UNIVERSIDAD COMPLUTENSE DE MADRID
FACULTAD DE CIENCIAS BIOLÓGICAS
Departamento de Bioquímica y Biología Molecular I

TESIS DOCTORAL

Modulación de la formación y de la diversidad estructural de amiloides

MEMORIA PARA OPTAR AL GRADO DE DOCTOR

PRESENTADA POR

Javier Alberto Martínez Fernández

Directora
María Gasset Vega

Madrid, 2016

UNIVERSIDAD COMPLUTENSE DE MADRID

FACULTAD DE CIENCIAS BIOLÓGICAS

BIOQUÍMICA Y BIOLOGÍA MOLECULAR I

"MODULACIÓN DE LA FORMACIÓN Y DE LA DIVERSIDAD ESTRUCTURAL DE AMILOIDES"

MEMORIA PRESENTADA POR JAVIER ALBERTO MARTÍNEZ FERNÁNDEZ PARA LA OBTENCIÓN DEL TÍTULO DE DOCTOR POR LA UNIVERSIDAD COMPLUTENSE DE MADRID

TESIS DOCTORAL

MADRID, 2015

DIRECTOR DE TESIS

MARÍA GASSET VEGA

María Gasset Vega, Investigadora Científica del CSIC

CERTIFICA, que el trabajo contenido en la memoria "***Modulación de la formación y de la diversidad estructural de amiloides***" presentada por D. Javier Alberto Martínez Fernández ha sido realizado en el Dpto de Química-Física Biológica del Instituto de Química-Física "Rocasolano" del CSIC, y financiada por una beca FPI (BES-2010-037134) los proyectos BFU2009-07971 y SAF2014-52661 del MINECO, una ayuda de la Fundación CIEN-Reina Sofía y de una acción de movilidad en la Universidad de Maryland (4-07-2013 al 5-10-2013) para la realización de experimentos en el laboratorio del Prof. Ilia V. Baskakov. Además, los trabajos aquí presentados son originales y la responsabilidad de la autoría ha sido avalada por todos los autores.

En Madrid, a 1 de septiembre de 2015

A mis padres

A mi hermana

A Alexia

Índice

Índice de tablas y figuras

Abreviaturas

AFM	Microscopía de Fuerzas Atómicas
BSA	Albúmina de Suero Bovina
CC1	Región Polibásica 1 de PrP
CC2	Región Polibásica 2 de PrP
CD	Dicroísmo Circular
CJD	Enfermedad de Creutzfeldt-Jakob
DLS	Dispersión de la Luz Dinámica
EDTA	Ácido Etilendiaminotetracético
FFI	Insomnio Familiar Fatal
FT	Región Efectora
FTIR	Espectrofotometría de Infrarrojo Transformada de Fourier
GAM-HRP	Anticuerpo secundario anti-ratón desarrollado en cabra fusionado a peroxidasa de rábano
GAR-HRP	Anticuerpo secundario anti-conejo desarrollado en cabra fusionado a peroxidasa de rábano
GD	Dominio Globular
GdnHCl	Cloruro de Guanidina
GPI	Glicosilfostatidilinositol
GSS	Síndrome de Gerstmann-Sträussler-Scheincker
HaPrP^{C}	Forma Celulara de la Proteína del Prión de Hámster
HC	Segmento Hidrofóbico
HPLC	Cromatografía Líquida de Alta Eficacia
HuPrP	Proteína Humana de Prión
KDa	Kilodalton
mAb	Anticuerpo Monoclonal
O.D. ^{n}	Valor de la absorbancia medida a la longitud de onda n (nm) en cubeta de 1 cm de paso óptico
OR	Octapéptido Repetido
ORF	Pauta de Lectura Abierta
PK	Proteinasa k
PMSF	Fluoruro de Fenilmetilsulfonilo
PRNP	Gen de la Proteína del Prión
PrP^{C}	Proteína Celular del Prión
PrP^{Sc}	Proteína Patógena del Prión (Sc de Scrapie)
PVDF	Fluoruro de Polivinilideno
RB	Región Bisagra
rSHaPrP	Proteína Recombinante que representa la secuencia madura de la Proteína PrP de Hámster Sirio
RMN	Resonancia Magnética Nuclear
SDS	Dodecilsulfato Sódico
SeMet, SeM	Selenometionina
ThT	Tioflavina T
Tween 20	Nombre comercial de Polioxietilensorbitan Monolaurato
WB	Electrotransferencia con posterior Inmunodetección
βME	β-Mercaptoetanol
ε^{n}	Coeficiente de Extinción Molar

Resumen / Summary

Resumen

Desde su descubrimiento como deshecho celular hasta la actualidad, los amiloides han adquirido la denominación de estado estructural provisto de actividad funcional. La estabilización de este estado requiere la presencia en la cadena de regiones adhesivas o proamiloidogénicas capaces de formar una lámina β-cruzada, su reactivación por exposición al medio y una concentración superior a una umbral para contrarrestar la barrera entrópica asociada a la adquisición del orden fibrilar. Estos requisitos pefilan un proceso de formación en varias etapas que permite la existencia de factores reguladores tanto intrínsecos como extrínsecos. Dentro de estos factores, se encuentran las mutaciones metabólicas derivadas de la sustitución de Met por SeMet, los códigos contenidos en la estructura de la carga y los cambios drásticos de entorno que modulen la unión de ligandos.

Para determinar el papel de la sustitución de Met por SeM, o mutación metabólica, en el ensamblaje de amiloides se eligieron regiones con uno (Aβ40, M35) o varios (HuPrP106-140; M109, M112, M129, M134) residuos. Estas secuencias y sus sustituciones se sintetizaron empleando métodos en fase sólida, y su capacidad para formar amiloides y la naturaleza de éstos se analizó utilizando cinéticas de unión de tioflavina T (ThT), electroforesis (PAGE-SDS), dicroísmo circular (CD), microscopía de fuerzas (AFM) y ensayos de citotoxicidad. En el caso de Aβ40, la sustitución de M35 por SeM impide la formación de fibras amiloides y da lugar a la formación de agregados no tóxicos tanto en reacciones de homo- ([SeM^{35}]Aβ40 con [SeM^{35}]Aβ40) como heteroasociación ([SeM^{35}]Aβ40 con [M^{35}]Aβ40). En el caso de HuPrP106-140, las distintas sustituciones generan un abanico de efectos entre los que se encuentran la inhibición (SeM129), la aceleración (SeM109 y SeM112), la reducción del rendimiento (SeM134), y cambios de forma, todos ellos correlacionados con alteraciones en la actividad citotóxica.

Para determinar el papel de la estructura de las cargas en la formación de amiloides, se eligió la cadena de PrP, en la que ésta presenta una distribución peculiar. En esta cadena el dominio N-terminal repetitivo está flanqueado por dos regiones polibásicas CC1 (23-30) y CC2 (101-110), mientras que el dominio C-terminal contiene la totalidad de los residuos ácidos, algunos de ellos expuestos. Para determinar el papel de la carga superficial en la formación y propiedades del estado amiloide de PrP, se generaron a partir de HaPrP(23-231) wt los mutantes K2(K24E,K27E), K4(K101,104,106,110E), K6 (K2-K4), K2-E200K, E200K, Q217R, Q219K, E221K y PrPΔ23-89. Las cadenas producidas de forma recombinante se caracterizaron empleando dispersión dinámica de luz (DLS), CD, AFM y microscopía de fluorescencia, mientras que las expresadas en células CHO mediante transfección transitoria se utilizaron en ensayos de procesamiento. La caracterización de la forma α (tipo PrP^{C}) indicó la existencia de un estado abierto y otro compacto más estable, cuya conversión depende de una interacción entre dominios, mediada por la región CC1 y la superficie electronegativa de α3. Esta interacción entre dominios dificulta la ruta de formación de amiloides. Por otra parte, la organización de la carga juega un papel clave en el estado amiloide, determinando su estructura y reactividad superficial.

El estudio del efecto de los cambios drásticos de entorno que incluyen alteraciones en la unión de ligandos estructurales se realizó empleando la proteína de unión de Ca^{2+} rGad m 1, el alérgeno dominante de pescado, y condiciones que simulan el tránsito gastrointestinal. En este caso

se emplearon análisis teóricos de secuencia y medidas de unión de ThT, SDS-PAGE, CD, DLS, AFM, proteólisis e inmunoensayos (dot blot) en condiciones de simulación gastrointestinal. Los resultados obtenidos indicaron que Gad m 1 forma amiloides a partir de su forma apo, estabilizada en condiciones de entorno gástrico o como en presencia de quelantes. Estos amiloides son responsables de la resistencia a proteasas y a la formación de distintos estados oligoméricos, de los cuales las oligoméricas tipo 2 dan cuenta de la unión de IgE de sueros de pacientes alérgicos al pescado.

Summary

Since their discovery as protein deposits, amyloids have progressively evolved to achieve the features of a structural state exhibiting function. To form amyloids, proteins first must contain in their sequence regions with cross-β sheet folding capacity. Second, such region must become prone to aggregation by solvent exposure. And third, the concentration of reactive regions must be overcome a threshold to counteract the entropic barrier of fibril ordering. These basic requirements describe amyloid formation as a multistep process under the control of both intrinsic and extrinsic factors. Among them, metabolic mutations resulting from Met substitution by SeMet, charge codes and drastic environmental changes with ligand binding impact could play yet unknown roles.

To gain insights the role of Met substitution by SeMet in amyloid assembly, the fibril-forming sequences of Aβ40 with one Met (M35) and HuPrP106-140 with several Met (M109, M112, M129, M134) were chosen. Sequences were synthesized using ad-hoc solid phase methods and their assembly properties analyzed using thioflavin T (ThT) binding kinetics, electrophoresis (SDS-PAGE), circular dichroism (CD), atomic force microscopy (AFM) and cytotoxicity assays. For Aβ40, substitution of M35 by SeM abrogated amyloid formation yielding non-toxic aggregates, both in homologous ([SeM^{35}]Aβ40 with [SeM^{35}]Aβ40) and heterologous ([SeM^{35}]Aβ40 with [M^{35}]Aβ40) reactions. For HuPrP106-140, single substitutions resulted in a variety of effects such as inhibition (SeM129), facilitation (SeM109 y SeM112), yield reduction (SeM134), and shape changes ape, all correlating with the cytotoxic activity.

To address the role of possible codes contained in the structure of exposed charges in amyloid assembly PrP chain was chosen. This two-domain chain contains a peculiar charge structure, with an N-terminal domain flanked by two polybasic clusters (CC1, residues 23-30, and CC2, residues 101-110), and a C-terminal harbouring all acid residues some of which are solvent exposed. HaPrP(23-230) wt chains and its various charge mutants (K2(K24E,K27E), K4(K101,104,106,110E), K6 (K2-K4), K2-E200K, E200K, Q217R, Q219K, E221K and PrPΔ23-89) were produced recombinantly and characterized using dynamic light scattering (DLS), CD, AFM and fluorescence microscopy. Also, the different chains were expressed in CHO cells using transient transfection assays, and the products characterized using enzymatic deglycosylations and immunodetections. Study of the α-fold showed the existence of an open and a compact forms and that their conversion is mediated by the interaction between CC1 and the electronegative surface of α3 that also impedes fibrillation. In the amyloid state, charges dictated the structure, the growth and the surface reactivity.

To analyze amyloid regulation by drastic environment changes with linked ligand binding effects, the dominant fish allergen Ca^{2+} binding Gad m1 and the simulated gastrointestinal transit were considered. Use of ThT binding, SDS-PAGE, CD, DLS, proteolysis and dot-blot assays showed that Gad m 1 forms amyloids from its apo form. Such form, stabilized both under gastric conditions or in the presence of chelates, forms amyloid depots which conferred protease resistance and yielded type 2 oligomers under intestinal conditions displaying the binding to allergic patient sera-contained IgE.

I. Introducción

1. El estado amiloide

La capacidad de las proteínas para experimentar cambios conformacionales es una propiedad esencial para la ejecución de su función de una forma regulada e integrada dentro de procesos biológicos. De todos los cambios conformacionales conocidos, los que han llamado más la atención por la naturaleza transgresora y las implicaciones en salud pública del producto final son aquellos que conducen a un estado rico en estructura β conocido como amiloide. Estos procesos se relacionan generalmente con la formación de agregados tóxicos que son patognomónicos de neurodegeneraciones tales como las enfermedades de Alzheimer, Parkinson, Creutzfeldt-Jakob o Huntington, entre otras [1-5]. Sin embargo, los amiloides no solo son relevantes en el contexto patológico, sino que su presencia acompaña a la adquisición de una larga lista de funciones beneficiosas como son la formación de corazas, el almacenaje de precursores, los procesos de adaptación rápida a cambios ambientales, y los fenómenos de memoria, entre otros [6-10]. La existencia de este estado, considerado como el estado estructural ancestral original, ha permitido ampliar las fronteras de las relaciones estructura-función de proteínas [11-16]. Actualmente, el estado amiloide se concibe como un estado estructural proteíco bien definido al que pueden acceder todas aquellas proteínas que cumplen unos requisitos de secuencia y se enfrentan a los entornos apropiados [12-14,16].

1.1. Su cronología.

El término amiloide se acuñó en la mitad del siglo XIX y desde entonces su significado ha evolucionado en paralelo al desarrollo tecnológico. La suma de la aparición de nuevas técnicas, sus aplicaciones, la incorporación de nuevos enfoques y el diálogo forzado o accidental entre distintos campos científicos (biología, física, química, medicina, etc) ha perfilado su significado dotándolo de identidad estructural y funcional.

Históricamente, el término amiloide surge en 1854, para definir al conjunto de anormalidades macroscópicas en tejidos teñidos con yodo que recordaban a los gránulos de almidón (Virchow, 1854). Años más tarde, el análisis de la composición reveló una naturaleza proteica excluyendo la presencia de carbohidratos (Kekulé, 1859). Ya en el siglo XX, la combinación de la tinción con Rojo Congo y el análisis mediante microscopía óptica con luz polarizada reveló la especificidad del colorante y una birrefringencia oro/verde (**figura 1.a-b**) [17-20]. Este rasgo de orden estructural se consolidó posteriormente con la incorporación de la tinción con acetato de uranilo y el análisis mediante microscopía electrónica, que permitió observar una estructura basada en un entramado de fibras de longitudes variables pero anchuras similares entre 80–100 Å (**figura 1.d**)[21].

Durante las dos décadas siguientes el estudio de amiloides persiguió incrementar la resolución estructural, identificando subunidades fibrilares con diámetros entre 25 y 35 Å [22,23]. En este periodo se desarrollan los protocolos de aislamiento de fibras a partir de tejidos y se optimizan los métodos de estudio *in vitro* [23-25]. En este sentido, la incorporación de agentes desnaturalizantes para la solubilización y disociación de las fibras aisladas de tejido, dictó el inicio de los estudios de secuenciación y de las relaciones entre patología, tipo de proteínas implicadas y proceso celular [26].

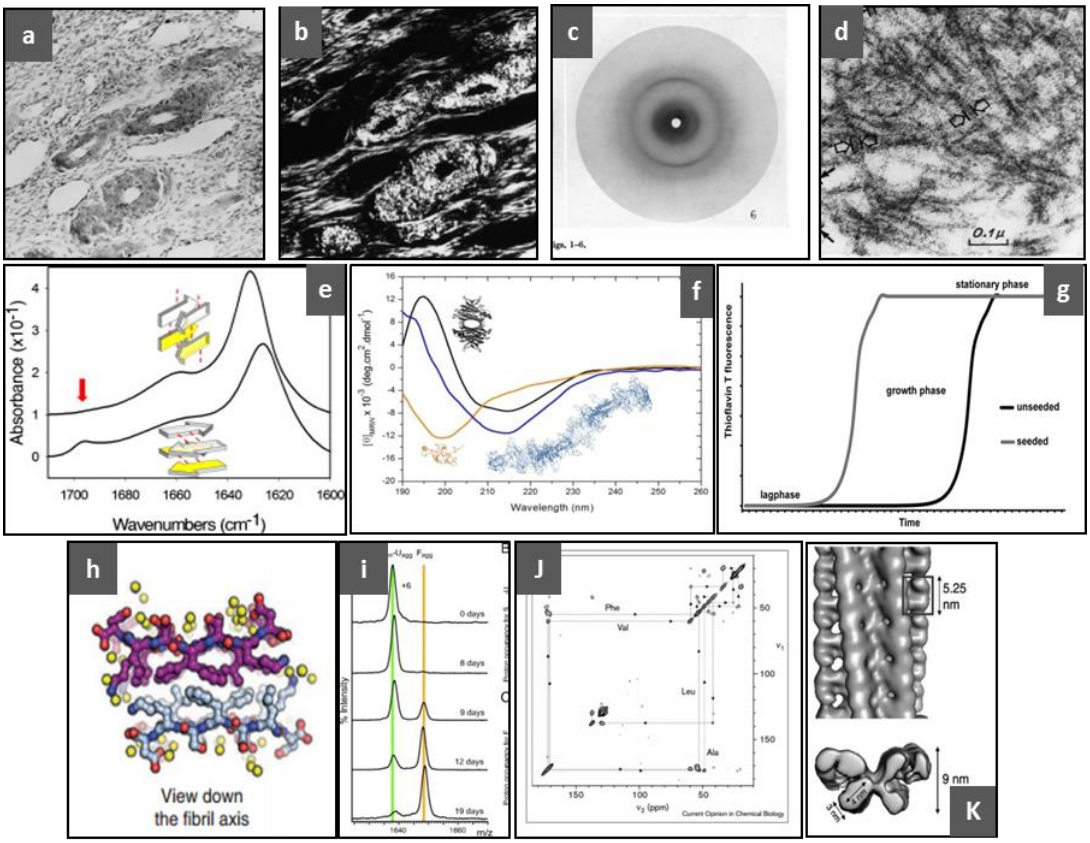

Figura 1. Cronología de la evolución del concepto estructural amiloide. Los paneles corresponden a: (**a**) tinción con Rojo Congo de la sección vascular de la pared muscular de útero amiloidótico [17]; (**b**) birrefringencia oreo/verde resultante de la visualización de la preparación anterior empleando polarizadores [17]; (**c**) patrón de difracción de rayos X de las fibras formadas después de desnaturalizar térmicamente la clara de huevo [27]; (**d**) imagen de microscopía electrónica de las fibras amiloides de bazo amiloidótico después de la tinción con acetato de uranilo (de The Journal of Cell Biology 1967 vol3); (**e**) espectros de FTIR de proteínas de estados amiloides [28]; (**f**) cambios en el espectro de dicroísmo circular de transtirretina (TTR) asociados a la formación de amiloides (Extraída web de RMBlab Protein Biophysics. Coimbra University); ((**g**) cinéticas modelo de formación de fibras construidas a partir medidas de emisión de fluorescencia de tioflavina T [29]; (**h**) estructura cristalina de amiloides mínimos secuencia segmento LSFSKD de β2-macroglobulina [30]; (**i**) cinética de la disociación de amiloides empleando intercambio isotópico HxD y espectrometría de masas[31]; (**j**) señal de NMR de estado sólido de las fibras amiloides formadas por el fragmento KLVFFAE de Aβ [32]; (**k**) reconstrucción de la estructura tridimensional de una fibra amiloide de la proteína β2-microglobulina a partir de imágenes de crio-EM [33].

Por otra parte, la generalización del uso de difracción de rayos X (figura 1c) y de espectroscopias de absorción (CD) y vibración (FTIR) (figura 1e, 1f) al estudio de fibras reveló como elemento estructural común la lámina β cruzada [34-39]. Este tipo de estructura había sido descrita con anterioridad para los estados térmicamente desnaturalizados de las proteínas de la clara de huevo y de fracciones de leguminosas e incorporada en los años 50 en los modelos de Pauling y Corey [27,40]. En las últimas dos décadas, los desarrollos de la producción de proteínas recombinantes, de la síntesis en fase sólida de péptidos, de técnicas de alta resolución para el análisis de estados sólidos (figura 1h-k) y de los sistemas de cálculo computacional ha permitido la descripción de los determinantes y requisitos para la formación de amiloides, la elaboración de modelos con resolución atómica de la organización de las fibras, la jerarquización de su ensamblaje y la existencia de polimorfismo, entre otras (ver más adelante).

Desde el punto de vista funcional el estado amiloide ha recorrido un camino largo, iniciado en su consideración como "basura proteica" y hasta su consolidación como elemento de transmisión de

información genética, similar a un ácido nucleico. Los estudios funcionales comienzan silenciosamente con el postulado de la hipótesis conformacional del prion de mamíferos (figura 2a,2b) [37,41,42]. Así el establecimiento del esqueleto amiloide de PrP^{Sc}, forma agregada de la proteína del prion con propiedades infecciosas, permitió abandonar el concepto de depósito inerte e incluir términos de transmisión y de propagación en el campo. Un poco más tarde, el campo de las levaduras empezó a manejar conceptos basados en elementos no genéticos y transmisibles de cambio de fenotipo y adaptación al medio [6] (figura 2c), describiéndose los amiloides transmisibles de las proteínas Ure2p y Sup35p. Desde entonces, la caracterización detallada de los procesos de transmisión de los amiloides ha permitido posicionarlos como moléculas de memoria hereditarias y con la capacidad de modificar los patrones de expresión del genoma (figura 2e) [9].

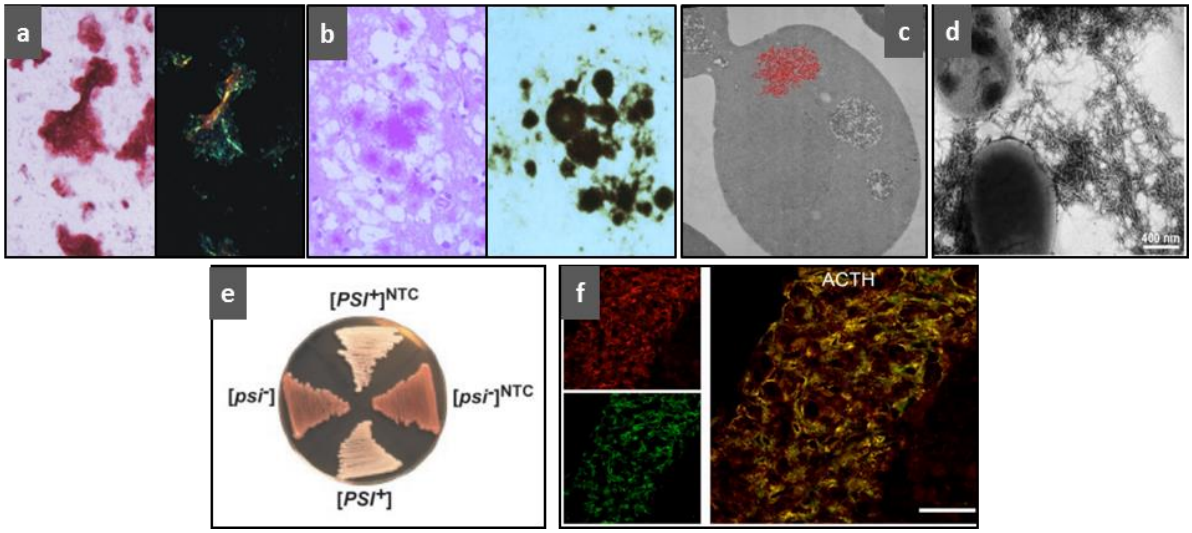

Figura 2. Cronología de la evolución del concepto amiloide desde el punto de vista funcional. Los paneles corresponden a: (**a**) birrefringencia oro/verde de los depósitos de proteínas teñidos con rojo congo [43]; (**b**) lesión vacuolar y depósitos amiloides del tejido cerebral provocada por la inoculación de fibras de PrP27-30 (priones) [44]; (**c**) fenotipo en levaduras debido a la aparición de fibras de Ure2p (Reed B. Wickner, Laboratory of Biochemistry and Genetics Web); (**d**) andamios de las biopelículas de *E.coli* sustentandos en las fibras de Curli [45]; (**e**) los priones de levaduras y sus fenotipos asociados se transmiten a células hijas [46]; (**f**) los almacenes intracelulares de la proforma de ACTH (rojo) son estados amiloide (verde) de acuerdo con las tinciones de una sección de pituitaria de ratón [7].

Por otra parte, los estudios de la arquitectura de las biopelículas bacterianas condujeron a la descripción de las fibras de Curli e identificarlas con un proceso complejo y regulado de ensamblaje de un amiloide (figura 2d) [8]. Este hallazgo condujo a acuñar el término de amiloide funcional y desde entonces se emplea para agrupar a un número creciente de actividades no tóxicas, como son los amiloides de Pmel y su papel en la formación de melanina, los amiloide de varias prohormonas y su almacén en los orgánulos de secreción de las mismas, entre otros (figura 2f) [7,47-50].

1.2. Su definición y características.

La definición del estado amiloide depende en gran medida del campo de estudio. En histología el término amiloide se emplea para referirse a fibras no ramificadas, normalmente extracelulares con capacidad para unir colorantes como el rojo Congo o la Tioflavina T o S y mostrar birrefringencia cuando se observan con luz polarizada o emitir fluorescencia [51]. Desde el punto de vista molecular, el amiloide es un estado estructural insoluble, polimérico, fibroso y

extraordinariamente ordenado [12,14,52]. La estructura de los amiloides se distingue de cualquier otro tipo de agregado fibrilar por su característico ordenamiento en forma de lámina-β cruzada (**figura 3**). En este tipo de ordenamiento varias copias de un segmento peptídico (de un péptido, de un fragmento de una proteína o de varias) adoptan una estructura secundaria de cadena β, que se ensamblan dando lugar a una lámina β, paralela o antiparalela, de extensión ilimitada y en la que la distancia entre cadenas unidas mediante puentes de hidrógeno es de 4.7 Å. Cada par de láminas se empaquetan mediante la interdigitación de las cadenas laterales a modo de cremallera estérica y generando una lámina β cruzada, cuya normal es perpendicular al eje fibrilar. La distancia entre láminas empaquetadas varía entre 6-11 Å, dependiendo de las cadenas laterales implicadas (**figuras 3a, b y c**) [27,53-56]. Las láminas β cruzadas, interaccionando entre sí, y trenzándose generan de forma jerarquizada protofibras (o protofilamentos), fibras (o filamentos) y fibras maduras [52,57,58].

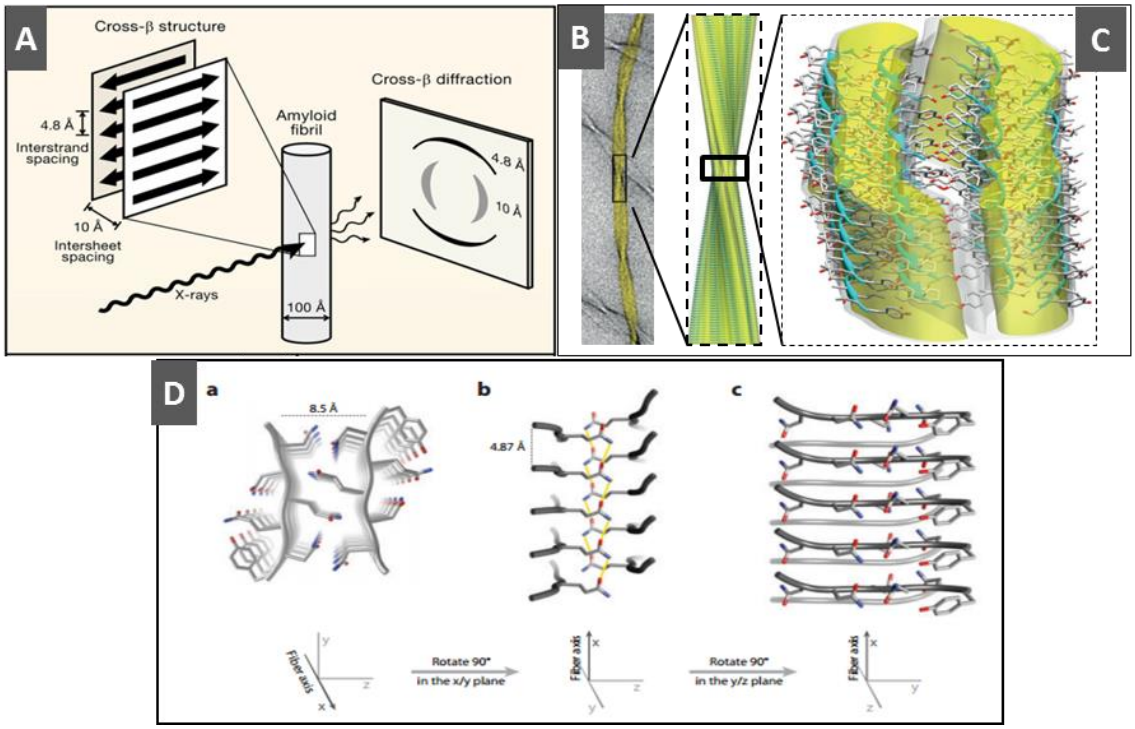

Figura 3. Estructura del estado amiloide. (**A**) las cadenas β (perpendiculares al eje de la fibra) forman láminas (paralelas al eje de la fibra) que se empaquetan inter-digitando las cadenas laterales a modo de cremallera. Esta disposición da lugar a las señales de las distancias entre cadenas de una lámina de 4.8 Å y la distancia entre láminas empaquetadas de alrededor de 10 [14]. Nivel de resolución de la estructura y jerarquía de un amiloide mediante (**B**) crio-microscopía electrónica, (**C**) NMR de estado sólido (las cintas verde representan la dirección de la cadena β, y las bolas en rojo, gris y azul representan los átomos de oxígeno, carbono, y nitrógeno, respectivamente) (Adaptado de [57]; (**E**) cristalografía de rayos X del péptido GNNQQNY. D-a) Vista inferior detallando la interdigitación de las cadenas laterales. D-b) Puentes de hidrógeno (amarillo) entre las cadenas laterales de las N de ambas láminas. D-c) Vista lateral mostrando la orientación de las cadenas laterales (Adaptado de Toyama et al. [59].

Estas características estructurales determinan unas propiedades mecánicas comparables a las del acero que distingue a los amiloides de otros filamentos biológicos, como son los formados por actina o tubulina [57,58]. Desde el punto de vista termodinámico, el amiloide representa un estado más estable que el del monómero precursor [12,60,61]. En esta estabilización participan factores de separación de fase (amiloide es un estado cuasi-sólido y el monómero es soluble) y cinéticos

(disociación de monómeros), que determina una gran resistencia a la degradación proteolítica (que ocurre a través del monómero) y a la solubilización por agentes químicos [60,61]. De este modo, los amiloides son resistentes a la acción del SDS, y su disociación con liberación de monómeros requiere agentes caotrópicos como cloruro de guanidina a altas concentraciones, ácido fórmico (FA) o hexafluor-2-propanol (HFIP) [62].

1.2.1. Predicción de secuencias amiloidogénicas.

El desarrollo de modelos de amiloides mínimos ha sido esencial para la descripción de determinantes estructurales. En primer lugar, la formación de un amiloide requiere un segmento con predisposición a adoptar una estructura de cadena β y formar una lámina β, tanto paralela como anti-paralela, propiedad que puede predecirse con algoritmos de tipo TANGO, AGGRESCAN y WALTZ [63-66] (tabla 1).

Tabla 1. Algoritmos para la predicción del comportamiento amiloide

Cadenas β con tendencia a agregar		
TANGO	http://tango.crg.es/	Se basa en las propiedades fisicoquímicas que hay detrás del plegamiento intermolecular en forma de lámina, el cual asume que las regiones de nucleación están completamente escondidas en el interior del agregado. Teniendo en cuenta estructuras secundarias, interacciones electrostáticas, enlaces de hidrógeno, hidrofobicidad, eneregías de solvatación, así como parámetros del entorno (pH, fuerza iónica, etc) [64].
AGGRESCAN	http://bioinf.uab.es/aggrescan	Permite predecir la capacidad de agregación e identifica regiones que participan en la agregación de proteínas [63]. Basado en experimentos in vivo realizados en bacterias y expresan el péptido β-amiloide el cual es empleado como modelo. Utilizan la región de agregación 18-20 y mediante mutaciones del residuo 19 van valorando las propiedades intrínsecas para la agregación de cada aminoácido [67].
ZYGGREGATOR	http://www.vendruscolo.ch.cam.ac.uk/zyggregator.php	Basado en las aproximaciones de Chiti y Dobson que demuestran las relaciones entre agregación de proteínas y tres propiedades físico-químicas como carga, hidrofobicidad y tendencia a formar α-hélice o hebras-β. Además de éstas, este algoritmo incluye como afectan las propiedades del entorno. Esta herramienta permite predecir agregación de cadenas polipeptídicas desplegadas, globulares y proteínas con dominios plegados y desplegados [68].
Amiloides		
WALTZ	http://waltz.switchlab.org	Utiliza una matriz que puntúa la capacidad de cada residuo en determinada posición-específica dentro del hexapéptido utilizando tanto métodos estructurales como biofísicos. Esta matriz se dedujo a partir de más de 200 secuencias de hexapéptidos. Por tanto determina la capacidad de cada aminoácido de forma posición-específica para cada aminoácido [66].
ZipperDB	http://services.mbi.ucla.edu/zipperdb/	Detecta las regiones propensas a formar amiloides en cada proteína. Funciona mediante el análisis de grupos de 6 residuos usando funciones de RosettaDesign para evaluar el ajuste a partir de la secuencia NNQQNY [56].

En segundo lugar y esencial, que dicha lámina β de lugar a caras capaces de interdigitarse, o lo que es lo mismo que las superficies generadas por las cadenas laterales de los aminoácidos sean parcial o totalmente complementarias de forma que el espacio entre láminas excluya las moléculas de agua (cremalleras estéricas secas)[14,69]. La tendencia intrínseca de un segmento a adoptar una estructura de cadena β y empaquetarse en cremallera estérica sólo puede predecirse *de novo* empleando el algoritmo ZipperDb, que arroja para parámetros de estabilidad secuencias mínimo de 6 aminoácidos [56,69]. No obstante, la capacidad predictiva de este algoritmo se limita a secuencias auto-complementarias, y no aborda la complementariedad de cadenas distintas que caracterizan las hetero-cremalleras [14].

1.2.2. Polimorfismo estructural de amiloides

Una misma secuencia puede dar lugar a diversas estructuras fibrilares que concurren con diferencias funcionales [12,14,70,71]. Este fenómeno, conocido como polimorfismo, se manifiesta en las características macroscópicas de las fibras (grosor, longitud, desviación del eje, ramificaciones, etc), los valores de masa por longitud, la estructura secundaria global, la naturaleza y reactividad de las superficies expuestas al solvente, la estabilidad relativa medida como resistencia a la disociación y la fragmentación, los patrones de difracción de rayos X, entre otras [72-81]. De forma importante, estas diferencias pueden transmitirse a fibras hijas, generadas a partir de núcleo de fibra "madre" y monómeros, o moldearse como consecuencia de cambios en el entorno [14,70,82-84].

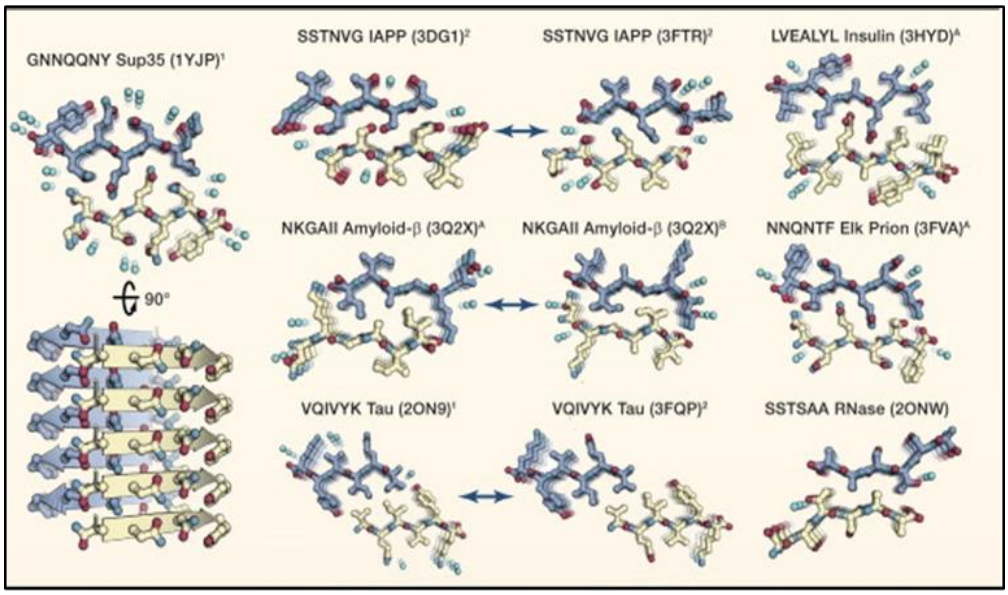

Figura 4. Cremalleras estéricas. Estructura atómica determinada por difracción de rayos X de los protofilamentos formados por hexapéptidos adhesivos de distintas proteínas, mostrando los polimorfismos debido a empaquetamientos alternativos. La ausencia de moléculas de agua (bolas azules) en el interior de las cremalleras demuestra su natulareza seca (Adaptado de Eisenberg and Jucke., 2012) [14].

La existencia de polimorfismo puede explicarse estructuralmente sobre el modelo de cremallera estérica. [12,14,43,56,71]. En primer lugar un mismo hexapéptido adhesivo puede experimentar distintos empaquetamientos y dar lugar a cremalleras con distintos mínimos de energías (figura 4). En segundo lugar, una cadena polipeptídica con varios hexapéptidos adhesivos puede dar lugar a distintas láminas β cruzada y sus estados superiores de polimerización dependiendo de cuál sea el

segmento iniciador. En este caso la posibilidad de que las láminas β no idénticas sean complementarias y formen una hetero-cremallera ofrece la posibilidad de un núcleo de crecimiento alternativo [12]. Además de la diversidad de los núcleos, la jerarquización del ensamblaje permite diferencias en el trenzado de los protofilamentos [14,43,76,85].

2. Mecanismo de formación de amiloides.

Desde el punto de vista cinético, la formación de amiloides obedece a una reacción de polimerización nucleada por condensación no covalente y puede determinarse experimentalmente empleando medidas de incremento de la fluorescencia de ThT y de incorporación de monómeros (figura 5). En este esquema básico, la primera etapa y limitante de la velocidad, consiste en la formación de un núcleo mínimo. El tiempo que tarda en constituirse este núcleo se denomina tiempo de retardo (Lag-phase) y distintos estudios sugieren una identidad de trímero o tetrámero para el mismo [54,86-89]. Una vez constituido el núcleo o administrado exógenamente (molde o semilla), se dispara la fase de crecimiento o elongación mediante la incorporación rápida de monómeros [16,43,54,90]. Esta etapa es compleja y el límite de crecimiento viene impuesto por la estabilidad del polímero que puede alcanzar un equilibrio de crecimiento/disociación o sufrir fragmentaciones que generen bien regiones nuevas de crecimiento o regiones incapaces de crecer (quenched). La información sobre la naturaleza del crecimiento está contenida en la fase exponencial y puede extraerse empleando modelos complejos de análisis [31,91-93]. La fase de elongación concluye en una fase estacionaria, en la que se alcanza el equilibrio entre crecimiento y fraccionamiento (figura 5).

Este mecanismo cinético subraya la naturaleza dinámica de los amiloides, descartando la característica de estado irreversible y explicando los fenómenos de latencia [94]. Así, de acuerdo con la ley de acción de masas y en condiciones de eliminación del monómero, como son las que hacen uso de digestiones proteolíticas prolongadas en condiciones diluidas y con homogeneidad de fase, los amiloides son disociables en su totalidad (figura 5). Igualmente, dependiendo de las propiedades del proceso de disociación los núcleos o fragmentos pueden existir en un estado latente y en presencia de monómeros iniciar procesos de polimerización, fenómeno que ha confundido durante tiempo a la comunidad científica del campo de los priones [95,96].

Estructuralmente la descripción de las cremalleras estéricas como esqueleto determina tres requisitos básicos en el proceso de formación. En primer lugar, que la proteína o fragmento de proteína implicada disponga en su secuencia de hexapéptidos adhesivos o segmentos capaces de constituir una lámina β cruzada estable, condición que puede determinarse mediante el análisis de las secuencias con ZipperDb [69]. En segundo lugar, los segmentos deben adquirir la capacidad de reacción mediante la exposición al medio a través de un desplegamiento parcial o local, un procesamiento proteolítico, la pérdida o ganancia de un ligando o una modificación covalente [14,97-99]. En tercer lugar, y como consecuencia de la barrera entrópica que conlleva la polimerización ordenada, ha de superarse una concentración umbral que explica que la amilogénesis se favorezca en condiciones de acumulación de monómeros y en regiones confinadas [100].

De forma general, el proceso de formación de amiloides lleva asociado la aparición de al menos dos tipos de oligómeros solubles que se distinguen en función de su relación con el polímero amiloide y en su immunorreactividad conformacional [78,101-112]. Los oligómeros de tipo I son el

resultado de en una ruta de plegamiento distinta de la que conduce a las fibras y son reactivos frente al anticuerpo A11, generado frente a láminas β antiparalelas desplazadas (out-of-register) [106,112,113]. Estos oligómeros no son propagativos pero si elevadamente tóxicos, actividad que se asocia con la formación de ensamblajes toroidales sobre las membranas biológicas [114-119]. Por el contrario, los oligómeros de tipo 2 se producen a lo largo del proceso de formación de las fibras amiloides y son reactivos frente al anticuerpo OC, que reconoce áminas β paralelas con cadenas dispuestas en registro [101,106,109,110]. Estos oligómeros son muy propagativos, debido a su comportamiento como núcleos de elongación [107,120-123].

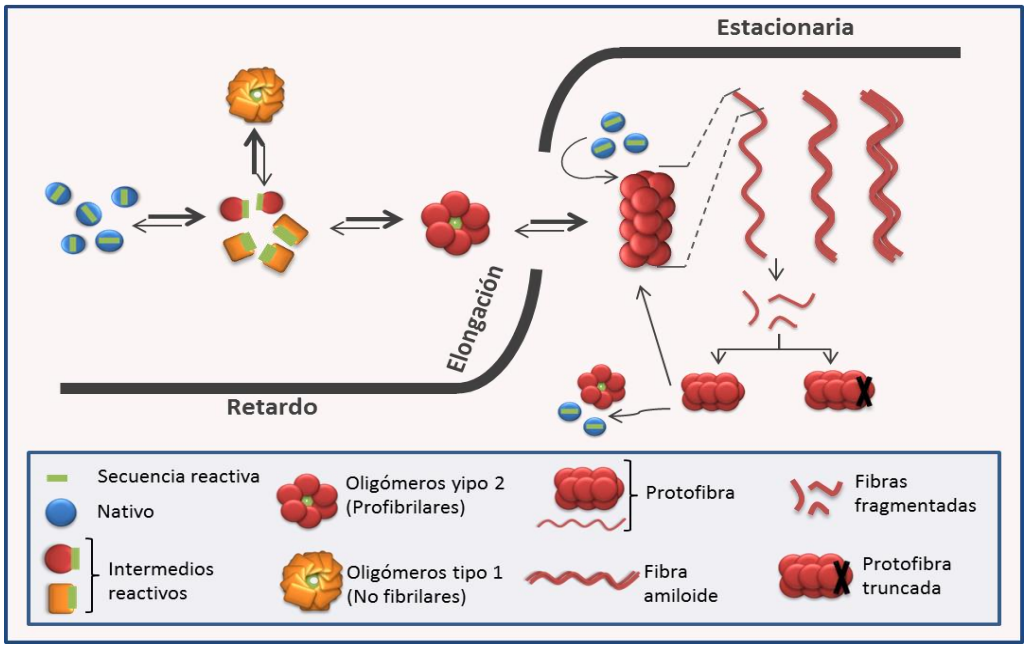

Figura 5.- Modelos cinético y estructural del proceso de formación de amiloides. Cinéticamente la formación de un amiloide obedece un patrón de polimerización nucleada por condensación no covalente. En la fase de retardo, las regiones adhesivas (línea gruesa verde) de los monómeros proteicos (esferas azules) se activan en cambios conformacionales que permite su exposición permitiendo la formación de dos tipos de oligómeros. Un tipo de estos actúa de núcleo de polimerización. En la fase de elongación, el núcleo crece por adición de monómeros para formare protofilamentos, que a su vez se unirán formando las fibras y éstas filamentos. En las fases de elongación y estacionarias pueden ocurrir fenómenos secundarios debidos a fraccionamientos y apagamientos del crecimiento.

3. Clasificación de los amiloides

La pérdida del papel de basura de los amiloides y la aceptación de su naturaleza de estado estructural, el amiloma o conjunto de proteínas que forman amiloides ha crecido significativamente y ha generado la necesidad de establecer una clasificación. En este sentido y por cuestiones históricas, los criterios de clasificación hacen referencia al grado o límite de propagación del polímero amiloide y al impacto tóxico o no de su formación (tabla 2).

3.1. Clasificación en función del alcance de la propagación

Debido a su mecanismo de formación los amiloides son polímeros que resultan del crecimiento de un núcleo mediante el reclutamiento de monómeros. Por lo tanto dependiendo de la

capacidad viajera del núcleo el proceso de propagación puede ser espacial y temporalmente restringido, o incluir transmisiones de orden superior como son la transcelular y entre organismos sin necesidad de iniciación del proceso [43,124-126] (**figura 6**). Es necesario destacar que la asignación de proteínas dentro de los distintos grupos no es fija, sino que a medida que se avanza en el conocimiento pueden producirse reclasificaciones (**tabla 2**).

3.1.1. Los amiloides: estructura sin dispersión. Es el grupo genérico que engloba a todas las proteínas capaces de ensamblarse en amiloides con restricción espacial y temporal, y por lo tanto que no cumplen los criterios de dispersión entre poblaciones celulares u organismos. Algunos ejemplos de estos amiloides son Pmel 17, varias prohormonas peptídicas, Curli, chaplinas, entre otros [7,8,127].

3.1.2. Los prionoides: amiloides transmisibles entre poblaciones celulares. Se denominan prionoides a aquellos amiloides cuya propagación ocurre al menos transcelularmente [124,125,128,129] (**figura 6**). De este modo, la denominación de prionoide en el caso de los amiloides de procariotas y de eucariotas unicelulares se confunde con el grado superior prion, y en el caso de los amiloides de organismos pluricelulares indica una capacitación para una transmisión todavía no determinada. Ejemplos de prionoides son RepA-WH1 causante de una prionopatía en *Escherichia coli* [130,131], TDP43 y FUS implicados en la aparición de esclerosis lateral amiotrófica (ELA)[132,133] o la huntingtina implicada en la enfermedad de Huntington [134] entre otras. Dos casos adicionales son los amiloides de MAVS (Mitochondrial antiviral-signaling protein) y de CPEB3 implicadas en la defensa frente a virus y en procesos de memoria, respectivamente [135-138]. En estos casos, la formación de amiloides es un proceso inducido con propagación intracelular, y transmisible transcelularmente en estudios modelo.

3.1.3. Los priones y cuasi-priones: amiloides transmisibles cuya propagación afecta a comunidades. El término prion, que procede de la conjunción de los términos proteína e infección para describir al agente causante de las encefalopatías espongiformes en mamíferos [2,139],se ha generalizado para referirse a estados amiloides cuya transmisión ocurre entre organismos o por herencia intracelular (citoplasmática o nuclear) en el caso de organismos unicelulares. Dentro de este grupo se encuentran los amiloides de PrP [2,139-144], de α-sinucleina [145], de SSA [146,147] y Aβ [148], y muy probablemente tau [149] en mamíferos. Como elemento de herencia citoplasmática, se encuentran los amiloides de levadura Sup35p, Ure2p, Rnq1p en *Saccharomyces cerevisiae* y HET en *Podospora anserina,* entre otros [150-155]. En muchos de estos casos, pero no en todos, las secuencias de la proteínas implicadas contienen un segmento de aproximadamente 40 aminoácidos ricos en Q/N y con una elevada repetición, al que se ha denominado dominio prion y que puede identificarse mediante el algoritmo PrionScan [156].

3.2. Clasificación en función de su actividad.

Por razones históricas los amiloides se han asociado preferentemente a la causa o consecuencia de patologías. No obstante, con el paso del tiempo se han incorporado un número elevado de proteínas cuyo estado amiloide desempeña una función beneficiosa para el huésped (**tabla 2**).

3.2.1. Amiloides funcionales. El término de amiloides funcionales agrupa al conjunto de estados amiloides de proteínas cuya aparición está relacionada con una función normal dentro de los procesos fisiológicos y no conlleva la toxicidad para el hospedador [12,157,158]. En muchos de estos casos la formación del amiloide ha de ser un proceso altamente regulado para evitar toxicidad [159].

3.2.1.1. Amiloides con funciones arquitectónicas. Dentro de los amiloides con funciones arquitectónicas se encuentran Curli, chaplina, rodlinas, hidrofobinas, y Pmel 17 [48,160]. En el caso de Curli su fibras amiloides forman los andamios de las biopelículas que recubren y preservan comunidades bacterianas en condiciones de estrés [45,161]. En este caso, la formación del amiloide es un proceso coordinado que implica la acción de distintas cadenas polipéptidcas y que supone una ventaja energética para la célula [162,163]. Del mismo modo, los amiloides de chaplinas, rodlinas e hidrofobinas permiten transiciones en las propiedades de las superficies celulares [160]. En el hombre, la formación del amiloide de Pmel17 da forma al andamio necesario para la polimerización de melanina [48,49,164,165]. Además, el estado amiloide de varias proteínas funciona como superficie activa para la activación del factor XII, serin proteasa implicada en procesos de homeostasis [48].

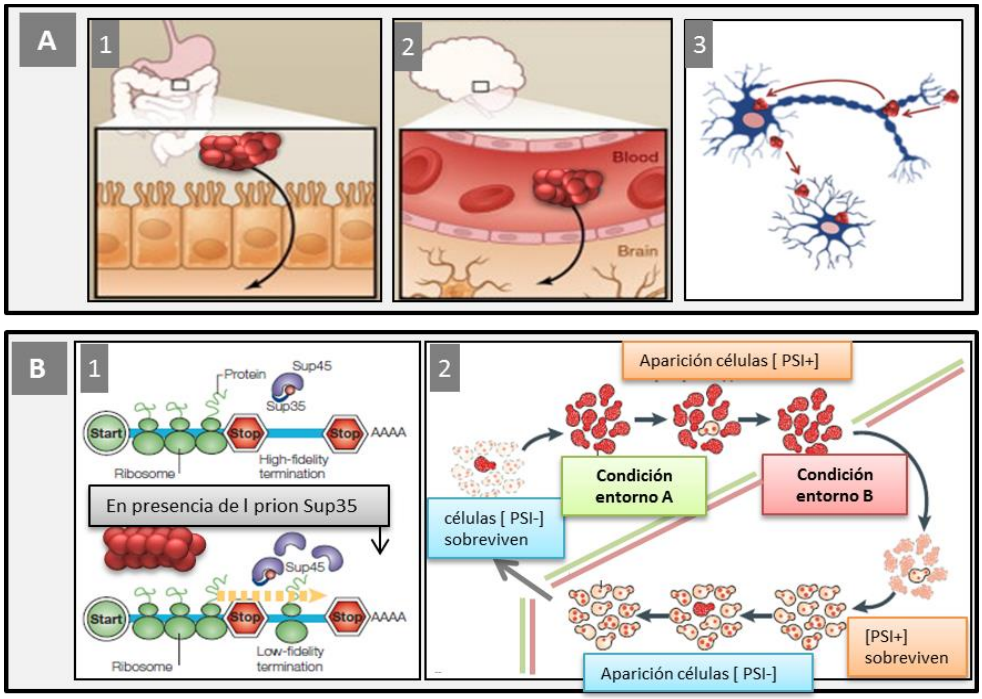

Figura 6. Los priones: amiloides con propagación tóxica o epigenética. A. Modelo de propagación del prion de PrP mediante la ruta oral incluyendo: 1) la estabilidad del estado amiloide frente a proteasas permite su preservación hasta alcanzar el intestino donde tiene lugar su absorción. 2) los núcleos amiloides son transportados acelular o celularmente atravesando la barrera hematoencefálica. 3) en las células donde existen monómeros se activa la fase de elongación que incide sobre la viabilidad celular (adaptada de Soto C. 2012 Cell). **B.** Modelo de propagación de priones de levadura. 1) Los amiloides de Sup35 interfieren en la terminación de la traducción, generando nuevas proteínas. 2) la aparición espontánea en una población de levaduras [PSI-] (células rojas) del prión Sup35 da a células [PSI+] (blancas con puntos rojos), que resisten un cierto entorno. Un cambio de las condiciones ambientales pueden revertir dicha selección o beneficiar nuevos fenotipos (Adaptada de Shorter & Lindquist 2005 Nat Rev).

3.2.1.2. Amiloides con funciones epigenéticas. Dentro de este grupo se encuentra la familia conocida como priones de levadura iniciada con Sup35p y Ure2p (**figura 6**) [6,166-168]. En este casos, las proteínas implicadas presentan una construcción en al menos dos dominios, uno de los cuales es un dominio PrD, caracterizado por una riqueza poco usual de residuos Q/N y repeticiones de aproximadamente 40 residuos. PrD es capaz de existir bajo un estado precursor y uno amiloide, y dependiendo de su

naturaleza dictar un cambio on/off en la función del dominio activo y una transición de adaptación del fenotipo [169].

3.2.1.3. Funciones de almacenaje. Más de treinta hormonas peptídicas, en su forma precursora de prehormona, se almacenan en forma de amiloides en los gránulos de secreción [7,47]. En este caso, los cambios en cofinamiento (concentración dentro del orgánulo frente a la dilución en su vertido), del pH y el procesamiento proteolítico de la prosecuencia determinan la disociación del amiloide en un proceso coordinado a la secreción del contenido del orgánulo [170].

3.2.2 Amiloides patógenos. Se denominan amiloides patógenos al conjunto de ensamblajes cuya formación es la causa o consecuencia de una enfermedad. Al conjunto de enfermedades relacionadas a la presencia de amiloides se las ha denominado tradicionalmente enfermedades conformacionales [171]. Dentro de estas se encuentran las enfermedad de Creutzfeldt-Jakob, Kuru, Gerstmann-Strussler-Sheinker e Insominio Familiar Letal asociadas al amiloide PrP [172], la enfermedad de Alzheimer, debida a los amiloides de Aβ y Tau (Busciglio et al., 1995; Kim and Tsai, 2009; Santacruz et al., 2005), la enfermedad de Parkinson y el amiloide de α-sinucleína [145,173-175], y la diabetes tipo 2 y el amiloide de IAPP [52,140,176,177]. De forma general, en estos casos la formación del amiloide implica la activación de una ruta de plegamiento minoritaria (generalmente llamada como "misfolding") que origina la pérdida de la función biológica del estado o estados nativos fisiológicos y la aparición de una función tóxica [52,65,171,176,178-182]. Esta función tóxica generalmente está mediada por oligómeros, que a diferencia de las fibras son solubles y tienen la capacidad de unirse a membranas y distorsionar su permeabilidad o disparar una cascada de señales tóxicas [183,184].

Tabla 2. Clasificación de amiloides

Criterio de clasificación			
Según su capacidad de propagación		**Según su funcionalidad**	
Amiloides	Sin dispersión	Funcionales	Estructurales (Pmel 17, Curli, Chaplinas, Rodlinas, Hidrofobinas)
			Almacenaje; prohormonas.
		Toxicos	
Prionoides	Propagación al menos es transcelular	Funcionales	Procesos de memoria (CPEB)
		Tóxicos	RepA1 (en *E.coli*), Hungtintina, MAVS
Priones	Transmisión entre organismos	Funcionales	Transmisión de caracteres (Sup35p, Ure2, Mot3, Rmq1p, HETs)
		Tóxicos	mamíferos(Aβ, PrP, Tau, α-synuclein, IAAP) Bacterias (microcina E92, harpinas)

3.2.2.1. Aβ40/42: uno de los amiloides de la enfermedad de Alzheimer. La enfermedad de Alzheimer (AD), la neurodegeneración dominante en el hombre, se caracteriza clínicamente por un deterioro cognitivo que conduce a un estado de demencia, e histológicamente por la aparición de placas de

amiloides, de ovillos neurofibrilares (NFTs) y la pérdida del contenido neuronal del hipotálamo y de la corteza cerebral [185,186]. El estudio de las dos lesiones patognomónicas ha permitido identificar como protagonistas patogénicos al péptido Aβ y sus distintos estados de asociación, como unidad constitutiva de las placas, y a la proteína asociada a microtúbulos tau y sus formas hiperfosforiladas, como entidad constitutiva de los NFTs [187-190]. La convergencia de ambas entidades moleculares ambas, Aβ y tau, ha dado forma a una cascada compleja de señalización en la que las aberraciones metabólicas en Aβ y en tau interaccionan recíprocamente hacia un estado patogénico común [191-193]. De todos los factores de riesgo implicados en el desarrollo de AD, el más significativo es el proceso de envejecimiento, entendido como la pérdida de armonía biológica. Así en humanos sanos existen mecanismos que permiten eliminar adecuadamente la familia de péptidos Aβ; y su fallo provoca la acumulación de Aβ y el incremento del riesgo de neurotoxicidad. Del mismo modo, la distorsión de la homeostasis de los procesos de fosforilación y desfosforilación de tau conduce a la acumulación de formas de tau hiperfosforiladas que carecen de la capacidad de unión de microtúbulos [187,188].

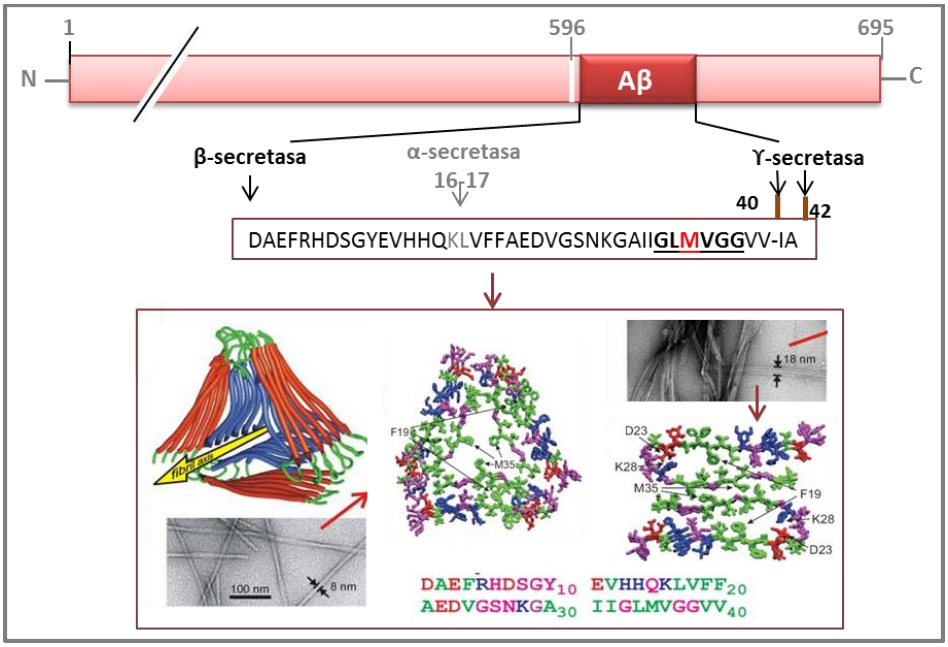

Figura 7.- Biosíntesis de los péptido Aβ y modelos estructurales de su empaquetamiento fibrilar. **A**) La proteína APP puede ser procesado a partir de α-, β- y γ-secretasas. La acción sucesiva de las β y γ-secretasas da lugar a los fragmentos Aβ40 y Aβ42. **B**) Modelos estructurales generados a partir de datos experimentales. Los residuos hidrofóbicos se representan en verde, los polares (magenta), con carga negativa (rojo) y con carga positiva (azul). (adaptado de Paravastu et al. 2008 PNAS).

Los péptidos Aβ son resultado del procesamiento proteolítico de la proteína precursora de amiloides (APP), proteína transmembrana tipo I implicada en el desarrollo neuronal, tráfico de proteínas y de señales de transducción [194-196]. APP experimenta dos tipos de procesamiento proteolíticos distintos (figura 7), uno amiloidogénico en el que se producen los fragmentos Aβ y otro no amiloidogénico [195,197]. El procesamiento amiloidogénico de APP implica un proceso complejo mediado por la acción de β-secretasa, (principalmente BACE1) y del complejo γ-secretasa, y su producto está constituido principalmente por Aβ40 y en menor medida el fragmento Aβ42 [196]. Los fragmentos Aβ40 y Aβ42 solapan en secuencia, diferenciándose en el dipéptido C-terminal IV

presente en Aβ42. Esta extensión incrementa la hidrofobicidad y capacita un segmento adhesivo adicional, que dicta la formación de amiloides más estables debido a impedimentos en la disociación [31,112,185,186,198-200]. Ambas secuencias comparten en el flanco C-terminal del segmento adhesivo central el residuo M35, cuya cadena lateral y sus cambios de polaridad mediante oxidación reversible (sulfóxido) o irreversible (sulfona) juega una papel clave en el ensamblaje y en la actividad [201-204].

3.2.2.1. PrP^{Sc}: el amiloide en las encefalopatías espongiformes transmisibles de mamíferos. Las encefalopatías espongiformes transmisibles son un conjunto de neurodegeneraciones letales de mamíferos caracterizadas por una lesión por vacuolización del sistema nervioso central, con hipertofia de astrocitos, proliferación de la microglia y en algunos casos de depósitos extracelulares amiloides de PrP [96,205-211]. En humanos, estas patologías se clasifican atendiendo a la etiología (genéticas, esporádica o adquirida) o al tipo de lesión (CJD, FFI, GSS, Kuru, etc) y sus prevalencias mínimas son de 2.5 casos por millón de habitante [206,212-219].

PrP^{Sc} es la forma patógena con estructura amiloide de la proteína del prión celular (PrP^{c}), formada en un proceso post-traduccional [172,220-227]. La cadena de PrP consta de unos 254 aminoácidos dependiendo de la especie, en la que los N- y C-terminales corresponden a secuencias señal proteolizables o transesterificables con un grupo GPI [228-231]. El resto de residuos está organizado en dos dominios N- y C-terminal separados por una región bisagra hidrofóbica. El dominio N-terminal, conocido como FT de cola flexible, tiene una estructura repetitiva en la que se distinguen secuencias de 11 y de 8 (OR) residuos, flanqueadas por dos regiones polibásicas denominadas CC1 y CC2 [232]. Este dominio aloja los sitios de unión de ligando tales como Cu^{2+}/Zn^{2+} en los OR y polianiones en CC1 y CC2 [233-242]. La región bisagra separa ambos dominios y es altamente maleable, apareciendo bien como segmento transmembrana en las formas integradas de PrP (^{Ctm}PrP y ^{Ntm}PrP), desordenada en modelos 3D de PrP^{c} y como núcleo amiloide en las placas tisulares [37,243,244]. El dominio C-terminal contiene la información para un plegamiento globular (de ahí su denominación de dominio globular, GD) sustentado en dos cadenas β (β1 entre 126-131, β2 en 161-164) y tres hélices α (α1 en 144-154, α2 en 175-193, y α3 en 200-227). Además, se distinguen dos posiciones susceptibles de glicosilación N181 y N197, y los residuos C179 y C214 que formando un puente disulfuro intramolecular sostienen el pilar estructural α2-α3 [124,243] (**figura 8**).

La cadena de PrP existe en dos estados estructurales principales. En el estado α o tipo PrP^{C}, el dominio C-terminal adopta una estructura globular con los elementos antes citados y el dominio N-terminal en función de la existencia o no de ligandos unidos se distribuye entre una estructura flexible desordenada y una más compacta que abraza el domino globular [245,246]. En el estado amiloide, la situación es más compleja y el uso de PrP^{Sc} aislada de tejido y cadenas producidas recombinantemente ha generado una colección extensa de confórmeros cuyo denominador común es la presencia de lámina β cruzada [83,247-249]. Estas formas β (o tipo PrP^{Sc}) se diferencian en la estructura secundaria, en su compacidad, en la facilidad de fragmentación y disociación, y en su capacidad para propagarse y causar las lesiones patognomónicas [250,251].

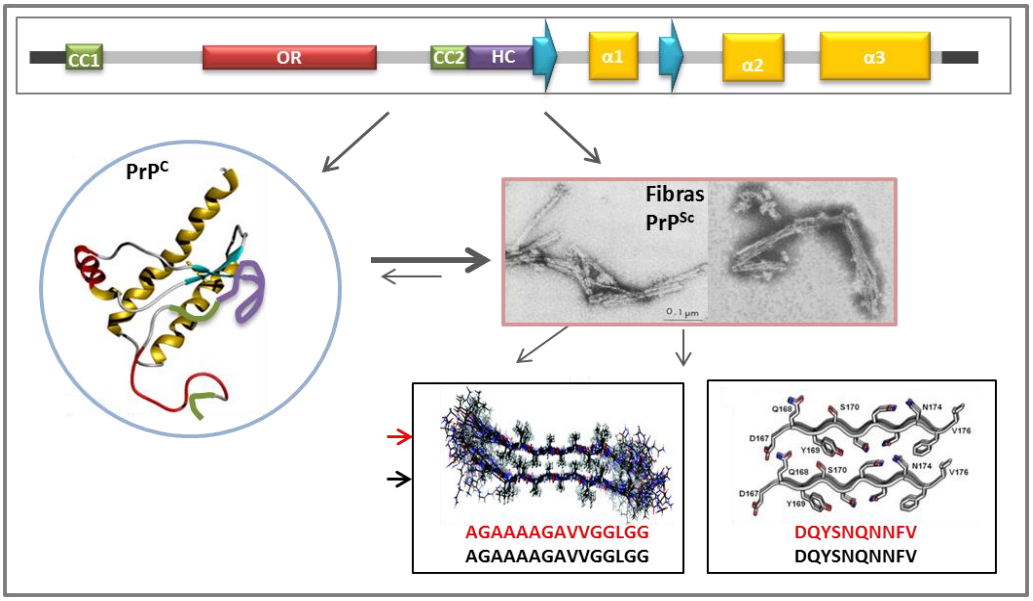

Figura 8.- Organización de la cadena polipeptídica de PrP y sus conformaciones PrP^C y PrP^{Sc}. A) La cadena polipeptídica de PrP está organizada en dos dominios N-y C- terminal separado por una bisagra hidrófobica (HC), y con secuencias señales en ambos extremos (banda gris oscura). Escindida la secuencia señal, el dominio N-terminal incluye las regiones ricas en aminoácidos básicos 1 (CC1 [23-30]) y 2 (CC2 [100-110]), y una región con cuatro repeticiones idénticas de un octapéptido (OR, [51-91]). El dominio C-terminal contiene los elementos capaces de plegarse generando dos cadenas β (flechas azules [126-131] y [161-164], y tres hélices α (α1 [144-154], α2 [173-194], α3 [200-221]. En este caso, la escisión de la secuencia señal incluye la adición de un grupo GPI (gris oscuro). **B**) Estructura del plegamiento o forma α , en la que el dominio N-terminal es una cola flexible (FT) y el C-terminal se comporta como un dominio globular (modificado de Jackson G lab. www.Prion.ucl.ac.uk/research/mrc-research-groups/molecular-diagnosis/). **C**) Estructura fibrilar PrP^{Sc} (Modificado de Merz et al. 1986 Journal of Virology), en la que participan al menos las regiones adhesivas 113-127 (Cheng H-M 2011 Biochemistry) y 167-176 (Kurt et al. 2014 JBC).

De todos las formas β generadas, sólo aquellas formadas a partir de la cadena en condiciones de desnaturalización parcial, ausencia de cofactores y agitación rápida conocidas como fibras tipo R son propagativas *in vivo* [242,252-254]. Estas fibras, preparadas a altas concentraciones de GdnHCl y por lo tanto muy estables, generan núcleos de resistencia proteolítica que incluyen las ocho regiones adhesivas detectadas por ZipperDb ([94]GTHSQW, [113]AGAAAAGAVVGGL, [130]LGSAMS, [170]SNQNNF, [179]CVNITIKQ, [193]TKGENF, [212]QMCITQ y [221]ESQAYY, en la secuencia de HuPrP) [253,255] y estructuras que contienen láminas paralelas β con cadenas en registro [256] (figura 8).Con respecto a la actividad, el uso de diferentes fibras recombinantes ha permitido demostrar la existencia de propagaciones silenciosas que pueden convertirse en patógenas sugiriendo la existencia de procesos de adaptación en los polímeros [83,248,257,258].

4. Modulación de la formación de amiloides

De acuerdo con el modelo estructural de formación de amiloides, la estabilización de una cadena polipeptídica dada en dicho estado depende principalmente de dos factores, los segmentos adhesivos y su activación por exposición. Estas características determinan que la formación de amiloides esté sujeta factores de regulación que impliquen la modulación de la secuencia de los segmentos adhesivos y de la conformación, de forma que los cambios en estos controlen la capacidad o no y la eficacia y condiciones de entono.

4.1.- Factores dependientes de la secuencia: mutaciones y modificaciones covalentes.

Dada la dependencia de la secuencia tanto de las propiedades adhesivas de un segmento como de la estabilidad de una conformación nativa, los cambios genéticos y metabólicos que se traducen en cambios en la secuencia actúan como reguladores potenciales de la formación de amiloides [69,98] .

Así, en el caso de transtirretina (TTR), cuyo tetrámero transporta la hormona tiroidea tiroxina en la sangre y fluido cerebroespinal y su agregación en amiloides extracelulares ocurre en la polineuropatía amiloidotica familiar (FAP) y en la cardiopatía amiloidótica familiar (FAC), se han descrito un número considerable de mutaciones patógenicas. Estas mutaciones causan fallos en el proceso de estabilización del tetrámero, desestabilizaciones de los monómeros e incremento de segmentos adhesivos [149,246,259-265].

En el caso de Aβ, las mutaciones detectadas en el precursor APP, incrementan la producción de segmentos (próximas a la zona de corte de la β-secretasa) o alteran la relación Aβ42/Aβ40 (próximas a la zona de corte de la γ-secretasa) [175]. Además, dentro de la secuencia de Aβ se han descrito las mutaciones conocidas como estirpes Flamenca (A21G) [266]; Ártico (E22G) [267,268], Holandesa (E22Q) [269], Italiana (E22K) [270] y de Iowa (D23N) [271], todas potenciadoras de toxicidad de los agregados [272] (figura 9B) .

Las mutaciones A30P, E46K, H50Q, G51D, A53E, y A53T en la α-sinucleina están ligadas a la aparición de la enfermedad de Parkinson [175]. Estos cambios de secuencia que favorecen los procesos de asociación también suponen distorsiones en su distribución en la célula [273-276] (figura 9C).

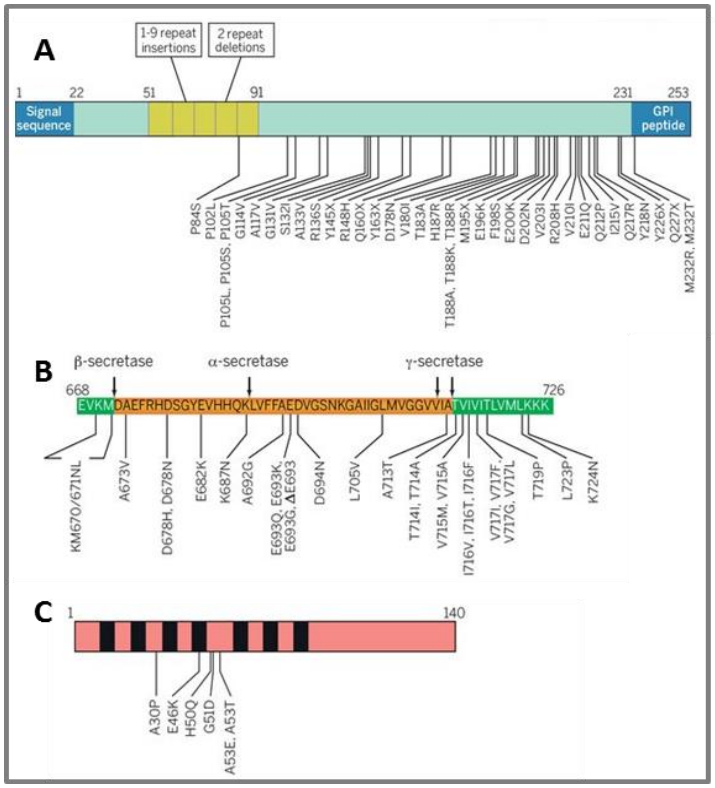

Figura 9.- Mutaciones patogénicas en los genes humanos que codifican (A) PrP, (B) APP y (C) α-sinucleina. (Modificado de Goedert, M. 2015).

En el caso de la lisozima, enzima que degrada los mucopolisacáridos de la pared bacteriana y que en humanos está presente en bazo, hígado , riñón y fluidos tales como plasma, saliva, leche y lágrimas, se han descrito 5 mutaciones patogénicas relacionas con una amiloidosis familiar sistémica no neuropática (I56T, F57I, W64R, D67H, W112R) [277]. Estas mutaciones impactan en el estado nativo estabilizando un estado parcialmente plegado en condiciones fisiológicas con propiedades de fibrilación, y expanden la longitud de la cadena implicada en las fibras [277,278].

En el caso de PrP, se han descrito más de quince mutaciones patogénicas que incluyen modificaciones en el número de repeticiones así como cambios puntuales como P102L, P105L, A117V, G131V, Y145, D178N, F198S, V180N, M232, T183A, E200K, D202N, R208H, V210I, Q217R y M232R/T [172]. Algunas de las mutaciones provocan pequeños cambios de estabilidad en el estado nativo, otras estabilizan formas integradas en membranas y un número considerable distorsiona la cooperatividad intramolecular incrementado directa o indirectamente la reactividad de algunos segmentos adhesivos [279,280] (figura 9A).

Al igual que las mutaciones, las modificaciones covalentes de las cadenas laterales de los aminoácidos pueden incidir y alterar la tendencia intrínseca de un segmento para auto-agregar o provocar cambios conformacionales que promuevan diferencialmente la ruta formación de amiloides. Estas modificaciones covalentes son el resultado de reacciones catalizadas o no enzimáticamente. Dentro de las modificaciones catalizadas enzimáticamente se encuentra la fosforilación y su efecto en la propiedades de agregación de tau [281]. En este caso, el desequilibrio entre los procesos de fosforilación y de desfosforilación conduce a formas de tau hipermodificadas que son inactivas en la función de unión a microtúbulos pero reactivas para agregación. Con respecto a las modificaciones resultantes de reacciones no catalizadas enzimáticamente, varios subproductos derivados del metabolismo del colesterol, de ácidos grasos y de la dopamina con grupos aldehídos y la tilolactona de la homocisteína reaccionan con las cadenas laterales de lisinas favoreciendo la amiloidosis de los péptidos Aβ, α-sinucleína y mioglobina [282-284]. Del mismo modo, las reacciones de Maillard con azúcares reductores y el ataque por las especies reactivas de oxígenos provocan cambios que generalmente promueven reacciones de amiloidogenésis [285-287].

Un tipo de modificación particular, es la oxidación de las cadenas laterales de metioninas catalizada por especies reactivas de oxígeno y reparada enzimáticamente [288,289]. La cadena lateral hidrofóbica de la Met es sensible a la oxidación química, dando lugar a la forma sulfoxidada hidrofílica (MSO), que puede oxidarse en un segundo paso a la sulfona correspondiente [290] (MSO_2) [291]. La reacción de sulfoxidación no es única, sino que conduce a dos isómeros R-sulfóxido o S-sulfóxido, y es reparada por los sistemas enzimáticos MsrA, específico para la reducción de los isómeros S [292-294], y MsrB, para los isómeros R [292,294,295]. Por el contrario, la oxidación de MSO en MSO_2 es irreversible y, aunque rara vez tiene lugar en sistemas biológicos, ésta se ha descrito en el caso de las M17 y M133 de DJ1 en pacientes con la enfermedad de Parkinson [296]. Las reacciones de sulfoxidación en general conllevan cambios de polaridad que se traducen en transiciones conformacionales [297,298]. En el caso de PrP, la sulfoxidación de las M menos expuestas al solvente (M205, M206 y M213) desestabilizada el plegamiento α y permite la ruta que conduce al estado amiloide [289,299-301]. Por otra parte, la sulfoxidación de M213 durante la biosíntesis impide la formación del puente disulfuro y la generación de oligómeros citotóxicos [302]. Del mismo modo, la oxidación de metioninas en Sup35 constituye el disparo conformacional para la formación de la forma prion [303,304].

4.2.- Factores dependientes de la conformación: ligandos y entornos.

La existencia de múltiples estados estructurales a lo largo del procesos de formación de amiloides cuya estabilización puede depender de la presencia o ausencia de un ligando dado impone otro conjunto de factores reguladores [283,305,306].

Así, la pérdida del grupo hemo de la mioglobina [307], la liberación de la tiroxina en TTR [264], o los cationes Zn^{2+} y Mn^{2+} en la superoxido dismutasa (SOD) [149], conduce a estados con flexibilidad estructural que favorecen la formación de amiloides. Del mismo, la interacción con algunos cationes metálicos como Ca^{2+}, Cu^{2+}, Zn^{2+} y Fe^{3+} favorecen la ruta de formación de amiloides en β-macroglobulina, α-sinucleina, Aβ y S100A8/A9 [250,262,265,283,308-311]. Otro grupo de ligandos reguladores de la formación de amiloides son los polianiones entre los que se encuentran polímeros como ácidos nucleicos y glucosaminoglicanos, y los ensamblajes formados por fosfolípidos ácidos. En el caso, los polianiones favorecen la adquisición de propiedades adhesivas, el proceso de nucleación o estabilizan el estado amiloide [266,267,283,312].

Dentro de los cambios de entorno drásticos que favorecen la formación de amiloides, se encuentra el definido por pH ácido en el cual se estabilizas estados no nativos. Así, las cadenas de PrP, ovoalbúmina, mioglobina, y lisozima, entre muchas otras, en medios a pH 1-2 se estabilizan en el estado amiloide [27,52,281,313-315]. Estas condiciones proamiloides han sido consideradas como entornos modelo para estudios biofísicos, alejados de la realidad. Sin embargo, existe un proceso fisiológico en el cual las proteínas son sometidas a cambios de pH desde 7 a 1.2 y luego a 7, y es el tránsito gastrointestinal de las proteínas contenidas en los alimentos.

4.3.- β-Parvalbúminas de pescado

La β-parvalbúmina es el alérgeno de tipo I dominante en la alergia alimentaria al pescado, reacción de hipersensibilidad mediada por IgE [316-322]. Estructuralmente, las β-parvalbúminas están constituidas por una única cadena de unos 110 aminoácidos en la que están presentes tres motivos de mano EF (hélice-loop-hélice) de unión de Ca^{2+} (figura 10). De estos motivos denominados AB, CD y EF, solo CD y EF son funcionales en la unión del catión. La forma unida a Ca^{2+} adopta un plegamiento helicoidal muy estable, que determina que la función alergénica resista los procesos de cocinado[319,323,324]. Por el contrario, la forma apo es estructuralmente más flexible y por ello más labil , y su estabilización parece reducir la capacidad de interacción con IgE de suero de pacientes alérgicos a pescado en magnitudes dependientes de la fuente de la secuencia [325-329].

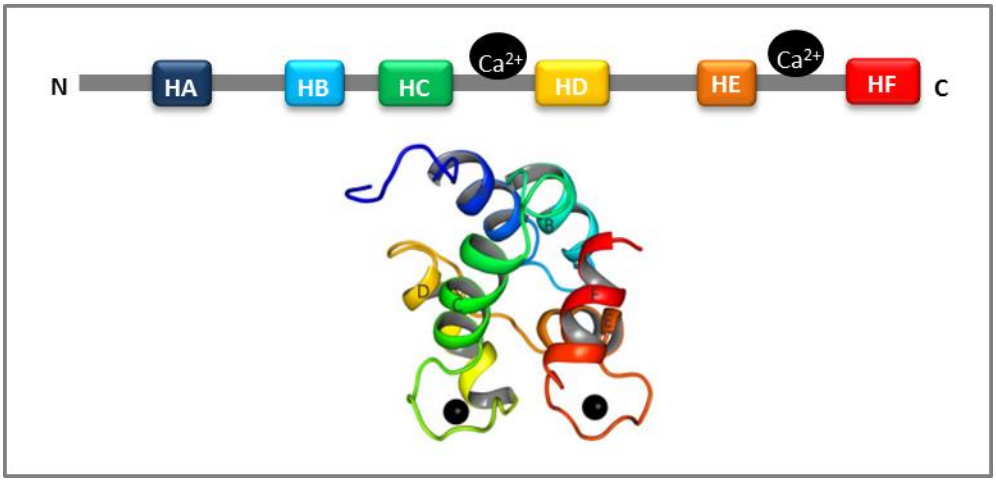

Figura 10.- Organización de la cadena polipeptídica de Gad m 1 y estructura. La cadena de Gad m 1, β-parvalbúmina de bacalo antlántico con propiedades alergénicas, consta de 110 aminoácidos que generan tres dominios de manos EF que corresponden a los motivos hélice loop-hélice (AB, CD y EF). De éstos sólo CD y EF unen calcio (bolas negras), generando un plegamiento todo α (Moraes et al. 2014 Proteins).

II. Objetivos

Si bien los amiloides y su formación han alcanzado ya los niveles de estado funcional y de transición conformacional general a muchas proteínas, todavía existen numerosas lagunas en el conocimiento de la naturaleza y características de sus procesos reguladores. Con el fín de contribuir al conocimiento de estos, en este trabajo se plantearon los siguientes objetivos:

1. Determinar y caracterizar el impacto de la sustitución Met por SeMet en la formación de amiloides en secuencias proamiloidogénicas con uno (Aβ40, M35) o varios (HuPrP106-140, M109,M112, M129 y M134) residuos.

2. Determinar el papel de la estructura de la carga de la molécula de PrP en la formación y propiedades del estado amiloide.

3. Determinar la posible relevancia del estado amiloide en los cambios de entorno asociados al proceso de digestión de alérgenos alimentarios de tipo I, modelizados con Gad m 1, y en su actividad alergénica, medida como la interacción con IgE de sueros de pacientes.

III. Resultados

Objetivo I. La incorporación de selenometionina en secuencias proamiloidogénicas regula su ensamblaje y toxicidad.

ANTECEDENTES: La estabilización del estado amiloide depende esencialmente de la existencia de segmentos adhesivos cuyas propiedades para ensamblarse en cremalleras estéricas son función de su secuencia y la de sus flancos [56,69]. De todos los residuos contenidos en estos segmentos, la Met es un caso particular debido a la capacidad de su cadena lateral para existir bajo estados reducido y oxidados (reversible como sulfóxido, irreversible como sulfona) [290]. Además, la incorporación de Met en proteínas en humanos, para los cuales su fuente es la dieta por ser un aminoácido esencial, compite con SeMet, también esencial [330-332]. La sustitución de un átomo de S por uno de Se introduce diferencias estéricas, de polaridad y de reactividad (susceptibilidad a la oxidación) [272,333,334].

OBJETIVO: Determinar el efecto de la sustitución de Met por SeM en el ensamblaje de secuencias proamiloidógenicas como son los fragmentos Aβ40 y PrP106-140, que con uno y varios residuos de Met, forman parte de las placas de amiloides en la enfermedad de Alzheimer y el síndrome de Gerstmann-Straussler-Scheinker, respectivamente.

METODOS: Las secuencias [M^{35}]Aβ40, [SeM^{35}]Aβ40, [SeM^{109}]HuPrP106-140, [SeM^{112}]HuPrP106-140, [SeM^{129}]HuPrP106-140, [SeM^{134}]HuPrP106-140, V-HuPrP106-140 y M-HuPrP106-140, fueron sintetizadas empleando métodos optimizados de fase sólida. La capacidad para formar amiloides y la naturaleza de los productos de las reacciones de ensamblaje se analizaron empleando ensayos cinéticos de unión de ThT, de solubilización (PAGE-SDS), dicroísmo circular y microscopía de fuerzas (AFM). La funcionalidad de los amiloides se evaluó como citotoxicidad empleando cultivos primarios de neuronas hipotalámicas embrionarias.

RESULTADOS: La caracterización del proceso de ensamblaje de los distintos péptidos puso de manifiesto que las sustituciones SeM^{35} en Aβ40 y SeM^{129} en HuPrP106-140 impiden la formación del estado amiloide, conduciendo a estados oligoméricos amorfos y con una citotoxicidad atenuada frente a las secuencias con M. El poder inhibidor de ambas sustituciones, SeM^{35} en Aβ40 y SeM^{129} en HuPrP106-40, se demostró también en ensayos de reacción conteniendo un exceso de las secuencias equivalentes con M o V indicando la existencia de especies mixtas. Por el contrario en HuPrP106-140, la presencia de SeM en las posiciones 109 o 112 acelera la reacción de polimerización con respecto al péptido control M-HuPrP y modula la forma del producto, mientras que la sustitución en 134 resta eficiencia al rendimiento.

CONCLUSIONES: Los efectos de la sustitución Met por SeM en secuencias proamiloidogénicas es un elemento regulador de las propiedades de ensamblaje, pudiendo desde inhibir hasta acelerar el proceso como alterar la forma del producto. Todos estos efectos reguladores, que ocurren con especificidad de sitio, podrían ser relevantes en los efectos de la dieta y en el origen de las cepas o strains.

Contribución: diseño, ejecución y análisis de los ensayos de unión de ThT, y experimentos de caracterización mediante CD, SDS-PAGE y AFM.

PLOS | ONE

Selenomethionine Incorporation into Amyloid Sequences Regulates Fibrillogenesis and Toxicity

Javier Martínez[1], Silvia Lisa[1], Rosa Sánchez[1], Wioleta Kowalczyk[2], Esther Zurita[3], Meritxell Teixidó[3], Ernest Giralt[3,4], David Andreu[2], Jesús Avila[5], María Gasset[1]*

[1]Instituto de Química-Física Rocasolano, Consejo Superior de Investigaciones Científicas, Madrid, Spain, [2]Department of Experimental and Health Sciences, Pompeu Fabra University, Barcelona Biomedical Research Park, Barcelona, Spain, [3]Institute for Research in Biomedicine, Barcelona, Spain, [4]Department of Organic Chemistry, University of Barcelona, Barcelona, Spain, [5]Centro de Biología Molecular Severo Ochoa, Consejo Superior de Investigaciones Científicas-Universidad Autónoma de Madrid, Madrid, Spain.

Citation: Martínez J, Lisa S, Sánchez R, Kowalczyk W, Zurita E, et al. (2011) Selenomethionine Incorporation into Amyloid Sequences Regulates Fibrillogenesis and Toxicity. PLoS ONE 6(11): e27999. doi:10.1371/journal.pone.0027999

Editor: Andrew Francis Hill, University of Melbourne, Australia

Received July 13, 2011; Accepted October 30, 2011; Published November 22, 2011

Competing Interests: The authors have declared that no competing interests exist.

Abstract

Background: The capacity of a polypeptide chain to engage in an amyloid formation process and cause a conformational disease is contained in its sequence. Some of the sequences undergoing fibrillation contain critical methionine (Met) residues which in vivo can be synthetically substituted by selenomethionine (SeM) and alter their properties.

Methodology/Principal Findings: Using peptide synthesis, biophysical techniques and cell viability determinations we have studied the effect of the substitution of methionine (Met) by selenomethionine (SeM) on the fibrillogenesis and toxic properties of Ab40 and HuPrP(106–140). We have found that the effects display site-specificity and vary from inhibition of fibrillation and decreased toxicity ([SeM35]Ab40, [SeM129]HuPrP(106–140) and [SeM134]HuPrP(106–140)), retarded assembly, modulation of polymer shape and retention of toxicity ([SeM112]HuPrP(106–140) to absence of effects ([SeM109]HuPrP(106–140)).

Conclusions/Significance: This work provides direct evidence that the substitution of Met by SeM in proamyloid sequences has a major impact on their self-assembly and toxic properties, suggesting that the SeM pool can play a major role in dictating the allowance and efficiency of a polypeptide chain to undergo toxic polymerization.

Introduction

Protein conformational diseases share the occurrence of a basic misfolding event that leads to the accumulation of proteins or fragments thereof as distinct oligomeric self-assemblies with gained toxic functions [1–3]. Among the various assemblies, amyloids refer to highly ordered cross β-sheet fibrillar aggregates resulting from tight interfacing of complementary β-sheets [4–7]. Despite the regulation by covalent modifications such as proteolytic cleavage, glycosilation and oxidation, among others, the gross information dictating the capacity of a polypeptide chain to form an amyloid is contained in its sequence [4,5,8]. Therefore, deciphering the rules for modulating these sequences, their conformation and their self-assembly preferences is fundamental for the design of preventive therapies.

Among the different strategies for modifying protein sequences, the replacement of Met residues by SeM is unique in that it occurs in the absence of changes at the nucleic acid level [9,10]. Like Met, SeM is an essential amino acid for humans and its availability is strictly related to diet [9,11,12]. SeM incorporates non-specifically into proteins in competition with Met [12]. As an organic part of the Se pool, the reduction of its levels has been correlated with an enhanced risk of aging disorders [13–15]. In principle, Met substitution by SeM is regarded as a structurally inert change that is exploited for the phasing of macromolecular structures in X-ray crystallography [10]. However, some reports indicate changes in the stability of proteins due to the increased hydrophobicity and distinct oxidation susceptibility of SeM compared to Met [16–21]. Thus, changes in the Met/SeM ratio can be considered as a source of transient, metabolic or non-coded mutations and their effect on proteins may vary as a function of residue location.

Of the various amyloid-forming sequences, the amyloid β peptides (Aβ40 and Aβ42) and the PrP(106–140) region are essential components of protein deposits in degenerative dementias and share the presence of regulatory Met residues [22–32]. Aβ40 and Aβ42, produced by sequential proteolytic cleavage of the amyloid β-protein precursor (APP) by β- and γ-secretase, accumulate both as extracellular amyloid deposits and synaptic oligomers in Alzheimer disease (AD) [27]. In both Aβ peptides, Met35, through the oxidation of its side chain, modulates the oligomerization kinetics, the shape of the final polymer (oligomer vs amyloid fibril) and the neurotoxic function [26,33–37]. In prion protein amyloidoses such as Gerstmann-Straussler-Scheinker syndrome and cerebral amyloid angiopathy, fragments overlapping the 106–140 region of the cellular prion protein (PrP^{C}) form the specific amyloid deposits [23,29,38]. This sequence (HuPrP) contains four Met residues (Met^{109}, Met^{112}, Met^{129}, Met^{134}) flanking either side of the palindromic AGAAAAGA region essential for assembly [38]. Of those, Met^{109} and Met^{112} are not conserved in mammalian PrP sequences and their mutation to Val does not impede fibrillation while it regulates the processing at the α-cleavage site [29,30,39]. On the other hand Met^{129} and Met^{132} are polymorphic positions in human and deer, respectively, and their substitution by Val or Leu regulates the disease phenotype and the ability to recognize and amplify exogenous prions [22,28,29,32,40].

To establish the role of Se intake as related to its specific incorporation as SeM into amyloid forming sequences, we have synthesized Aβ40 and HuPrP(106–140) sequences containing SeM as a replacement for Met. In contrast to the single Met^{35} substitution in Aβ40, the presence of

four methionines in HuPrP(106–140) allows to investigate the role of the replacement site on fibril formation. Herein we show that the substitution of Met by SeM in Aβ40 and HuPrP(106–140) regulates both amyloid formation and toxicity. For HuPrP(106–140), the inhibitory effect displays site-specificity, with the activity varying from inhibition of fibrillation and decrease in toxicity ([SeM^{35}]Aβ40 and [SeM^{129}]- HuPrP(106–140)) to accelerated fibrillation and modulation of the polymer shape with retention of toxicity ([SeM^{109}]HuPrP(106–140) and [SeM^{112}]HuPrP(106–140)).

Results

SeM incorporation to amyloid sequences. Figure 1 shows the sequences of Aβ40 and HuPrP(106–140), both with amyloid-forming capacity and with one or more Met residues with relevant roles [27,29]. The single methionine (Met^{35}) in Aβ40 allowed an unambiguous SeM replacement, while the four (Met^{109}, Met^{112}, Met^{129}, Met^{134}) in HuPrP(106–140) required a more extensive investigation of the site-specificity of SeM replacement. Hence, the wt HuPrP(106–140) sequence with four SeM residues (all-M), a non-oxidizable variant sequence (all-V) with all four Met residues mutated to Val, plus four analogs with single SeM replacements at either position 109, 112, 129 or 134, and Val at the other positions, were prepared. While all seven peptide sequences are of a size generally regarded as viable for solid phase synthesis methodologies, their well-known tendency to aggregate clearly placed them in the ''synthetically difficult'' category [41]. This fact, plus the need for cost-effective handling of the high-priced Fmoc-SeM building block, called for highly optimized, state of the art synthetic strategies. Thus, for [SeM^{35}]Aβ40, the O-acyl isopeptide approach [42] to difficult sequences was applied, whereby a soluble precursor, 26-O-isoacyl- [SeM^{35}]Aβ(1–40), was prepared and purified to near-homogeneity, then incubated at pH 7.4 to give the target peptide in precipitate form. For its part, [SeM^{109,112,129,134}]HuPrP(106–140) (all-M), its all-Val counterpart and the four site-specifically SeM- substituted analogs were efficiently assembled by microwaveassisted solid phase synthesis on ChemMatrixH, a resin proven successful in preventing aggregation during the synthesis of large, complex peptides [43]. Peptides were successfully purified from the crude material and their identity and homogeneity confirmed by mass spectrometry [44]. Full details on the synthesis, purification and analytical documentation of all peptides are given in the **Supporting Information S1** file.

PEPTIDE	SEQUENCE
Aβ 40 M35	DAEFRHDSGY EVHHQKLVFF AEDVGSNKGA IIGL MVGGVV
Aβ 40 SeM35	DAEFRHDSGY EVHHQKLVFF AEDVGSNKGA IIGLSeMVGGVV
Aβ 42 M35	DAEFRHDSGY EVHHQKLVFF AEDVGSNKGA IIGL MVGGVVIA
PrP M	KTNMKHM AGAAAAGAVVGGLGGY MLGSA MSRPIIH
PrP V	KTNVKHV AGAAAAGAVVGGLGGY VLGSA VSRPIIH
PrPSeM109	KTNSeMKHV AGAAAAGAVVGGLGGY VLGSA VSRPIIH
PrPSeM112	KTNVKHSeM AGAAAAGAVVGGLGGY VLGSA VSRPIIH
PrPSeM129	KTNVKHV AGAAAAGAVVGGLGGY SeMLGSA VSRPIIH
PrPSeM134	KTNVKHV AGAAAAGAVVGGLGGY VLGSASeMSRPIIH

Figure 1. Proamyloid sequences used as templates for the substitution of Met by SeM. Residues are depicted following one-letter code except for selenomethionine that is abbreviated as SeM.

SeM^{35} impedes Aβ40 fibrillation. To investigate the ability of SeM to modify the aggregation properties of Ab40 we set up a ThT binding kinetics assay. To this end, either wt Aβ40 (Met^{35}) or [SeM^{35}]Aβ40 were incubated at 20–40 mM concentration in PBS in the presence of 15 µM ThT and the increase in fluorescence emission as consequence of its binding to cross β-sheets was monitored (see methods). **Figure 2A** shows that wt Aβ40 at 20 µM and 30°C provokes a time-dependent increase in ThT fluorescence compatible with the known fibrillation process [45]. Importantly, the kinetic trace was reproducible in independent experiments with different batches, with an average lag-phase of 13±2 h. In contrast, incubation of [SeM^{35}]Aβ40 under similar conditions did not cause any detectable change in ThT fluorescence. Increasing [SeM^{35}]Aβ40 concentration up to 200 µM and the incubation time up to 1 week did not provoke any significant or additional change. These results suggest that the substitution of Met by SeM has a clear deleterious impact on amyloid formation.

To confirm the previous findings we analyzed the reaction products by Atomic Force Microscopy (AFM). **Figure 2C** shows that, as expected from the ThT fluorescence readings, Aβ40 assembles into long (>200 nm length) and thin (7 nm height and about 2x40 nm diameter) fibrils that appear decorated by globular particles of about 4 nm in height and 40–80 nm in diameter [**Figure 2C insert**].

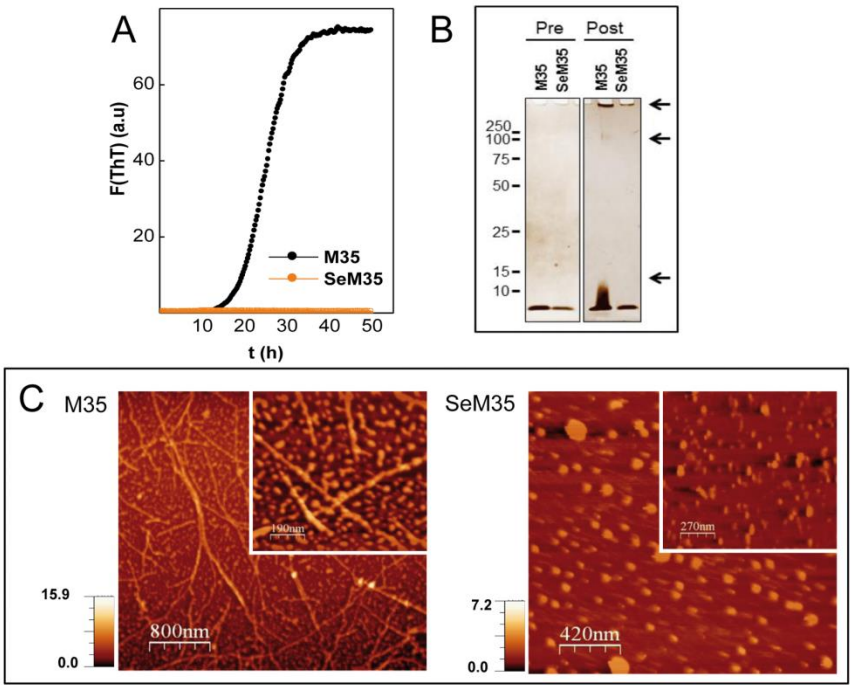

Figure 2. Effect of the incorporation of SeM on the Ab40 amyloid formation. (A) Fibrillation kinetics followed by ThT binding. The displayed curves were obtained by continuous incubation of 20 µM peptide solutions in PBS containing 15 µM ThT at 30°C run in triplicate, and represent the average of three independent experiments. (B) Representative silver-stained SDS-PAGE gel of [Met^{35}]Aβ40 and [SeM^{35}]Aβ40 before (pre) and after 80 h (post) of incubation under aggregating conditions. Arrows indicate the distinct oligomers. (C) AFM topography imaging of the aggregation reaction products of [Met^{35}]Aβ40 and [SeM^{35}]Aβ40 after 80 h of incubation. Inserts displayed the magnification of a representative area of each case.

In contrast, [SeM^{35}]Aβ40 uniquely yields globular aggregates characterized by 3.5–7 nm height and 35 nm average diameter, corroborating the impair- ment of the fibrillation process. On

the other hand, [SeM^{35}]Aβ40 aggregates yielded electrophoretic patterns different from those of toxic Aβ40 oligomers [**Figure 2B**] [46].

SeM effect on fibrillation displays site-specificity. To ascertain whether the previous findings are uniquely related to the Aβ40 sequence and the essential role played by Met^{35}, or can take place also in other sequences, we analyzed the effect of this substitution on the fibrillation properties of HuPrP(106–140). In this case, given the presence of four Met residues and the possible interference of undesired oxidations in long time incubations, we investigated a non-oxidizable version (all-V, all four Met replaced by Val), as well as single SeM replacements with Val at the other positions [**Figure 1**].

Figure 3A shows that, at 30°C, 20 μM concentration in PBS and with mild orbital shaking, both all-M and all-V HuPrP(106– 140) undergo fibrillation, though with notable kinetic differences. Thus, all-M HuPrP(106–140) exhibits the kinetic profile of a highly cooperative process, characterized by an average lag time of 33.8±2.0 h and a final arbitrary ThT fluorescence intensity of 60±5, whereas fibrillation of the all-V variant is characterized by a lag-phase of about 16.4±2.0 h and a final ThT intensity reading of 40±4 [**Figures 3A and 3B**]. These differences found here for the (106–140) sequence regions agree with previous findings reporting the faster polymerization of [Val^{129}]PrP compared to [Met^{129}]PrP and the higher propensity of [Met^{129}]PrP(109–135) over its Val^{129} variant to form β-sheet stabilized fibers [40,47]. Placing SeM at position 109 slightly reduces both the lag phase and the final ThT intensity of the fibrillation kinetics. However, the absence of a clear statistical significance in these changes suggests that SeM^{109} behaves as an all-Val variant. On the contrary, placing SeM at position 112 significantly increases the lag time to 19.7±1.2 h with no effects in the maximum ThT intensity. Surprisingly, the introduction of SeM at position 129 drastically impairs the fibrillation process. Prolonged incubations (up to 1 week) yielded ThT intensity increases below 2.5 with averaged lag phases of >72 h. Along similar lines but to a lesser extent, placing SeM at position 134 allowed a slight fibrillation process featured by a final ThT intensity of 8 and a lag time of 31.5±2.0 h.

To confirm these findings we analyzed by AFM the products of the aggregation reactions [**Figure 3C**]. In agreement with the ThT kinetics, the all-M, all-V, SeM^{109} and SeM^{112} versions of HuPrP(106–140) yielded fibrillar structures, of which those formed by SeM^{112} differed notably from the others by appearing as regular straight rods with a high homogeneity in length. On the contrary, the reaction product of the SeM^{129} analog yielded mainly amorphous aggregates with rarely the presence of fibrillar aggregates. The SeM^{134} peptide displayed an intermediate behaviour, showing few but detectable fibrillar assemblies. The aggregation profile was also studied by SDS-PAGE. **Figure 4A** shows that on aggregation all-M, all-V, SeM^{109} and SeM^{112} versions of PrP(106–140) yielded bands of SDS-resistant aggregated species, whereas SeM^{129} and SeM^{134} ran mainly as monomers.

Taken together these data indicate that, as for the case of Aβ40, SeM incorporation also impairs HuPrP(106–140) fibrillation, but in this case the inhibitory process is highly dependent on the replacement site, with position 129 and to a lesser extent 134 being essential in this respect.

SeM modulates fibril shape. As noted above, [SeM^{112}]HuPrP(106–140) forms fibrillar aggregates that differ notably from those obtained from all-M, all-V and SeM109 peptides. To gain an insight on the basis of this polymorphism, the fibrils were isolated from the aggregation reactions by centrifugation and, after resuspension, were characterized for their ThT binding on fibril molar basis and by far-UV CD for comparison with previous reports [48]. It must be noted that SeM^{129} and SeM^{134} peptides were not considered in this study given their failure to form fibrils with minimal efficiency.

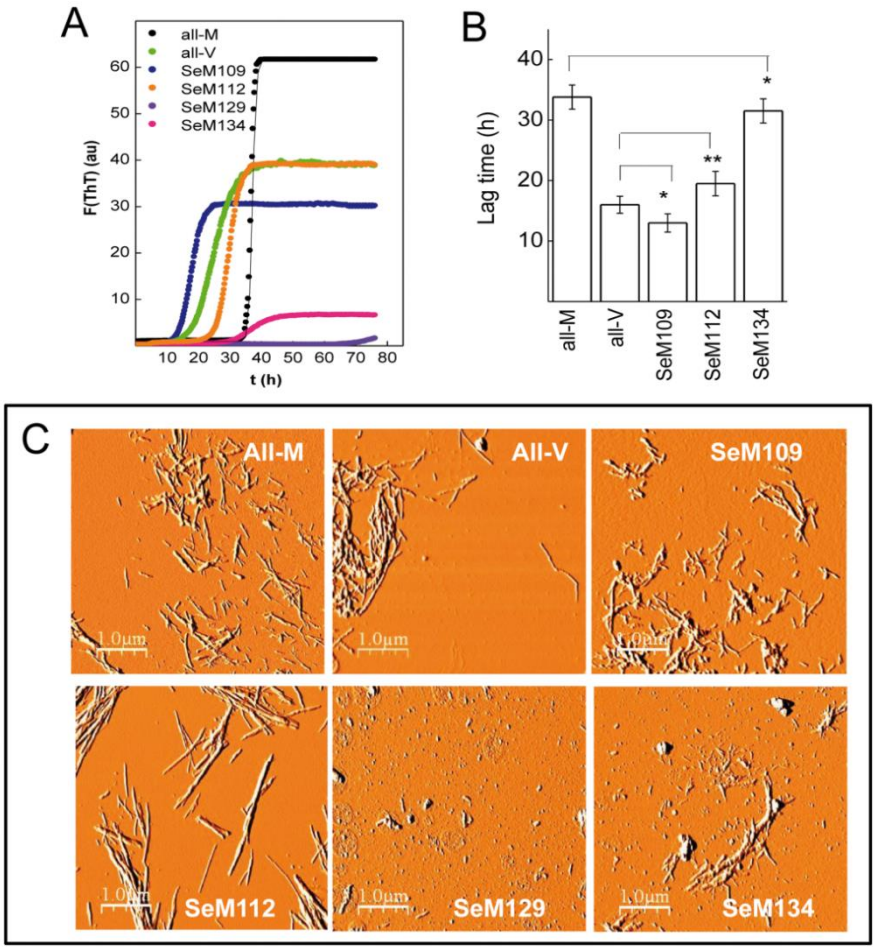

Figure 3. Effect of the incorporation of SeM in HuPrP(106–140) on its amyloid formation. (A) Representative fibrillation kinetics of HuPrP(106–140) sequences followed by ThT binding. The color code of the traces is depicted as an insert in each panel. The displayed curves were obtained by continuous incubation of 20 µM peptide solutions in PBS containing 15 µM ThT at 30°C run in triplicate, and represent the average of three independent experiments. (B) Lag times of the fibrillation kinetics of HuPrP(106–140) and of its variants. Lag times were calculated independently from each curve and analyzed statistically using the Student's t-test tool provided by Origin 6 software: *, non-significant; **, $P \prec 0.05$. (C) Phase images of the molecular species formed after 80 h incubation of HuPrP(106–140) sequences. The displayed fields for all-V, all-M, SeM^{109} and SeM^{112} sequences represent most frequent areas (9 out 10 analyzed 1 µm x 1 µm regions). For SeM^{129} and SeM^{134} the displayed fields represent the minor hits (1 out of 20 analyzed 1 µm x 1 µm regions).

Figure 4B shows that the fibrillar aggregates of all-M, all-V, SeM^{109} and SeM^{112} recovered by centrifugation from the aggregation reactions and resuspended to similar molar concentration yield similar ThT intensity, and the minor variations are not statistically significant. Figure 4C shows that the all-M, all-V and SeM^{109} peptides shared a common spectrum, featured by a double minimum at

208 and 220 nm suggesting an altered β-sheet structure. On the contrary, the spectrum of the SeM^{112} analog displayed the features of a pure β-sheet structure. The results thus support that, depending on its incorporation site, SeM can modulate the secondary structure and subsequently sculpture its self-assembly shape.

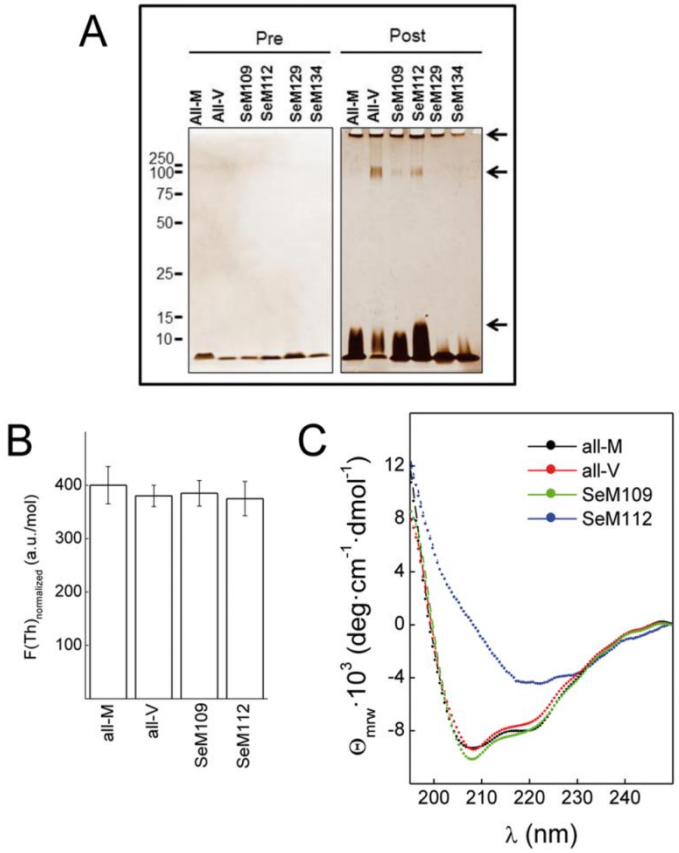

Figure 4. Aggregation profiles of HuPrP(106–140) sequence variants. (A) Typical aggregation pattern of HuPrP(106–140) and of its variants probed by silver-stained SDS-PAGE. Peptide aliquots (1 mg) before (pre) and after 80 h (post) of aggregation were separated in TGX-Precast BioRad gels and then silver stained. (B) Normalized ThT binding of the insoluble aggregates formed by HuPrP(106–140) peptides. Aggregated peptides were isolated as insoluble pellets of 30 min centrifugations at 15000 rpm, resuspended in PBS at 60 μM concentration. ThT binding of the resuspended aggregates was measured by fluorescence at 20 μM peptide and 15 μM ThT concentrations. (C) Far-UV CD spectral features of the insoluble aggregates formed by HuPrP(106–140) peptides. Insoluble pellets were prepared as in panel B in PBS and the spectra recorded at 60 μM. At least three separate experiments were performed to confirm these results.

Interestingly, these distinct spectral features have been previ- ously reported for the R- and S-fibrils formed by the full length PrP resulting from the aggregation using two different conditions [48]. In fact the morphological and spectral features herein found for the aggregates formed by the SeM^{112} analog resemble those described for S-fibrils, which can be formed with the HaPrP but not with the MoPrP [48,49]. Similarly, the features of the fibrils formed by the all-M, all-V and SeM^{109} peptides resemble the properties described for the R-fibrils which can be formed by both HaPrP and MoPrP [48,49]. Among other sequence differences, HaPrP and MoPrP differ in the residue at position 112, Met in HaPrP and Val in MoPrP. Since Met though not Val can be metabolically replaced by SeM, it is tempting to speculate that the formation of S-fibrils could be dictated at least

in part by the presence of chains containing SeM in position 112, which can uniquely occur with HaPrP, not with MoPrP.

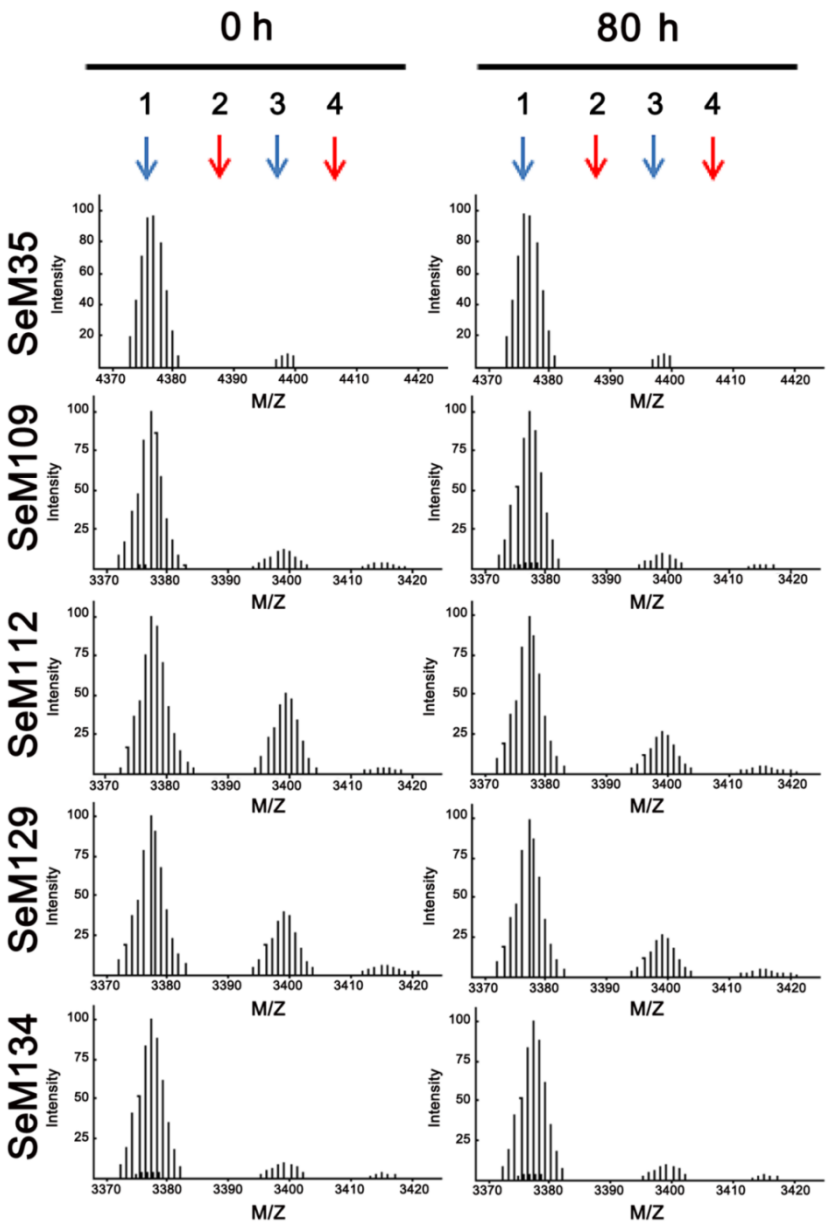

Figure 5. MALDI FT-ICR profiles of SeM-containing Aβ40 and HuPrP(106–140) peptides. Representative m/z patterns of the distinct peptides after 80 h of incubation under aggregating conditions. Measurements were performed using samples of at least two separate experiments. Arrows indicate the theoretical positions for the m/z values of: 1) +1, 2) +16 (selenoxide), 3) +23 (Na+-adduct) and 4) +32 (selenone). For SeM^{35} the values are: 4376.1, 4381.1, 4388.1, 4408.1. For SeM analogs of HuPrP(106–140) the values are: 3377.2, 3393.2, 3399.2, 3409,2. The peak complexity arises from the Se isotopic distribution [20].

SeM effects on fibrillation are unrelated to oxidation. As with Met, the SeM side chain can undergo oxidation to selenoxide and selenone, and if so could drastically modify the process of amyloid formation [26,33–37]. To investigate whether the observed differences in fibrillation were related to SeM oxidation we analyzed by MALDI FT-ICR the peptides before and after the aggregation reaction. In all cases, m/z patterns of pre-aggregated and post-aggregated samples were

superimposable and peaks reproduced the theoretical predicted charged masses [**Figure 5, Supporting Information**]. Importantly, no peaks at +16/+32 Da expected for the oxidized variants were detected [**Figure 5**]. Despite the non-quantitative nature of the mass spectrometry method, it plausible discards that undesired side chain oxidations play a role in the amyloid formation traits.

SeM containing sequences also function as exogenous fibrillation regulators. Consistent with the previous findings and with the fact that Met substitution by SeM would be hardly ever quantitative under physiological conditions, we next tested the capacity of the SeM- containing sequences to modulate the amyloid formation process of the unlabelled sequences. As amyloid formation can be essentially view as a seeded-polymerization in which nucleation, elongation and polymer fragmentation are critical steps, the SeM effects could also provide mechanistic information [1–7]. The results are shown in **Figure 6**.

Co-incubation of [SeM^{35}]Aβ40 with Aβ40 and with its longer and more fibrillogenic form Aβ42 impaired their fibrillation process [**Figure 6A**]. These impairments could not be attributed to dilution since, in the absence of [SeM^{35}]Aβ40 and at equal concentration, both Aβ40 and Aβ42 undergo fibrillation. Rather, the results agreed with an inhibition process and suggested that [SeM^{35}]Aβ40 interacts with Met^{35}-bearing peptides, and halts their productive aggregation through the formation of growth-impaired oligomers.

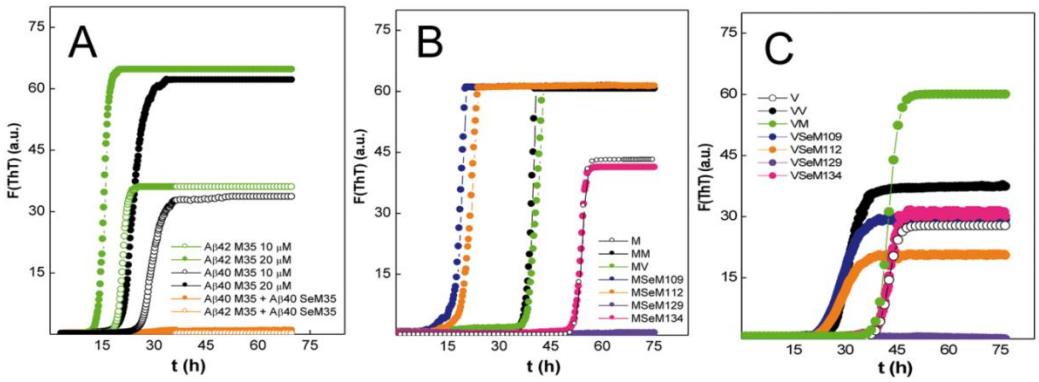

Figure 6. Analysis of the regulatory cross-talk between SeM-tagged and wt sequences. (A) ThT binding kinetics of Aβ40 and Aβ42 in the absence (10 and 20 μM) and presence of [SeM^{35}]Ab40 (10 μM of each peptide). (B) Time evolution of the ThT binding of mixtures of 10 μM all-M HuPrP(106–126) in the absence and presence of 10 μM of HuPrP(106–126) sequence variants. (C) ThT binding kinetics of mixtures of 10 μM all-M HuPrP(106–126) in the absence and presence of 10 μM of HuPrP 106–126 sequence variants. The color code of the different traces is indicated at the right hand side of each panel. The displayed curves were obtained by continuous incubation of the different peptide solutions in PBS containing 15 μM ThT at 30°C in duplicate, and represent the average of three independent experiments.

Similarly, in the HuPrP(106–140) case, co-incubation of 10 μM SeM^{129} analog with 10 μM of either all-M [**Figure 6B**] or all-V [**Figure 6C**] peptides inhibited amyloid formation. Again, such inhibitions could not be attributed to dilution effects, since the latter peptides, at 10 μM and in the absence of the SeM^{129} analog, yielded ThT binding kinetics compatible with fibrillation reactions. Hence, the inhibition trend suggests that [SeM^{129}]HuPrP(106–140), acting like a quencher, interacts with either all-M or all-V HuPrP(106–140), giving rise to oligoheteromeric species that do not sustain

growth. This data agreed with previous findings indicating the essential role of identity in position 129 for the allowance of formation of a stable steric zipper [50].

On the contrary, [SeM^{134}]HuPrP(106–140), of very low efficiency in fibrillogenesis, when mixed with either all-M or all-V does not alter significantly the ThT binding pattern of the previous peptides [**Figure 6B and 6C**]. These results suggest that SeM^{134} precludes stable interaction and therefore causes its segregation. Since position 134 has not been found to play a fundamental role in amyloid formation, then the segregating behavior seems related to SeM hydrophobic properties and their provoked reactions [5,51,52].

On the other hand, SeM^{109} and SeM^{112} when mixed 1:1 with either all-V or all-M peptides altered the ThT binding kinetics, imposing their characteristic lag-phase and allowing the final ThT intensity of the SeM-free peptide [**Figure 6B and 6C**]. This observation strongly suggests that positions 109 and 112 determine the efficiency of seed formation and therefore the speed of the polymerization reaction [1–7].

SeM-containing sequences can ameliorate toxicity. To investigate the structure–activity relationship of the SeM substitutions we analyzed the effect of the aggregation reaction products on the viability of rodent primary cortical neurons [**Figure 7**]. For this purposes, the different peptides and their combination were incubated for 80 h at 30°C at 0.10–0.15 mM in PBS and then diluted to a final concentration of 10 µM in the cell medium and allowed to incubate for 48 h. Under the assay conditions, all peptides except [SeM^{35}]Aβ40 and the SeM^{129} and SeM^{134}-analogs of HuPrP(106–140) and their mixtures have completed their fibrillation process as judged by parallel ThT reading, and the untreated cells yielded cell viability values that amounted to 97.5±1%.

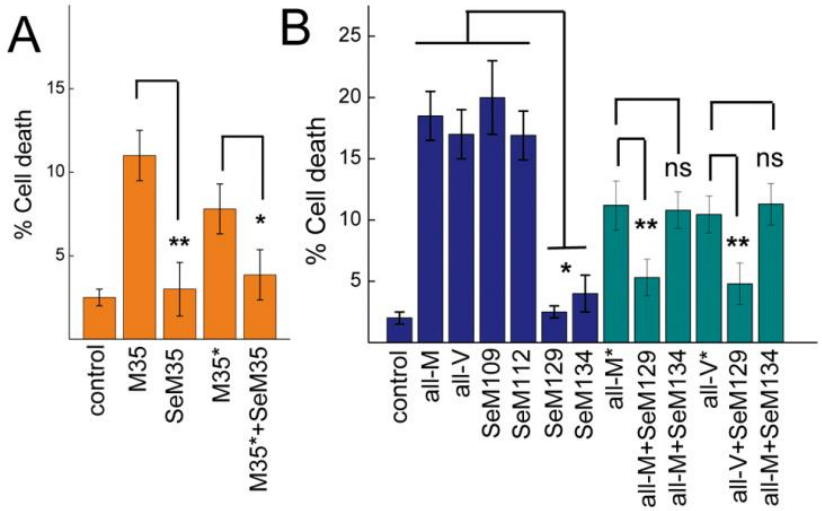

Figure 7. Cytotoxic potential of SeM containing sequences and of their mixtures. Rodent primary cortical neurons were cultured for 7 days on poly-D-lysine-coated coverslips and treated with 10 µM of each peptide or 1:1 molar ratio mixture of peptides for 48 h. The cells were then probed with LIVE/DEAD kit. The percentage of dead cells was obtained dividing the number of dead cells by the total (live and dead) number of cells. The results are the means ± SD of three independent experiments ran in duplicate. Statistical analysis was performed with the Student's *t* test tool of Origin software. ns, non-significant. *, $P < 0.05$;**, $P < 0.005$.

Aβ40 was found to cause 11±1% cell death, in agreement with previous reports [27,37,53]. Interestingly, [SeM^{35}]Aβ40 reduced cell death to 3±1.5%, thereby excluding any relationship between its assemblies and the highly neurotoxic nonfibrillar oligomers formed by Aβ peptides [27]. This reduction pattern was maintained for its 1:1 mixture with Aβ40, which cannot be explained solely on the basis of [Met^{35}]Aβ40 dilution as judged from the concentration control.

As for HuPrP(106–140), the aggregation reaction products of all-M and all-V caused about 20±2% of cell death, in agreement with the toxicity levels described for the polymers formed by HuPrP(82–146) [54]. SeM^{109} and SeM^{112} analogs caused cell death to a similar extent, in agreement with their similar amyloid forming ability at long incubation times [**Figure 3A**]. On the contrary, SeM^{129} and to a lesser extent SeM^{134} caused minor effects on cell viability (1.1±0.5 and 4±0.6, respectively). As in the case of [SeM^{35}]Aβ40, these statistically significant reductions in the extent of cell death compared to that caused by the amyloid-assembled sequences discards active oligomeric species. Moreover, the aggregation products of the all-M and all-V peptides mixed with SeM^{129} and SeM^{134} reproduced the profiles observed in kinetic experiments [**Figure 6B and 6C**]. Mixing SeM^{129} 1:1 with either all-M or all-V decreases cell death extent to almost abrogation, and the effect cannot be explained solely in terms of the reduction all-M and all-V concentration as shown by the concentration controls. On the contrary, mixing the SeM^{134} analog 1:1 with either all-M or all-V reproduces the cell death percentage of diluted all-M and all-V peptides.

Discussion

Unveiling the ways proamyloid sequences can be modulated to impede their productive engagement into self-assembly processes yielding toxic events is essential for designing preventing strategies for conformational diseases. The pioneer study of Goldschmidt et al [5] has solidly established as general principle that the capacity of a protein to form the b-sheet based fibrillar amyloid structures is coded in its sequence, although its display may depend on structural and environmental regulatory factors [55]. One possible modulatory event is that involving metabolic changes of Met and SeM pools and consequently of their competitive incorporation in proteins through the AUG codon. Taking the advantage of synthetic approaches we have substituted Met by SeM in amyloid forming sequences and we have found dramatic effects on their polymerization and toxicity. These effects varied from inhibition ([SeM^{35}]Aβ40 and [SeM^{129}]PrP(106–140)), polymerization kinetics perturbation to polymer shape determination ([SeM^{112}]PrP(106–140)) [**Figure 8**].

Despite the consideration of Met and SeM as structurally equivalent, the change of a sulfur by a selenium atom involves major steric and reactivity differences. Se is slightly larger than S (atomic radius of 1.17 vs 1.04 Å) and has also a larger van der Waals radius (1.90 vs 1.80 Å).Since the spines of amyloid fibrils consist in steric zippers formed by the interdigitation of β-sheets through their side chains, any steric perturbation may lead to clashes which may reduce the stability of this unit or even preclude its formation [5,50]. This might be the case of the fibrillation impairments of [SeM^{35}]Aβ40 and [SeM^{129}]PrP(106–140) peptides, for which the crystal structure of shorter fragments have shown Met^{35} and Met^{129} actively participating in the inter-sheet packing [50,56]. Also, since the interdigitations are not unique but can involve distinct patterns, the side chain size

increase together with its position can dictate the preference for specific stacking patterns over others that as seeds will produce distinct fibril shapes as for SeM[109] and SeM[112] analogs of PrP(106–140) [5,50,56]. The larger size of Se than S also causes SeM to have a larger surface area and hence hydrophobicity than Met. Since amyloid formation is a complex process involving the construction of oligomeric species undergoing growth, fragmentation and quenching or arrest, minor changes in hydrophobicity may trigger significant alterations in the solubility of the distinct oligomeric species as well as in the the features of the interacting surfaces [1–7,50]. For instance, by its increased hydrophobicity SeM can decrease the efficiency of amyloid formation in [SeM[134]]PrP(106–140), which retains the ability to engage in the process but does it with a very low efficiency.

SeM also differs from Met in its side chain oxidation process. SeM can undergo oxidation by peroxynitrites to selenoxide but, unlike the sulfoxide, the selenoxide is easily reduced by organic thiols as glutathione and does not required enzymatic assistance [20,52,57]. Although SeM oxidation is not a major event in our experimental setup, since sulfoxide formation is known to impair fibrillation in Aβ40 and PrP(106–126), the chemical differences of the reaction could add novel regulatory steps to the polymerization [24–26,34,35,58]. To address this possibility, improved basic knowledge is required on reaction conditions and product characterization of SeM oxidation as a part of a protein and free in solution [52,57].

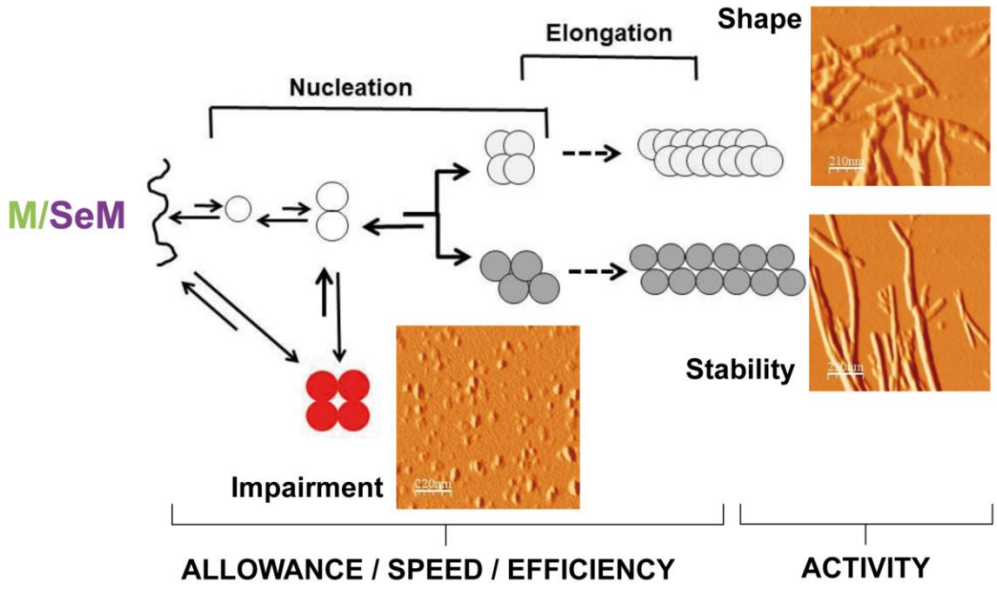

Figure 8. Summary of the effects of SeM introduction in amyloid forming sequences. Replacement of methionine (M) residues by its metabolic competitor selenomethionine (SeM) in proamyloid sequences involves changes in local hydrophobicity and steric factors. With a site-dependence, the replacement can promote side association reaction that either decrease the efficiency and speed or impair amyloid formation. In other cases, by regulating the seed packing can generate distinct fibrilar assemblies.

For Aβ40 the Met35SeM non-coded or metabolic mutation impairs amyloid formation but stabilizes oligomeric assemblies as shown by AFM. Based on shape considerations, the oligomers might be suspected to act as the actual neurotoxins. However, both PAGE-SDS analysis and toxicity evaluation discard such assemblies being deleterious and support the importance of the amyloid

pathway as a source of toxic species. This rationale can be extended to the [SeM^{129}]HuPrP(106–140) analog, which in addition to its impaired fibrillation and lack of toxic activity, prevents the fibrillation and toxicity of all-V and all-M. For these two cases, the incorporation of SeM into an essential position functions as a physiological anti-amyloid metabolic defense. However, the effect of SeM incorporation is not homogeneous. For instance, the SeM^{109} and SeM^{112} analogs of HuPrP(106–140) displayed differences in kinetics and in fibril shape, and such morphological differences can have important functional implica tions [59]. In this sense, fibrils of the SeM^{112} -shape are expected to be more toxic that fibrils with shapes of the SeM^{109}-analog, whereas if fragmented the toxicity profile inverts [59]. In our set up, both assemblies yielded statistical similar toxicity traits suggesting that SeM substitution could also play a role in the in vivo stability (fragmentation or recycling) of the polymers so activity differences in the 48 h assay become averaged. In this line, H/D exchange experiments have shown that isolated fibrils can display significant distinct recycling properties, with changes in fibril dissolution rate constant of about two orders of magnitude (0.6 s^{-1} and 1.0x10^{-2} s^{-1} for Aβ40 and Aβ42, respectively) [60].

As summarized in **Figure 8**, these evidences clearly indicate that SeM incorporation into pro-amyloid sequences results in various effects as a function of its location and suggest that metabolic changes in the Met/SeM pool can exert important modulatory effects in amyloid diseases.

Materials and Methods

Peptides and aggregation reactions. The SeM-substituted versions of Aβ40 and HuPrP(106–140) (**Figure 1A**) were synthesized by solid phase methods, purified by HPLC and characterized by mass spectrometry. Details are given in the **Supporting Information S1** file. For control studies, Aβ40 and Aβ42 were obtained from GenScript. Lyophilized peptide stocks were dissolved in HFIP, aliquoted and dried under N2 for storage at -80°C. Samples were reconstituted in 5 mM NH4OH pH 8.0 at about 2 mg/ml concentration and filtered through 0.2 µm membranes before use. Peptide concentrations were determined by UV spectroscopy and by amino acid analysis. Peptide stock solutions were diluted with PBS at 100–200 µM concentrations and kept at 4°C for less than 30 min. The aggregation reactions were performed both in eppendorf tubes and in wells of a 96-well plate by incubating 20-200 µM peptide monomers in PBS at 30°C with orbital shaking (100 rpm).

Thioflavin T binding kinetics. The kinetics of thioflavin T (ThT) binding was monitored by bottom reading of fluorescence intensity in a POLARstar microplate reader (BMG Labtech) as described [51]. Measurements were performed using 450 nm excitation and 480 nm emission filters, 0.20 ml samples and 15 µM ThT concentration. The measurement program consisted of 10 flashes reading every 10 min with 1-min of orbital 1-mm diameter shaking at 100 rpm with the temperature controller set at 30°C. All measurements were done in triplicate and the experiments were repeated at least twice using two different peptide batches. When required, the lag-phase was determined as described [61].

PAGE analysis. Peptide samples before and after 80 h of aggregation were removed and diluted 1:1 in β-mercaptoethanol-free Laemmli buffer and, omotting the thermal denaturation step, loaded

in BioRad precastTGX-gels. After silver staining, gel images were captured and analyzed using the Molecular Imager ChemiDocTM XRS+ Imaging system and ImageLab 3.0.1 (beta2) software (BioRad).

Mass spectrometry analysis. Aliquots of the peptide solutions before and after aggregation were removed, treated with HFIP for aggregate disruption and analyzed using a-hydroxy-cinnamic acid matrix and a MALDI FT-ICR 930-MS (Varian) instrument operating at 7 T and 10^{-9} Torr and with OMEGA software.

Atomic force microscopy (AFM). Ten ml-samples of peptide solution after 70 h incubation were diluted to 2 µM with ddH2O and applied onto freshly cleaved mica surfaces to adhere for 15 min. After washing with ddH2O, samples were dried with N_2. AFM imaging was then performed using a PicoSPM™ (Molecular Imaging, Phoenix, AZ), operating the AFM scanner in acoustic alternating current mode with Si,N- ACT type cantilevers (ScienTec) with a tip radius <10 nm and a spring constant of 25–75 N/m [51]. The images (1x1 mm scans) were collected at a scan rate of 1 line per second and analyzed using WSxM 5.0 Nanotec software.

Circular dichroism (CD) spectroscopy. CD spectra were recorded in the far-UV region with a Jasco J-810 spectropolarimeter in continuous scan mode (250-190 nm) and a 0.1 cm path length quartz cuvette (Hellma) as described previously [51].

Citotoxicity assays. Mice were obtained from the Centro de Biolog´ıa Molecular and treated following the guidelines of Council of Europe Convention ETS123, recently revised as indicated in the Directive 86/609/EEC. Animal experiments were performed under protocols (P22/ P23) approved by the Centro de Biolog´ıa Molecular Severo Ochoa Institutional Animal Care and Utilization Committee (CEEA- CBM, Madrid, Spain). Primary cortical neurons were obtained from the cerebral cortex of C57B16 E18 rat embryos, by enzymatic dissociation with papain (Worthington Biochemical) in EBSS for 45 min at 37°C. Cells were resuspended in Neurobasal medium with 2% B27, 0.25% 200 mM Gln, 1% Glutamax and 1% penicillin/streptomycin and seeded on cover slips pre-coated with poly-D-Lys (10 µg/ml). Two days later, 5 µM Ara-C was added to the medium. Seven days later, peptides preincubated in PBS were added at a final concentration of25 µM. After 48 h incubation at 37°C, neuronal cell death was determined using the LIVE/DEAD kit (Invitrogen) for mammalian cells. Live cells (stained with calcein-AM) and dead cells (stained with red-fluorescent ethidium homodimer-1) were counted and the percentage of dead cells calculated.

References

1. **Carrell RW, Lomas DA** (1997) Conformational disease. *Lancet* 350: 134–138.
2. **Stefani M, Dobson CM** (2003) Protein aggregation and aggregate toxicity: new insights into protein folding, misfolding diseases and biological evolution. *J Mol Med* 81: 678–699.
3. **Chiti F, Dobson CM** (2006) Protein misfolding, functional amyloid, and human disease. *Annu Rev Biochem* 75: 333–366.
4. **Maji SK, Wang L, Greenwald J, Riek R** (2009) Structure-activity relationship of amyloid fibrils. *FEBS Lett* 583: 2610–217.
5. **Goldschmidt L, Teng PK, Riek R, Eisenberg D** (2010) Identifying the amylome, proteins capable of forming amyloid-like fibrils. *Proc Natl Acad Sci U S A* 107: 3487–3492.
6. **Toyama BH, Weissman JS** (2010) Amyloid Structure: conformational diversity and consequences. *Annu Rev Biochem* 80: 557–585.
7. **Shewmaker F, McGlinchey RP, Wickner RB** (2011) Structural insights into functional and pathological amyloid. *J Biol Chem* 286: 16533–16540.
8. **Wiltzius JJ, Landau M, Nelson R, Sawaya MR, Apostol MI, et al.** (2009) Molecular mechanisms for protein-encoded inheritance. *Nat Struct Mol Biol* 16: 973–978.

9. **Schrauzer GN** (2000) Selenomethionine: a review of its nutritional significance, metabolism and toxicity. *J Nutr* 130: 1653–1656.
10. **Yokoyama S** (2003) Protein expression systems for structural genomics and proteomics. *Curr Opin Chem Biol* 7:39-43.
11. **Griffiths NM, Stewart RDH, Robinson MF** (1976) The metabolism of (75Se) selenomethinine in four women. Br J Nutr 35: 373–382.
12. **Rayman MP** (2008) Food-chain selenium and human health: emphasis on intake. Br *J Nutr* 100: 254–268.
13. **Méplan C** (2011) Trace elements and ageing, a genomic perspective using selenium as an example. *J Trace Elements Med Biol* 255: 511–516.
14. **McCann JC, Ames BN** (2011) Adaptative dysfunction of selenoproteins from the perspective of the triage theory: why modest deficiency may increase risk of diseases of aging. *FASEB J* 25: 1793–1814.
15. **Shahar A, Patel KV, Semba RD, Bandinelli S, Shahar DR, et al.** (2010) Plasma selenium is positively related to performance in neurological tasks assessing coordination and motor speed. *Mov Disord* 25: 1909–1915.
16. **Budisa N, Huber R, Golbik R, Minks C, Weyher E, et al.** (1998) Atomic mutations in annexin V: thermodynamic studies of isomorphous protein variants. *Eur J Biochem* 253: 1–9.
17. **Gassner NC, Baase WA, Hausrath AC, Matthews BW** (1999) Substitution with selenomethionine can enhance the stability of methionine-rich proteins. *J Mol Biol* 294: 17–20.
18. **Hakansson K, Broder D, Wang AH, Miller CG** (2000) Crystallization of peptidase T from Salmonella typhimurium. *Acta Crystallogr D Biol Crystallogr* 56: 924–926.
19. **Wernimont AK, Huffman DL, Finney LA, Demeler B, O'Halloran TV, et al.** (2003) Crystal structure and dimerization equilibria of PcoC, a methionine-rich copper resistance protein from Escherichia coli. *J Biol Inorg Chem* 8: 185–194.
20. **Le DT, Liang X, Fomenko DE, Raza AS, Chong CK, et al.** (2008) Analysis of methionine/selenomethionine oxidation and methionine sulfoxide reductase function using methionine-rich proteins and antibodies against their oxidized forms. *Biochemistry* 47: 6685–6694.
21. **Yamniuk AP, Ishida H, Lippert D, Vogel HJ** (2009) Thermodynamic effects of noncoded and coded methionine substitutions in calmodulin. Biophys J 96: 1495–1507.
22. **Collinge J, Palmer MS, Dryden AJ** (1991) Genetic predisposition to iatrogenic Creutzfeldt-Jakob disease. *Lancet* 337: 1441–1442.
23. **Ghetti B, Piccardo P, Spillantini MG, Ichimiya Y, Porro M, et al.** (1996) Vascular variant of prion protein cerebral amyloidosis with tau-positive neurofibrillary tangles: the phenotype of the stop codon 145 mutation in PRNP. *Proc Natl Acad Sci U S A* 93: 744–748.
24. **Palmblad M, Westlind-Danielsson A, Bergquist J** (2002) Oxidation of methionine 35 attenuates formation of amyloid b-peptide 1–40 oligomers. *J Biol Chem* 277: 19506–19510.
25. **Bitan G, Tarus B, Vollers SS, Lashuel HA, Condron MM, et al.** (2003) A molecular switch in amyloid assembly: Met35 and amyloid β-protein oligomerization. *J Am Chem Soc* 125: 15359–15365.
26. **Butterfield DA, Boyd-Kimball D** (2005) The critical role of methionine 35 in Alzheimer's amyloid β-peptide (1–42)-induced oxidative stress and neurotoxicity. *Biochim Biophys Acta* 1703: 149–156.
27. **Haass C, Selkoe DJ** (2007) Soluble protein oligomers in neurodegeneration: lessons from the Alzheimer's amyloid beta-peptide. *Nat Rev Mol Cell Biol* 8: 101–112.
28. **Green KM, Browning SR, Seward TS, Jewell JE, Ross DL, et al.** (2008) The elk PRNP codon 132 polymorphism controls cervid and scrapie prion propagation. *J Gen Virol* 89: 598–608.
29. **Aguzzi A, Calella AM** (2009) Prions: protein aggregation and infectious diseases. *Physiol Rev* 89: 1105–1152.
30. **Haigh CL, Lewis VA, Vella LJ, Masters CL, Hill AF, et al.** (2009) PrPC-related signal transduction is influenced by copper, membrane integrity and the alpha cleavage site. *Cell Res* 19: 1062–1078.
31. **Lee S, Antony L, Hartmann R, Knaus KJ, Surewicz K, et al.** (2010) Conformational diversity in prion protein variants influences intermolecular beta-sheet formation. *EMBO J* 29: 251–262.
32. **Parchi P, Strammiello R, Giese A, Kretzschmar H** (2011) Phenotypic variability of sporadic human prion disease and its molecular basis: past, present, and future. *Acta Neuropathol* 121: 91–112.
33. **Näslund J, Schierhorn A, Hellman U, Lannfelt L, Roses AD, et al.** (1994) Relative abundance of Alzheimer Ab amyloid peptide variants in Alzheimer disease and normal aging. *Proc Natl Acad Sci USA* 91: 8378–8382.
34. **Butterfield DA, Bush AI** (2004) Alzheimer's amyloid beta-peptide (1–42): involvement of methionine residue 35 in the oxidative stress and neurotoxicity properties of this peptide. *Neurobiol Aging* 25: 563–568.
35. **Clementi ME, Marini S, Coletta M, Orsini F, Giardina B, et al.** (2005) Abeta(31–35) and Abeta(25–35) fragments of amyloid beta-protein induce cellular death through apoptotic signals: Role of the redox state of methionine-35. *FEBS Lett* 579: 2913–2918.
36. **Johansson AS, Bergquist J, Volbracht C, Païviö A, Leist M, et al.** (2007) Attenuated amyloid-beta aggregation and neurotoxicity owing to methionine oxidation. *Neuroreport* 18: 559–563.
37. **Maiti P, Piacentini R, Ripoli C, Grassi C, Bitan G** (2010) Surprising toxicity and assembly behaviour of amyloid β-protein oxidized to sulfone. *Biochem J* 433: 323–332.
38. **Gasset M, Baldwin MA, Lloyd DH, Gabriel JM, Holtzman DM, et al.** (1992) Predicted alpha-helical regions of the prion protein when synthesized as peptides form amyloid. *Proc Natl Acad Sci* U S A 89: 10940–10944.
39. **Salmona M, Morbin M, Massignan T, Colombo L, Mazzoleni G, et al.** (2003) Structural properties of Gerstmann-Straussler-Scheinker disease amyloid protein. *J Biol Chem* 278: 48146–48153.

40. **Petchanikow C, Saborio GP, Anderes L, Frossard MJ, Olmedo MI, et al.** (2001) Biochemical and structural studies of the prion protein polymorphism. *FEBS Lett* 509: 451–456.
41. **Dettin M, Pegoraro S, Rovero P, Bicciato S, Bagno A, et al.** (1997) SPPS of difficult sequences. A comparison of chemical conditions, synthetic strategies and on-line monitoring. *J Pept Res* 49: 103–111.
42. **Sohma Y, Hayashi Y, Kimura M, Chiyomori Y, Taniguchi A, et al.** (2005) The 'O-acyl isopeptide method' for the synthesis of difficult sequence-containing peptides: application to the synthesis of Alzheimer's disease-related amyloid beta peptide (A-beta) 1–42. *J Pept Sci* 11: 441–451.
43. **Garcia-Martin F, Quintanar-Audelo M, Garcia-Ramos Y, Cruz LJ, Gravel C, et al.** (2006) ChemMatrix, a poly(ethylene glycol)-based support for the solid-phase synthesis of complex peptides. *J Comb Chem* 8: 213–220.
44. **Grillo-Bosch D, Rabanal F, Giralt E** (2011) Improved Fmoc-based solid-phase synthesis of homologous peptides fragments of human and mouse prion proteins. *J Pept Sci* 17: 32–38.
45. **LeVine H** (1993) Thioflavine T interaction with synthetic Alzheimer's disease beta-amyloid peptides: detection of amyloid aggregation in solution. *Protein Sci* 2: 404–410.
46. **Itkin A, Dupres V, Dufrêne YF, Bechinger B, Ruysschaert JM, et al.** (2011) Calcium ions promote formation of amyloid β-peptide (1–40) oligomers causally implicated in neuronal toxicity of Alzheimer's disease. *PLoS One* 6: e18250.
47. **Baskakov I, Disterer P, Breydo L, Shaw M, Gill A, et al.** (2005) The presence of valine at residue 129 in human prion protein accelerates amyloid formation. *FEBS Lett* 579: 2589–2596.
48. **Ostapchenko VG, Sawaya MR, Makarava N, Savtchenko R, Nilsson KP, et al.** (2010) Two amyloid States of the prion protein display significantly different folding patterns. *J Mol Biol* 400: 908–921.
49. **Makarava N, Ostapchenko VG, Savtchenko R, Baskakov IV** (2009) Conformational switching within individual amyloid fibrils. *J Biol Chem* 284: 14386–14395.
50. **Apostol MI, Sawaya MR, Cascio D, Eisenberg D** (2010) Crystallographic studies of prion protein (PrP) segments suggest how structural changes encoded by polymorphism at residue 129 modulate susceptibility to human prion disease. *J Biol Chem* 285: 29671–29675.
51. **Lisa S, Meli M, Cabello G, Gabizon R, Colombo G, et al.** (2010) The structural intolerance of the PrP alpha-fold for polar substitution of the helix-3 methionines. *Cell Mol Life Sci* 67: 2825–2838.
52. **Smith JL, Thompson A** (1998) Reactivity of selenomethionine-dents in the magic bullet? *Structure* 6: 815–819.
53. **Dahlgren KN, Manelli AM, Stine WB, Baker LK, Krafft GA, et al.** (2002) Oligomeric and fibrillar species of amyloid-beta peptides differentially affect neuronal viability. *J Biol Chem* 277: 32046–32053.
54. **Fioriti L, Angeretti N, Colombo L, De Luigi A, Colombo A, et al.** (2007) Neurotoxic and gliotrophic activity of a synthetic peptide homologous to Gerstmann-Sträussler-Scheinker disease amyloid protein. *J Neurosci* 27: 1576–1583.
55. **Duennwald ML, Jagadish S, Muchowski PJ, Lindquist S** (2006) Flanking sequences profoundly alter polyglutamine toxicity in yeast. *Proc Natl Acad Sci U S A* 103: 11045–50.
56. **Sawaya MR, Sambashivan S, Nelson R, Ivanova MI, Sievers SA, et al.** (2007) Atomic structures of amyloid cross-β spines reveal varied steric zippers. *Nature* 447: 453–457.
57. **Krause RJ, Elfarra AA** (2009) Reduction of L-methionine selenoxide to seleno- L-methionine by endogenous thiols, ascorbic acid, or methimazole. *Biochem Pharmacol* 77: 134–140.
58. **Bergström AL, Chabry J, Bastholm L, Heegaard PM** (2007) Oxidation reduces the fibrillation but not the neurotoxicity of the prion peptide PrP106–126. *Biochim Biophys Acta* 1774: 1118–1127.
59. **Lee YJ, Savtchenko R, Ostapchenko VG, Makarava N, Baskakov IV** (2011) Molecular structure of amyloid fibrils controls the relationship between fibrillar size and toxicity. *PLoS One* 6: e20244.
60. **Sánchez L, Madurga S, Pukala T, Vilaseca M, López-Iglesias C, et al.** (2011) Aβ40 and Aβ42 amyloid fibrils exhibit distinct molecular recycling properties. *J Am Chem Soc* 133: 6505–6508.
61. **Bishop MF, Ferrone FA** (1984) Kinetics of nucleation-controlled polymerization. A perturbation treatment for use with a secondary pathway. *Biophys J* 46: 631–644.

Acknowledgments: Angel Cuesta, Natalia Carulla, Juan Dávalos and Javier González are acknowledged for their advice on AFM and MALDI FT-ICR measurements.

Author Contributions: Conceived and designed the experiments: MG JA DA EG. Performed the experiments: JM SL RS WK EZ MT MG. Analyzed the data: MG JM SL. Contributed reagents/materials/analysis tools: WK EZ MT EG DA JA. Wrote the paper: MG DA.

Funding: This work was supported in part by gra'ts BFU2009-07975 (MG), BIO2008-04487-CO3-02 (DA) and BIO2008-00799 (EG) from the Spanish Ministry of Science and Innovation, from the Fundacio´ n Cien-Fundacio´ n Reina Sofia, and from Generalitat de Catalunya (XRB and Grups Consolidats). Wioleta Kowalczyk is supported by a Juan de la Cierva fellowship from the Spanish Ministry of Science and Innovation. The funders had no role in study design, data collection and analysis, decision to publish, or preparation of the manuscript.

Supporting Information

1. Materials and Methods for [SeM^{35}]Aβ(1-40)

Abbreviations: DCM, dichloromethane; DIEA, N,N-diisopropylethylamine; DIPCDI, diiso-propylcarbodiimide; DMF, N,N-dimethylformamide Fmoc, 9-fluorenylmethoxycarbonyl; HBTU, 2-(1H-benzotriazol-1-yl)-1,1,3,3-tetramethyluronium hexafluorophosphate; HPLC, high performance liquid chromatography; MALDI-TOF, matrix-assisted laser desorption ionization time-of-flight; MS, mass spectrometry; SeM, selenomethionine; SPPS, solid phase peptide synthesis; TFA, trifluoroacetic acid; TIS, triisopropylsilane.

Chemicals. Fmoc-protected amino acids were obtained from Senn Chemicals (Dielsdorf, Switzerland). Fmoc-L-SeM-OH was from AnaSpec (San Jose, CA, USA), and Boc-Ser(Fmoc-Gly)-OH from Novabiochem (Läufelfingen, Switzerland). Fmoc-Rink-amide ChemMatrix resin was from Matrix Innovation (Montreal, Canada). HPLC-grade acetonitrile, and peptide synthesis-grade DMF, DCM, DIEA and TFA were from Carlo Erba-SdS (Sabadell, Spain). All other reagents were of the highest quality commercially available.

26-O-isoacyl-[SeM^{35}]Aβ(1-40). The synthetic approach is illustrated on **Figure S1**. Automated synthesis was performed in an ABI433 synthesizer (Applied Biosystems) running FastMoc protocols at 0.08 mmol scale on Fmoc-Rink-amide ChemMatrix resin [1]. 10-fold molar excess of Fmoc-L-amino acids and HBTU/HOBt, in the presence of 20-fold molar excess of DIEA, were used for coupling, with DMF as solvent. Side-chains were protected with the TFA-labile groups t-butyl (Asp, Glu, Ser, Tyr), t-butyloxycarbonyl (Lys), 2,2,4,6,7-pentamethyldihydrobenzofuran-5-sulfonyl (Arg), and trityl (Asn, Gln, His). Boc-Ser(Fmoc-Gly)-OH was coupled in the manual mode (polypropylene syringe with a porous polyethylene disk) in 4-fold molar excess in the presence of an equivalent amount of DIPCDI and HOBt in DMF. After synthesis completion, the protected peptide resin was N-deblocked with piperidine/DMF (20% v/v) prior to full deprotection and cleavage with TFA/H2O/TIS (95:2.5:2.5 v/v, 90 min, 25 ºC). The peptide was precipitated by addition of chilled diethyl ether, taken up in aqueous acetic acid (10% v/v) and lyophilized.

Analytical RP-HPLC was done on a C8 column (4.6×50 mm, 3 μm, Phenomenex) in a LC-2010A system (Shimadzu). Solvents A and B were 0.045% and 0.036% (v/v) TFA in H2O and MeCN, respectively. A linear 20-50% gradient of B into A over 15 min at 1mL/min flow rate was used for elution, with UV detection at 220 nm. Preparative HPLC was done on a C8 column (10×250 mm, 10 mm, Phenomenex) in a Shimadzu LC-8A system. Solvents A and B were 0.1% TFA (v/v) in H2O and MeCN, respectively. A linear 20-35% gradient of B into A over 30 min was used for elution, at 5 mL/min flow rate, with UV detection at 220 nm. Fractions of satisfactory purity (>95%) by analytical HPLC were pooled and lyophilized (**Figure S2**). The purified peptide was satisfactorily checked for identity by MALDI-TOF MS in a Voyager DE-STR instrument (Applied Biosystems), in the reflector mode, with α-hydroxy-cinnamic acid matrix: calculated MW for C194H296N54O57Se1= 4374.1089 (monoisotopic), found: [M+H+] 4375.45.

[SeM^{35}]Aβ(1-40). The target product was obtained in an O-N acyl shift reaction [2,3] upon incubation of purified 26-O-isoacyl-[SeM^{35}]Aβ(1-40) in PBS, pH 7.4 for 4 h at 37°C. The peptide precipitate was centrifuged and washed with water. Progress of the rearrangement reaction is shown in **Figure S3**. The end product was satisfactorily characterized by MALDI-TOF MS, as above. Calculated MW for C194H296N54O57Se1= 4375.7718 (monoisotopic), m/z found: [M+H+]: 4375.6

2. Materials and Methods for HuPrP(106-140) and analogs

Abbreviations: DCM, dichloromethane; DIEA, N,N-diisopropylethylamine; DMF, N,N-dimethylformamide; Fmoc, 9-fluorenylmethoxycarbonyl; TBTU, 2-(1H-benzotriazole-1-yl)-1,1,3,3-tetramethyluronium hexafluoro-phosphate; HPLC, high performance liquid chromatography; MALDI-TOF, matrix-assisted laser desorption

ionization time-of-flight; MS, mass spectrometry; SeM, selenomethionine; SPPS, solid phase peptide synthesis; TFA, trifluoroacetic acid; TIS, triisopropylsilane.

Chemicals. Fmoc-protected amino acids and linkers were from Luxembourg Industries (Tel-Aviv, Israel), Neosystem (Strasbourg, France), Calbiochem-Novabiochem (Laüfelfingen, Switzerland), Bachem AG (Bubendorf, Switzerland) and Iris Biotech (Marktredwitz, Germany). 4-Aminomethyl ChemMatrix resin was from Matrix Innovation (Montreal, Canada). DIEA and TIS were from Sigma (St. Louis, MO). TBTU was from Iris Biotech. Solvents for peptide synthesis and HPLC were from Carlo Erba-SdS (Sabadell, Spain). TFA was from Fluorochem Ltd (Derbyshire, UK). All other chemicals were purchased from Sigma-Aldrich at the highest quality available.

Peptide synthesis and characterization. Peptides were synthesized at 100 µmol scale [4]. Fmoc-Rink amide linker was manually coupled in a 4-fold molar excess to 4-aminomethyl ChemMatrix resin (0.57 mmol/g) in the presence of TBTU (4-fold excess) and DIEA (8-fold excess) in 3 mL of DMF, with 5 min preactivation followed by 90 min coupling to the resin. Completeness of coupling was estimated by the Kaiser test [5]. Peptides were assembled on this resin by automated Fmoc synthesis protocols (see above) run on a Liberty-12-channel synthesizer (Matthews, NC). Briefly, Fmoc groups were removed with piperidine/DMF (+0.1M HOBt; 1:4) using a short (37 W, 79 ºC, 30 s) followed by a long cycle (37 W, 79 ºC, 180 s). After DMF and DCM washings, coupling was carried out with a 0.2 M solution of Fmoc-amino acid, in the presence of 0.5 M TBTU and 2 M DIEA at 21 W, 79 ºC for 5 min. Fmoc-Arg(Pbf) required an additional coupling step consisting of a long cycle at 0 W, 25 ºC for 25 min followed by two short cycles at 21W, 75 ºC for 5 min. For Fmoc-His(Trt), deprotection was at 50 ºC to avoid racemization, and a specific coupling cycle, again to avoid racemization, was used, consisting of an initial step at 0 W, 50 ºC for 4 min followed by another at 15 W, 50 ºC for 5 min. After synthesis completion, the N-deblocked peptide resins were side-chain deprotected and cleaved from the resin using TFA/H2O/EDT/TIS (94:2.5:2.5:1, 3 h) with mild orbital shaking. The peptides were precipitated by addition of chilled diethyl ether, taken up in aqueous acetic acid (10% v/v) and lyophilized.

Peptides were analyzed by HPLC on a Sunfire C18 column (4.6×100 mm, 3.5 µm) in a Waters 2695 system equipped with a 996 PDA and Empower software. Solvents A and B were 0.045% and 0.036% (v/v) TFA in H2O and MeCN, respectively. Linear 0-100% gradients of B into A over 8 min at 1 mL/min flow rate were used for elution, with UV detection at 220 nm. Preparative HPLC was done on a Symmetry C18 column (30×100 mm, 5 mm, Waters) in a Waters 600 system. Solvents A and B were 0.1% TFA (v/v) in H2O and 0.05% TFA (v/v) in MeCN, respectively. Linear 10-60% gradients of B into A over 30 min were used for elution, at 10 mL/min flow rate, with UV detection at 220 nm. HPLC traces and purities of the purified peptides are shown in Figure S3 and Table S1, respectively. Peptides were satisfactorily checked for identity by mass spectrometry on MALDI-TOF/TOF 4700 (Applied Biosystems) and (for higher resolution) LTQ-FT Ultra (Thermo Scientific) systems.

Mass data are given in **Table S1**. Peptide quantification was done by amino acid analysis with the Waters AccQ-Tag system.

3. References

1. Fields GB, Noble RL. (1990) Solid phase peptide synthesis utilizing 9-fluorenylmethoxycarbonyl amino acids. Int J Pept Protein Res 35: 161-214
2. Sohma Y, Kiso Y. (2006) Click peptides"--chemical biology-oriented synthesis of Alzheimer's disease-related amyloid beta peptide (abeta) analogues based on the "O-acyl isopeptide method. Chem. Biochem. 7: 1549-1557
3. Sohma Y, Yoshiya T, Taniguchi A, Kimura T, Hayashi Y, et al. (2007) Development of O-acyl isopeptide method. Biopolymers 88: 253-262.
4. Grillo-Bosch D, Rabanal F, Giralt E. (2011) Improved Fmoc-based solid-phase synthesis of homologous peptide fragments of human and mouse prion proteins. J. Pept. Sci. 17: 32-38.

5. Kaiser E, Colescott RL, Bossinger CD, Cook PI. (1970) Color test for detection of free terminal amino groups in the solid-phase síntesis of peptides. Anal. Biochem. 34: 595-598.

Table S1. HPLC and mass spectrometric characterization of HuPrP peptides

Peptide	**Purity**	**Theo. Mass**	**Mass [M+ H^+]**
all-M	98.3%	3423.751	3424.725
all-V	99.2%	3295.862	3296.932
[SeM^{109}]HuPrP(106-140)	98.4%	3375.779	3376.470
[SeM^{112}]HuPrP(106-140)	96.5%	3375.779	3376.854
[SeM^{129}]HuPrP(106-140)	97.8%	3375.779	3376.927
[SeM^{134}]HuPrP(106-140)	97.5%	3375.779	3376.882

4. Supporting Information Legends

Figure S1

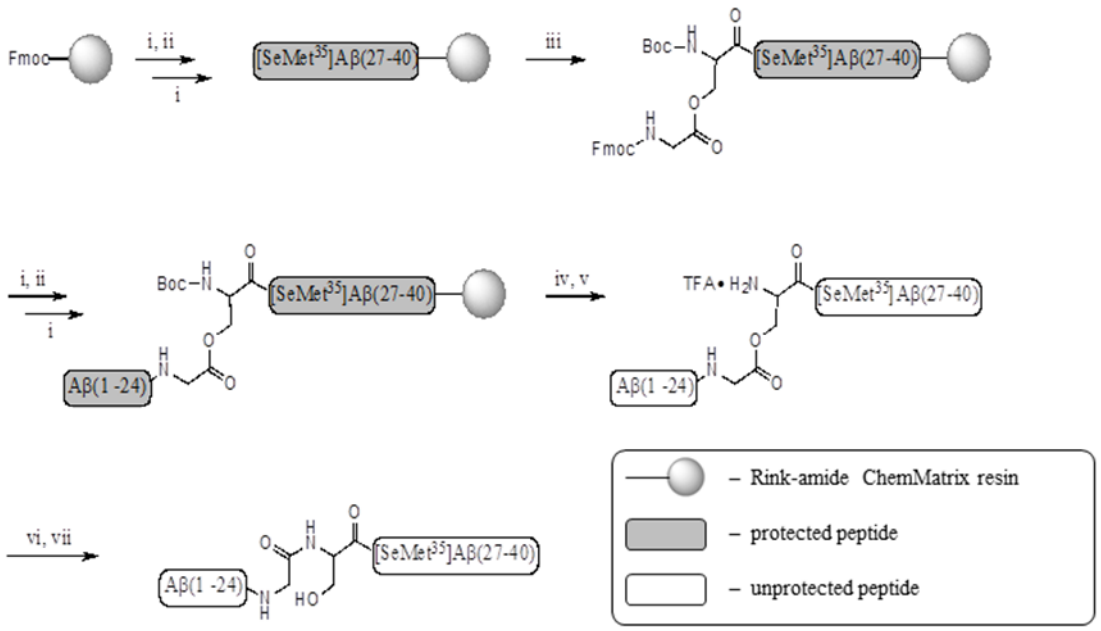

Figure S1: Synthesis of [SeM35]Aβ(1-40) by the O-acyl isopeptide method: (i) deprotection with 20% piperidine in DMF; (ii) coupling of Fmoc-L-AA/HBTU/HOBt/DIEA (10/10/10/20 eq); (iii) coupling of Boc-L-Ser(Fmoc-Gly)-OH/DIPCDI/HOBt (4/4/4 eq); (iv) cleavage: TFA/H2O/TIS (95:2.5:2.5, v/v); (v) HPLC purification; (vi) rearrangement: PBS, pH 7.4, 37°C, 3 h; (vii) H2O washes. Sequences (X=SeM): Aβ(27-40) = NKGAIIGLXVGGVV; Aβ(1-24) = DAEFRHDSGYEVHHQKLVFFAEDV

Figure S2.

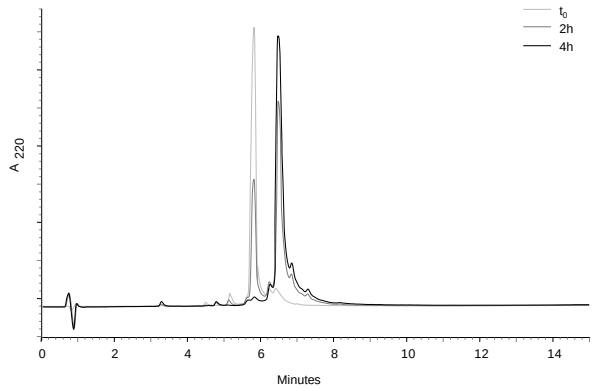

Figure S2: Progress of the O→N shift reaction of 26-O-isoacyl-[SeM35]Aβ(1-40) to [SeM35]Aβ(1-40) by incubation in PBS at pH 7.4, 37 ºC, for 4 h. HPLC conditions as described in text above.

Figure S3.

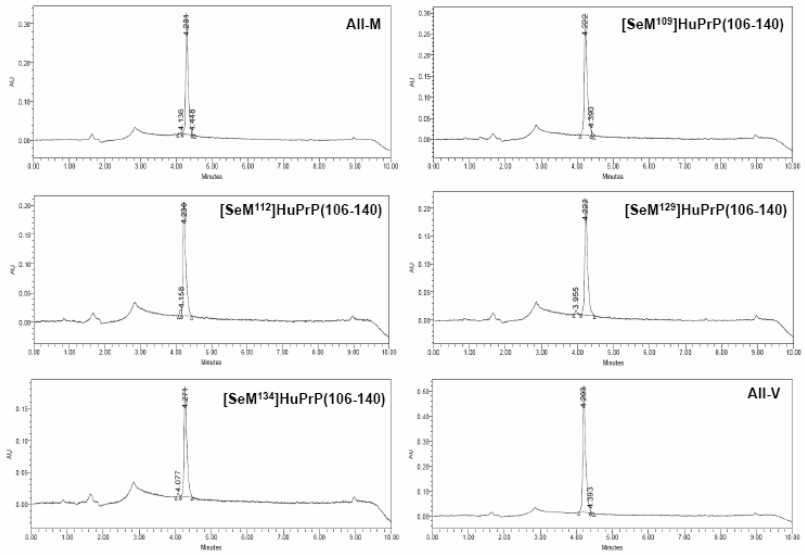

Figure S3: HPLC characterization of (left to right, top to bottom) all-M, [SeM109]HuPrP(106-140), [SeM112]HuPrP(106-140), [SeM129]HuPrP(106-140), [SeM134]HuPrP(106-140) and all-V peptides. HPLC conditions in text above.

Objetivo II: La estructura de la carga de PrP codifica interacciones entre dominios

ANTECEDENTES: La distribución o estructura de la carga en las proteínas funciona a modo de código interno clave para el plegamiento, las interacciones intermoleculares y la actividad [276,335,336]. En el caso de PrP, con una construcción en dos dominios N- y C-terminal separados por una bisagra, esta estructura es muy peculiar. En esta, el dominio N-terminal (FT) contiene dos regiones polibásicas CC1 (23-30) y CC2 (101-110), y varía entre un estado flexible y uno estructurado interaccionando con el C-terminal [243,245,278,337]. Por el contrario, el dominio globular C-terminal y proamiloidogénico todos los residuos ácidos, algunos constituyen los sitios de mutaciones patológicas (D178N, E196K, E200K, D202N, E211Q, Q212P, Q217R, Q227X) [140,172,280,338-340].

OBJETIVOS: Determinar el papel de la disposición peculiar de las cargas en PrP en el plegamiento y estabilidad del estado de referencia nativo (forma α), en la predisposición para formar el estado amiloide y en las características estructurales y reactividad del mismo.

MÉTODOS: El análisis del papel de la carga se realizó mediante comparación de las cadenas rHaPrP (23-230) wt y sus mutantes de carga K2 (K24,27E), K4 (K101, 104, 106, 110E), K6 (K2-K4), K2-E200K, E200K, Q217R, Q219K, E221K y PrP Δ23-89, producidos bien recombinantemente o mediante transfección transitoria en células CHO. La caracterización biofísica de las cadenas plegadas en forma-α y su ensamblaje en forma-β se realizó empleando dicroísmo circular (CD), dispersión dinámica de luz (DLS), microscopía de fuerzas (AFM) y microscopía de inmunofluorescencia. El procesamiento in vivo se determinó después de la desglicosilación enzimática de las cadenas producidas en células transfectadas seguida de inmunodetección en western-blot.

RESULTADOS: La caracterización hidrodinámica y conformacional mediante DLS y CD, respectivamente, de las distintas cadenas de PrP plegadas en su forma-α permitió establecer que las cargas en CC1 (mutadas en K2,K6) y en la superficie electronegativa de la región α3 (mutadas en E200K, Q217R y E221K) están implicadas en una interacción electrostática que conduce a una forma cerrada, más estable termodinámicamente que la forma abierta, y que impide la formación de amiloides. De las distintas cargas, sólo las contenidas en CC1 y CC2 son responsables del procesamiento in vivo que conduce a C1 (escisión proteolítica alrededor del residuo 110). Por otra parte, la caracterización del estado amiloide mediante CD puso de manifiesto que las cargas determinan la estructura secundaria del polímero, de forma que cualquier mutación salvo el polimorfismo Q219K, estabiliza las fibras de tipo R. El empleo de AFM y microscopia de fluorescencia permitió observar diferencias en las asociaciones laterales y la reactividad superficial entre las fibras S formadas por wt y Q219K. Del mismo modo, en las fibras de tipo R se observaron diferencias dependiendo de las cargas sustituidas. Así, los polímeros de K2 eran fibras finas y reactivas superficialmente, mientras que los de K4 y K6 eran gruesos e inactivos, subrayando que si bien el dominio N-terminal no forma parte del núcleo amiloide si modula sus propiedades estructurales. En el caso de las mutaciones en α3, el producto consistió en fibras más finas y cortas tipo varillas en E200K y Q217R y esféricas en E221K. La exposición a POM17 de E200K y Q217R era similar al wt mientras que en E221K los epítopos estaban ocultos.

CONCLUSION: La estructura de la carga en PrP actúa como un código que regula la interacción entre dominios y su patogenicidad. En el estado nativo (forma α) las cargas definen la estabilización de un estado compacto (CC1 y α3) y la extensión del procesamiento que conduce a una cadena no convertible (CC1 y CC2). En el estado amiloide, las cargas de las regiones CC1, CC2 y α3 determinan el tipo de estructura secundaria, la jerarquía del ensamblaje y la longitud de las fibras.

Contribución: Diseño y desarrollo experimental y análisis de resultados, incluyendo estudios con cultivos celulares, ensayos de transfección y western-blot. El entrenamiento en el análisis mediante immunofluorescencia de fibras fue adquirido en una estancia breve en la Universidad de Maryland.

SCIENTIFIC REPORTS

PrP charge structure encodes interdomain interactions

Javier Martínez[1], Rosa Sánchez[1], Milagros Castellanos[2], Natallia Makarava[3], Adriano Aguzzi[4], Ilia V. Baskakov[3] & María Gasset[1]

[1]Instituto Química-Física "Rocasolano", Consejo Superior de Investigaciones Científicas, Madrid 28006, Spain. [2]Centro Nacional de Biotecnología, Consejo Superior de Investigaciones Científicas, Madrid, Spain; IMDEA- Nanociencia, Madrid 28049, Spain. [3]Center for Biomedical Engineering and Technology, University of Maryland School of Medicine, Baltimore, MD 21201, USA. [4]Institute of Neuropathology, University Hospital of Zürich, Zürich 8091, Switzerland. Correspondence and requests for materials should be addressed to M.G. (email: maria.gasset@csic.es)

Scientific Reports | 5:13623 | DOi: 10.1038/srep13623, Received: 11 June 2015; Accepted: 31 July 2015; Published: 01 September 2015, How to cite this article: Martínez, J. et al. PrP charge structure encodes interdomain interactions. Sci. Rep. 5, 13623; doi: 10.1038/srep13623 (2015).

Abstract

Almost all proteins contain charged residues, and their chain distribution is tailored to fulfill essential ionic interactions for folding, binding and catalysis. Among proteins, the hinged two-domain chain of the cellular prion protein (PrP^C) exhibits a peculiar charge structure with unclear consequences in its structural malleability. To decipher the charge design role, we generated charge-reverted mutants for each domain and analyzed their effect on conformational and metabolic features. We found that charges contain the information for interdomain interactions. Use of dynamic light scattering and thermal denaturation experiments delineates the compaction of the α-fold by an electrostatic compensation between the polybasic 23–30 region and the α3 electronegative surface. This interaction increases stability and disfavors fibrillation. Independently of this structural effect, the N-terminal electropositive clusters regulate the α-cleavage efficiency. In the fibrillar state, use of circular dichroism, atomic-force and fluorescence microscopies reveal that the N-terminal positive clusters and the α3 electronegative surface dictate the secondary structure, the assembly hierarchy and the growth length of the fibril state. These findings show that the PrP charge structure functions as a code set up to ensure function and reduce pathogenic routes.

Introduction

The charge organization in proteins defines the inter- and intramolecular ionic interactions essential for folding, binding and catalysis[1–3]. Altered charges modify the structural dynamics, the aggregation, and amyloid formation propensity, among others, of elementary proteins processes in all protein conforma- tional diseases[4–14]. In prion disorders, the prion protein (PrP), a two-domain chain with an N-terminal effector tail (FT) hinged to a C-terminal globular domain (GD), forms transmissible amyloids[15,16]. Although the information for both folding and misfolding is contained in the 90–231 sequence region, the regulatory role exerted by the charged FT and the pathogenicity of mutations related to exposed charges underline an intramolecular code that remains to be elucidated[10,17–30].

PrP displays a peculiar charge pattern in its two domain chain, with a polybasic FT and all acid residues located at the GD. The FT is composed of repeats flanked at either side by positively charged clusters, known as CC1 (residues 23–30) and CC2 (residues 101–110). Despite its intrinsically disordered tail, the protein undergoes ligand-induced folding and can wrap around the GD facing the α2–α3 exposed surface, which induces compaction of the α-fold[19,27,31,32]. Removing the CC1 cluster alters the α-fold stability, early nucleation steps, the polymer shape and the prion propagation efficiency[17,18,20–26,28–30]. CC2 plays a very active metabolic role, participating in both biogenesis and processing[33,34]. Importantly, its charge abrogation yields amyloids with PrP^{Sc}-like features[35]. The spacing between CC1 and CC2 affects disease onset, GD stability and the FT effector function[28,30,36,37]. On the contrary, the GD contains all the acid residues of the chain. Among them, D144, D147, D178, E196 and E211 (numbered according to the human sequence) are involved in salt bridges that either stabilize (α1/α3) or link structural elements (β2 to α2 and α1 to α2/α3)[38–41]. Other residues, such as E146 and E152 in α1, D167 in β2-α2, and E200, D202, E207, E221 and E228 in α3, expose their side chains to solvent, thus defining electronegative surface clusters[39]. Of these charges, the structural D144 and D147 residues and their respective salt bridges stabilize PrP^{C}, preventing conversion to protease resistance forms, whereas D178, E196 and E211 are prone sites for pathogenic mutations upon charge alteration[38,42]. Moreover, pathogenic mutations, such as E200K and Q217R, and the dominant negative E219K polymorphism alter the α3 surface electrostatic potential, inducing minor folding effects[39].

To unveil the information encoded in the complementary solvent-exposed charge structure, we constructed several mutants consisting of charge reversions and inclusions and tested their effects on the properties of both the α-folded and fibrillar states. These modifications avoid the formation of non-polar surface patches resulting from abrogating charges and it solubility effect[43]. At the FT, both the CC1 and CC2 regions were modified by substituting their K residues with E (K2: K24EK27E, K4: K101EK104EK106EK110E and K6: K2–K4). At the GD, the α3 electronegative surface was perturbed by replacing E200 and E221 with K and by replacing Q217 and Q219 with charged R and K, respectively. We found that charges dictate a variety of structural and metabolic traits mostly through communication between domains. Effects such as the stabilization of the native α-fold, dictating the efficiency of the α-cleavage, attenuating the fibrillation propensity and yielding the most benign amyloids suggest that the charge design ensures PrP^{C} functions.

Results

To gain insight into the charge design of the PrP chain, we utilized reversion and insertion approaches using the rHaPrP (23–230) (PrP wt) as template (**Fig. 1a**). This choice preserved surface charge avoiding solubility effects resulting from charge abrogation[43]. At the FT, both the CC1 and CC2 charges were reversed (K2: K24EK27E, K4:K101EK104EK106EK110E and K6: K2-K4). At the GD, the α3 charge surface was modified by independent E200K, Q217R, Q219K, and E221K substitutions. Of these chains, K4 is equivalent to MoFBOM122, E200K and Q217R are pathogenic mutations found in humans[44,45], and Q219K represents the dominant-negative variant of MoPrP Q218K46. All of these chains were produced recombinantly, yielding cooperative folds with a predominantly α-helical secondary structure (**Fig. 1b**).

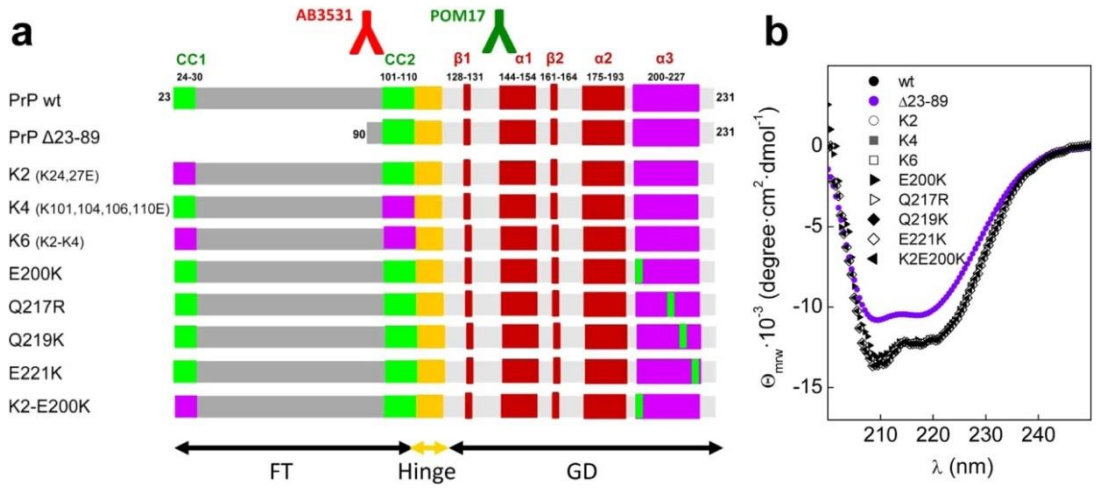

Figure 1. Charge structure of the PrP chain. (**a**) Modular organization of the PrP chain into an N-terminal domain (FT) hinged to a C-terminal globular domain (GD), displaying the location of the charged regions and their mutations that were considered in this study. Epitopes for Ab3531 and POM17 are depicted using the color codes of fluorescence microscopy. (**b**) Far-UV CD spectra in 10 mM MES pH 6.5 of PrP wt and of its charge and length mutants due to their α-folding.

PrP charge structure encodes an interdomain interaction promoting the α-fold compaction. Because charges are fundamental for intra- and intermolecular interactions, we probed the fold hydrodynamic properties using dynamic light scattering (DLS) (**Fig. 2**). To minimize insolubility interferences, measurements were performed using 15 µM protein concentrations at pH values of 4.5 and 6.5, for which open and closed PrP wt states have been reported, respectively[27,40]. **Figure 2a** shows that PrP wt yielded monodisperse species with RH of 3.2 ± 0.1 (pH 4.5) and 2.6 ± 0.1 (pH 6.5) nm, whereas its GD as PrPΔ23–89 yielded an RH of 2.1 ± 0.1 nm at both pH values[47,48]. Of these values, only the 2.6 nm for the PrP wt and 2.1 nm for the PrPΔ23–89 were comparable to the theoretical RH values of globular protein spheres with the same molecular weight (2.25 and 1.96 nm, respectively), whereas the value of 3.2 nm for the PrP wt at pH 4.5 deviated from the ideal behavior, agreeing with the open state indicated via NMR. Importantly, the RH values at pH 6.5 remained constant in the presence of 10 mM Tris used as a cation quencher, ruling out the effects of cation traces (**Fig. 2a**).

At pH 4.5 all charge mutants yielded an RH (approximately 3.2 ± 0.1 nm) similar to the PrP wt, ruling out perturbations in the open state (**Fig. 2b**). On the contrary, at pH 6.5, the RH of K4 and Q219K decreased to 2.6 ± 0.1 nm, whereas the RH values of K2 (both independently or combined with K4 as K6), E200K, Q217R and E221K remained unaltered. The lack of an RH difference for these mutants suggests an impaired compaction and a structural role of CC1, E200, Q217 and E221 in such process. Given the hydrodynamic invariability of the GD and the pH-induced electropositive charge changes (His residues in octarepeats) in the FT, the impaired RH reduction for the CC1, E200, Q217 and E221 mutants suggests that compaction involves an electrostatic interaction between the electropositive CC1 and the electronegative α3 surface, which is altered in Q217R. To further test this possibility, we constructed a K2-E200K mutant containing a double reversion and, after verifying its cooperative folding (**Figs 1** and **3a**), we tested its hydrodynamic properties. **Figure 2b** shows that the K2-E200K mutant behaved similar to the PrP wt, supporting the idea that the α-fold undergoes a compaction due to a long-range electrostatic interdomain interaction between the CC1 and α3 surface charges. The interaction driving the interdomain lock in monomeric PrP wt is weak, and NaCl concentrations above 50 mM provoke the emergence of species corresponding to the open (3.2 ± 0.1) and oligomeric (5.6 ± 0.2 nm) states (**Fig. 2a**), agreeing with the relevance of stabilizing factors such as coordinated cations[27,49].

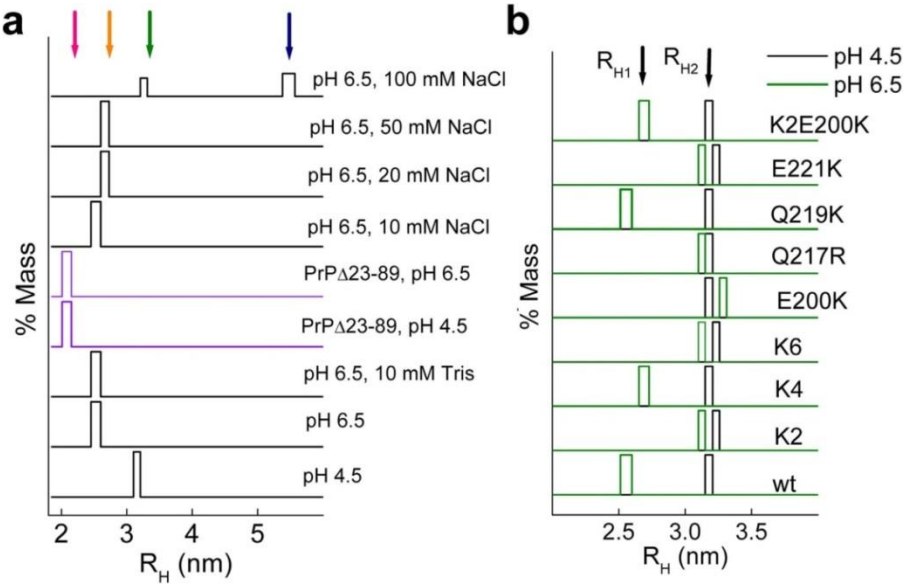

Figure 2. Effect of charges on the PrP hydrodynamic features. (a) Mass size distributions of PrP wt and PrPΔ23–89 as a function of pH and NaCl concentration. The theoretical values of RH for spheres with similar MWs to PrP wt and PrPΔ23–89 are 2.25 and 1.96 nm, respectively. (b) Mass size distributions of PrP mutants in 10 mM NaAc pH 4.5 (black) and 10 mM Mes pH 6.5 (green). The measurements were performed at 25 °C using at least two different protein batches. Column widths show the standard deviation among measurements. Arrows at the top indicate the different RH values.

Charge structure regulates α-fold stability through interdomain interactions in the native and denature states. To gain insights on the effect of the PrP charge structure on its thermodynamic stability, we analyzed the thermal denaturation curves, as shown in **Fig. 3**. It must be noted that measurements were performed in the absence of described interdomain cation stabilizers to avoid effects other than their complexation with His residues of the N-terminal octarepeats[27,49]. With the exception of

K4, all of the thermal denaturations were reversible, as indicated by the recovery of at least 90% of the initial signal after cooling from the highest temperature. K4 denaturation was irreversible, and insoluble aggregates were detected upon cooling from the highest temperature (data not shown). **Figure 3a,b** show that the mutants with impaired compaction, such as K2, K6, E200K, Q217R, E221K and Δ23–89, unfolded with Tm values lower than that of wt PrP. This effect varied according to K6 ≈ E221K ≈ Q217R >Δ23–89> E200K ≈ K2, leading to decreases in the free energy of unfolding of about 1.2–6 kJ/mol. On the contrary, Q219K and K2-E200K, which undergo compaction, exhibited a PrP wt-like denaturation profile. Notably, the K4 mutant, exhibiting PrP wt-like hydrodynamic properties, yielded the most thermally labile fold, possibly due to its singular irreversible denaturation. Thus, with the exception of K4, these results indicate that altering the charges that mediate the interdomain lock decrease the native fold stability.

The destabilization pattern of the mutants precluding compaction agree with the effects described for the chains containing N-terminal truncations at pH > 6.0 and slightly differ from that described for PrP chains consisting in mutant GD moieties[20,21,37,50–52] (**Fig. 3b**). By virtue of its additivity, the ΔG of folding of a two-domain protein (TD or full length) can be expressed as the sum of the contributions arising from the folding of each of domain (ΔGFT and ΔGGD) and from their interaction (ΔGFTGD). Since the ΔGFT and ΔGFTGD are linked in PrP, their sum (ΔG*FT) can be calculated as ΔG*FT = ΔG TD - ΔGGD. For the PrP wt and a GD consisting in PrPΔ23–89, ΔG*FT corresponded to 3 ± 0.7 kJ/mol (−ΔΔG* in Fig. 3b), which agree with the 3.2 ± 1 kJ/mol value that can be calculated for GD consist- ing in PrPΔ32–89 chains[20].

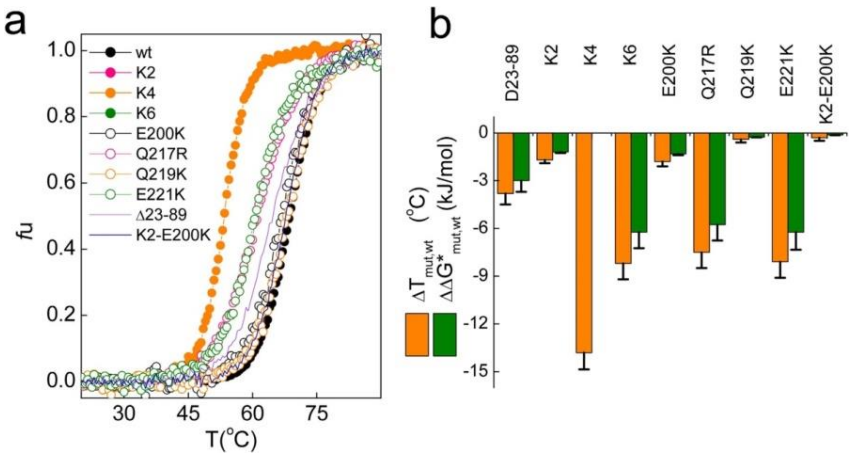

Figure 3. Effect of domain charges on the PrP stability. (a) Thermal denaturation of PrP wt and mutants. The unfolded fraction was calculated using the Θ222 temperature function according to a two-state transition, as described[48]. (b) Differences in the unfolding temperature (ΔTm) and in the free energy of unfolding (ΔΔG*) induced by the charge mutations. ΔTm is the difference between the denaturation temperature of PrP mutant (PrPmut or PrP90–231 wild type) and full length PrPwt (Tmmut −Tmwt). Tm values were obtained as the midpoints of the temperature denaturation curves. ΔΔG* was obtained as ΔH,wt × (1−Tmwt/Tmmut), where ΔHvH is the van´t Hoff enthalpy of PrP wt denaturation (255 kJ/mol). ΔΔG* < 0 indicates adestabilization of the mutant chain compared to the wt. Displayed data are the average of three independentmeasurements, performed with at least two different protein batches. Error bar represents the standard deviation (s.d.). Calculations for K4 were omitted given its irreversible denaturation.

For mutants exhibiting either identical GD as K2 or negligible effects on its free energy of unfolding as E200K[50,51], which increasing GD breathing facilitates M213 sulfoxidation[53], ΔG*FT can be approximated to ΔGTDwt-ΔGTDmutant difference (−ΔΔG* in **Fig. 3b**). This approach yielded values of 1.2 ± 0.2 and 1.5 ± 0.7 kJ/mol for K2 and E200K respectively.

Taken together the values of PrPΔ32–89, K2 and E200K yielded an averaged estimation of ΔG*FT of approximately 2 kJ/mol. On the hand, for Q217R the ΔΔG*Q217R reported for the GD chains was −8.9 ± 2 kJ/mol[50,51] and the calculated for the TD amounted to −5.8 ± 1 kJ/moly. As with Q217R, K6 reversing the charge of FT flanks provoked a similar ΔΔG* of −6.2 ± 1 kJ/mol. The higher destabilization of Q217R and K6 compare to PrP Δ23–89 suggested that in these mutants their charge changes affected interdomain interactions not only in the native state but also in their denature state[54].

Charges are gatekeepers of PrP fibrillation. Although most PrP amyloids generated in vitro lack the infectivity and proteolytic signatures of PrP^{Sc}, their formation models the chain propensity and the conformational changes required for GD self-assembly[55,56]. To test whether the charge structure, through either the α-fold stabilization described above or the initial self-assembly step, impacts the fibrillation, we performed time-dependent Thioflavin T (ThT) binding experiments using the various PrP chains at pH 6.5 and calculated the lag-phase as indicator of propensity (**Fig. 4**).

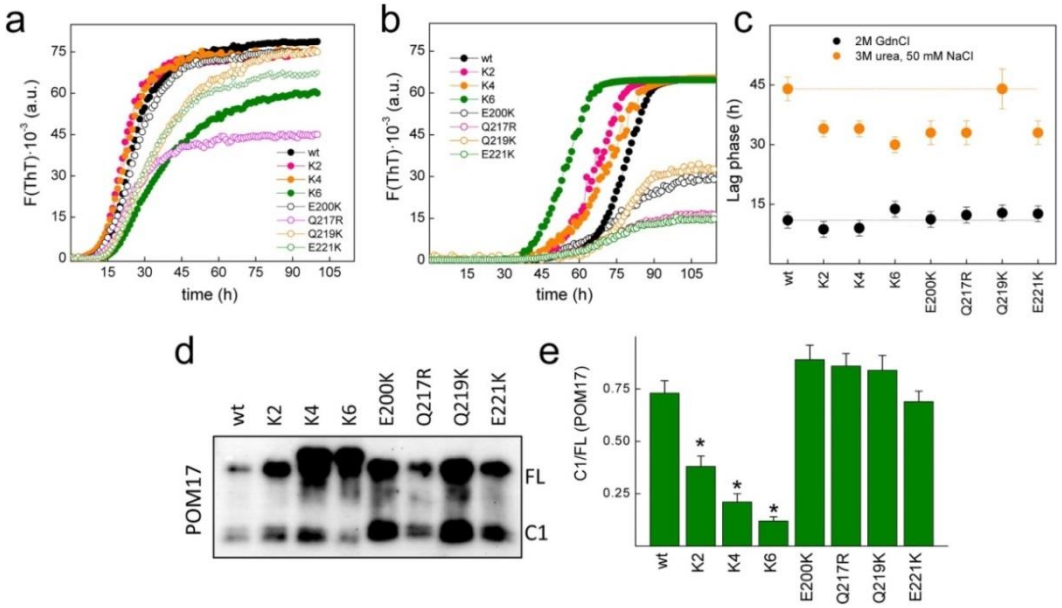

Figure 4. Charge changes modify the fibrillation propensity and processing of PrP. Time-dependence of ThT binding of the PrP wt and mutants (40 μM protein concentrations) in 50 mM MES pH 6.5 at 37 °C containing (a) 2 M GdnCl and (b) 3 M urea and 50 mM NaCl. The curves represent the average of three independent measurements, performed in triplicate. (c) Lag-phases of the fibrillation reactions of the PrP wt and mutants in 50 mM Mes pH 6.5 containing either 2 M GdnCl or 3 M urea with 50 mM NaCl. The depicted values correspond to three independent experiments, each performed in triplicate. (d) Western blot of PNGase-treated cell lysates of CHO cells transfected with PrP wt and the charged mutants. Detection was performed using POM17, and the positions of the full-length (FL) and N-terminal-truncated (C1 fragment) chains are depicted. (e) Variations in the C1/FL ratio of the PrP chains. Quantifications are the average of two independent transfection assays. Error bar represents the standard deviation (s.d.). *p < 0.01.

To induce the required mild denaturation, we used either 2 M GdnCl (conventional ionic media) or 3 M urea containing 50 mM NaCl (low salt). As anticipated from the exposed character of the mutated charges and the high ionic strength of the media, fibrillation in 2 M GdnCl (**Fig. 4a**) yielded lag-phases that were roughly similar for all chains, with minor reductions (K2,K4) or enhancements (K6) (**Fig. 4c**).

On the contrary, reactions in the low salt media containing 3 M urea and 50 mM NaCl revealed that with the exception of Q219K, all mutants form fibrils faster than the PrP wt as indicated by their higher lag-phases (**Fig. 4b,c**). Kinetic curves also showed that charge changes in the GD (E200K, Q217R, Q219K and E221K) decrease the ThT fluorescence increment linked to fibrillation predominantly under low salt (**Fig. 4a,b**), suggesting off-pathway events.

The observed reduction in the lag-phase in the low salt reaction media in K2, K4, K6, E200K, Q217R and E221K variants indicated that CC1, CC2 and the α3 electronegative caps function as fibrillation gatekeepers. Since K2, K6, E200K, Q217R and E221K impeded domain compaction and K4, with preserved compaction, lack the charges preventing the PrP fibril N-terminal packing[35], together their effects suggest that charges regulate fibrillation propensity through their role in both the native fold compaction and the packing of critical regions for the seed stability. This charge effect agree with the increased propensity of PrP Δ23–89 compared to the full length chain[57,58] and the dependence of anionic cofactors for functional fibrillation[59].

FT charges regulate the efficiency of C1 production. PrP processing into C1 chains is essential for the abrogation of prion formation and propagation, involving a complex cleavage within the interdomain hinge (around residue 110)[60–62]. To test whether the PrP charge structure plays a role in this processing, CHO cells were transfected with plasmids coding for PrP wt or its mutants, and the expressed chains were analyzed using POM 17 after PNGaseF digestion. **Figure 4d,e** shows that among the different PrP chains, only K2, K4 and their combination as K6 drastically reduced the efficiency of C1 production compared to wt PrP, which is in agreement with previous reports that showed impaired C1 production for mouse variants of K4 and PrPΔ23–31 in both Hpl cells and transgenic mice[22,25]. On the contrary, the mutants including modifications of the α3 surface charge impairing the interdomain lock, such as E200K, Q217R and E221K, yielded C1 levels similar to the PrP wt (**Fig. 4d,e**). Differences in the dependence of C1 production on the charge structure of either domain indicated that processing through the α-cleavage site is highly dependent on the FT charge structure but fairly independent of their role in driving the α-fold compaction. Thus, C1 production may require the recognition of the FT through its charge clusters by an unknown anionic ligand[52,63–65], implying conditions with unlocked α-fold. These results suggest that the PrP charge structure regulates processing through its role in interactions.

Charges impact the secondary to quaternary structure of the fibrils. Similar to the α-folded wt PrP chain, variants with altered charge structure form fibrils that differ in their shape and proteinase-resistant core[21,35]. To gain insight into the effects of the charged design on the fibril structure and its properties, we used the reaction conditions yielding PrP wt S-fibrils with resolution for imaging analysis. S-fibrils, produced under slow orbital agitation as opposed to the fast rotation leading to the R-polymorph, are featured by a β-sheet-like far-UV CD spectrum along with a thin and

curvy fibril topology that expose the 90–102 region while partially shield the POM17 epitope[66] (**Figs 5–7**). It must be stressed that this fibrillation reaction was performed in the presence of 2 M GndCl, which abrogates the charge effects on the native α-fold and permits the assignation of the deviations from the wt behavior to differences in the assembly process. Fibrils formed by all PrP mutants displayed a reduced specific ThT binding, suggesting major structural differences (**Fig. 5a**).

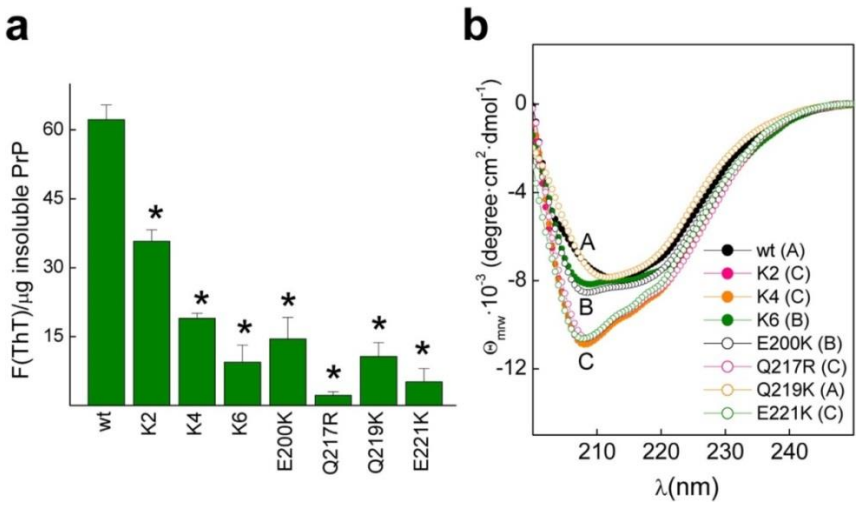

Figure 5. Properties of the PrP wt and mutant fibrils. (a) Specific ThT binding of the PrP wt and mutant fibrils. Typically 50 µM of fibrils in 10 mM ammonium acetate pH 5 were incubated for 10 min with ThT (15 µM) before fluorescence determination. ThT fluorescence intensities were corrected for the background (absence of fibrils) and divided by the protein amount in the pellet of a 12000 rpm 20 min centrifugation..The depicted data represent the average of two independent experiments performed in duplicate (*p < 0.01). (b) Far-UV CD spectra of the PrP wt and mutant assemblies in 10 mM ammonium acetate pH 5. The fibrils were formed in 50 mM MES pH 6.5 containing 2 M GdnCl at 37 °C under continuous rotation at 24 rpm, and then dialyzed against 10 mM ammonium acetate pH 5.

Among the fibrils, only those formed by Q219K exhibited an S-like CD spectrum (**Fig. 5b**), whereas the assemblies formed by K2, K4, K6, E200K, Q217R and E221K displayed R-like CD spectra featuring a higher negative ellipticity, a minimum at 207 nm, and a shoulder at 217 nm of the β-sheet and turn structures (**Fig. 5b**). These data suggest a strict dependence of the S-fibril on CC1, CC2, and α3 surface charges. Because only the R-type fibril exhibited in vivo infectivity, the PrP charge structure appears to drive the fibrillation path to the less pathogenic S-type state[67]. The blockage of S-fibril type formation in K2, K4, K6, E200K, Q217R and E221K mutants also suggest that these charges may behave as sites for cofactor binding that, through their shielding, may shift the conversion route to the most infectious path[35,68,69]. Accordingly, in addition to known anionic cofactors which may function recognizing CC1 and CC2 regions may be molecules that exhibiting a basic charge would produce similar effects shielding the α3 surface charges , which would amplify the group of molecules functioning as cofactor inconversion[35,59,68,69].

The Q219K substitution forms S-type-fibrils as PrP wt, but their assembly exhibited several differences. First, AFM imaging revealed that the Q219K fibrils, which were similar in dimension to those formed by the PrP wt, displayed a high degree of lateral association, yielding fibril layers rarely observed in PrP wt (**Fig. 6**). Second, the immunofluorescence analysis resolving fibrils in the µm range

showed that in the wt and the mutant fibrils, the 90–102 (red, Ab3531 epitope) region is exposed along the fibril axis, whereas POM17 epitopes (140/145 region) were detected as discrete regularly spaced dots (green), which after treatment with 3 M GdnCl become disrupted in the wt fibrils but persist in the Q219K fibrils (**Fig. 7a**). These differences in the POM17/Ab3531 overlap both in the absence and presence of denaturant treatment are depicted in **Fig. 7b**.Thus, the lateral association and the attenuated surface reactivity of the Q219K fibrils may presumably contribute to the dominant-negative property of this charge insertion.

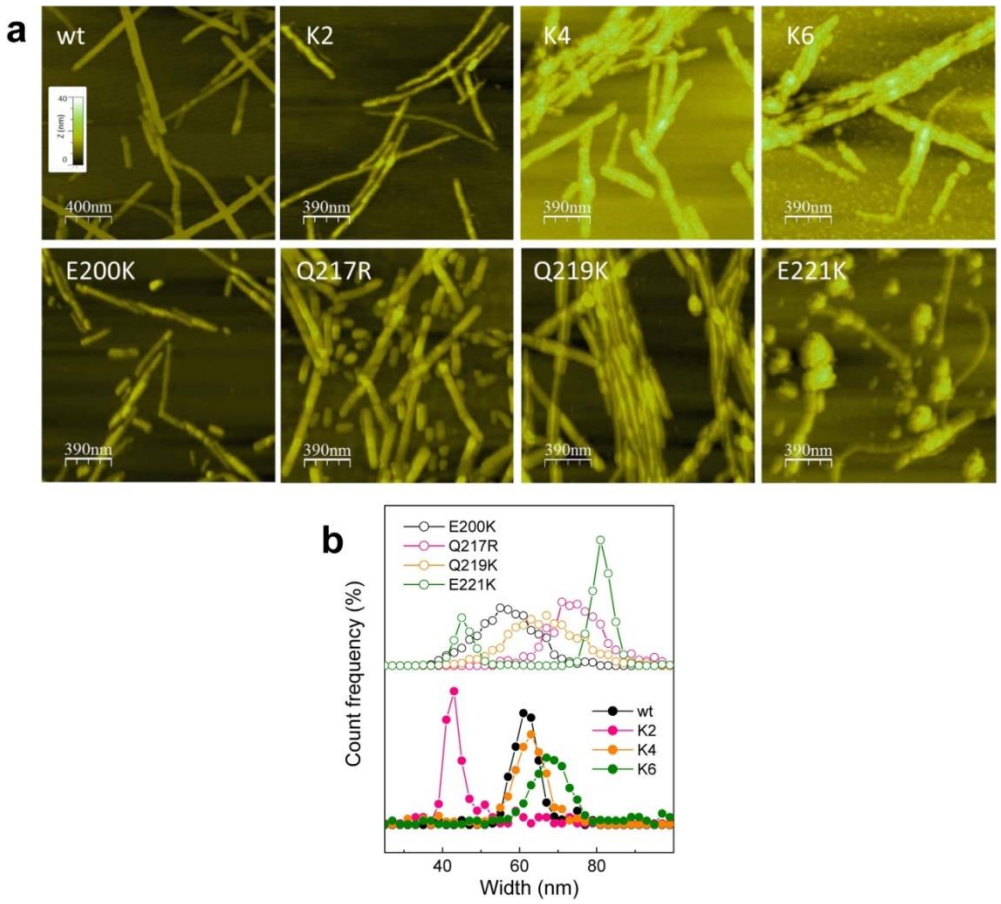

Figure 6. Topology images of the PrP wt and mutant fibrils. (a) AFM images of the PrP wt and mutant fibrils corresponding to the topology mode. The z-axis was fixed for all graphs, and the color scale is displayed as an insert in the PrP wt panel. (b) Histogram of the width distribution of the distinct PrP assemblies.

The K2 fibrils were thinner than the wt fibrils and tending to arrange into Y-shapes (**Fig. 6**). The immunofluorescence analysis revealed that the POM17 epitope was fully exposed in the absence of denaturant treatment (**Fig. 7**). On the contrary, K4 and K6 formed thick fibrils, indicating a higher assembly complexity. Of them, the peculiar stacking of the K6 assemblies resembled the aggregates of PrP27–30 rods[35,70]. Immunostaining revealed that the POM17 epitope was highly secluded in the K4 and K6 assemblies, resisting treatments, with distinct GdnCl concentrations (**Fig. 7**). These results indicate that CC1 and CC2 charges, in addition to allowing for S-type fibrillation, govern the evolution of the hierarchical assembly and the surface exposure of the region 140–145. CC1 appeared to work during the initial assembly step involving the shielding of the 140–145 region, whereas CC2 in a dominant fashion functioned during later assembly steps, compromising the discrete POM17 epitope

exposure. These effects suggest that the FT charges modulate properties of the fibril state of the C-terminal domain.

Changes in the α3 charge structure resulted in R-type (**Fig. 5b**). AFM imaging revealed thicker fibrils compared to those of the PrP wt and images that were rich in short structures, rod-shaped in E200K and Q217R and spherical in E221K (**Fig. 6**). Interestingly, the E221K mutant revealed extremely thin, curvy fibrils emerging from the spherical aggregates (**Fig. 6**). The E200K and Q217R fibrils displayed a surface reactivity similar to that of the PrP wt but with green dots at reduced spacing, suggesting POM17 epitope location at the joint of the short rod-shaped structures (**Fig. 7**). In both assemblies, mild denaturing treatment increased POM17 staining but to a lesser extent that in the wt fibrils, suggesting differences in the folding of the 140–145 region. On the contrary, the E221K fibrils resembled those formed by K4, with a complete seclusion of the POM17 epitope and a discrete exposure upon treatment with 3 M GdnCl (**Fig. 7**). Taken together, these features suggest that the charges of the α3 primarily regulate the fibril length by either limiting growth or promoting fragmentation and the exposure of the POM17 epitope.

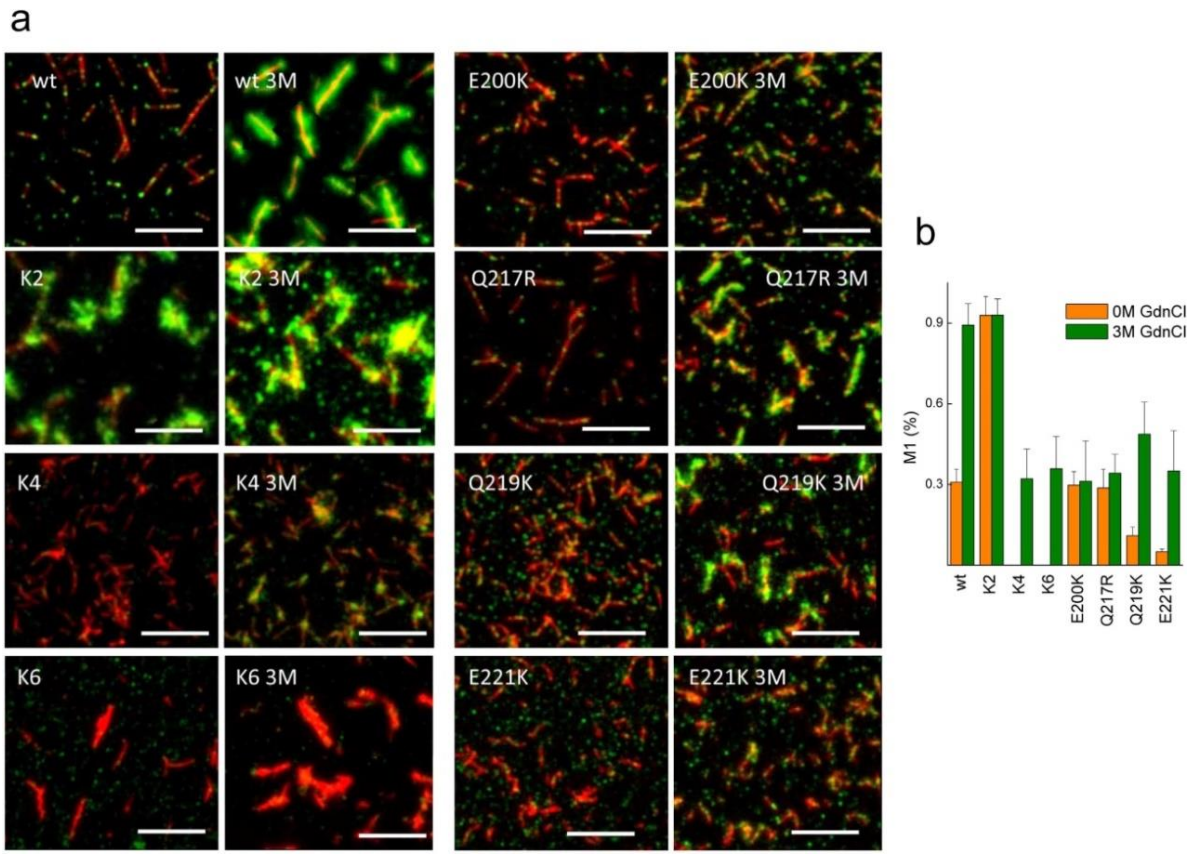

Figure 7. Surface reactivity of PrP wt and mutant fibrils. (a) Representative fluorescence images of the fibrils formed by the PrP wt and mutant fibrils stained with AB3531 (red) and POM17 (green). Pretreatment with 3 M GdnCl is indicated as 3 M. The white bar represents 5 µm. (b) Effect of charges on the variation of the POM17 overlap with AB3531 (Manders overlap coefficient) based on the denaturant concentration. Error bar represents the standard deviation (s.d.).

Discussion

Here, we show that the PrP charge structure considered as solvent exposed contains information regarding interdomain interactions in both the PrP^{C}-like conformation and the fibrillar

state. In the PrP^{C}-like formation, FT wraps the GD via the interaction between the N-terminal polybasic motive (CC1) and the α3 electronegative surface. This complementary charge interaction is relatively weak, and in the absence of stabilizers such bound Zn^{2+} the modifications provoked by the ionic strength or diminished surface electronegativity (single charge reversion or inclusions along the helix) impaired it. Notwithstanding, the interdomain interaction adds to the global fold a stabilization lower threshold of approximately 2 kJ/mol which interferes with fibrillation. Independent of this structural effect, the FT charge design also dictates the efficiency of cleavage between domains through the α-site indicating that the production of neuro- protecting fragments involves conditions with unlocked domains. In the fibrillar state, the PrP charge structure regulates the assembly process, dictating the secondary structure of the scaffold, the allowance of different (initial, intermediate and late) assembly steps, and the polymer length.

The sequence of proteins contains the protein's functional information, including signaling mechanisms for maturation, sorting, covalent modification, and folding regulation, whereas other functions are encrypted and operate metabolically. The PrP sequence exhibits an unusual abundance of encrypted codes. The abundance of Met residues in the PrP chain allows for the translation of a minor chain that segregates out of the major secretory route, a structural regulation through a redox process, and a metabolically controlled substitution by SeMet[71–73]. Similarly, the His distribution entails a complex pH-regulated, cation binding trait in the FT that provides a diverse structural landscape with functional consequences[27,32,63,74]. Regarding charges, the complementary polybasic stretches in the FT and electronegative surfaces from the GD folding provide the basis for molecular compaction and its regulation by FT and GD ligands. Charge structures also participate in the fibrillation process, bestowing interdomain-dependent and domain-specific growth and assembly features.

The PrP charge structure seems to encode information for latent states with balanced ligand binding functions. The interdomain lock, functionally in non-transmembrane PrP formations, may sense changes in the length and flexibility of the FT, which depend on the number of repeats, the pH and cation binding[27,28,30,36,37,75]. Indeed, the interaction can be isolated either under partial protonation of the octarepeat His, as described here, or stabilized by Zn^{2+} binding[27] to ensure ionic strength resistance. FT ligands that recognize its charge clusters regulate the cleavage of domains, suggesting that this process that monitors the dose of prion precursors uses as substrate the unlocked domain molecule. On the other hand, GD ligands precluding the lock by shielding the interacting motives (POM 4,10,19 and α-219–232) or by providing steric impediments (POM1) allow for FT toxic signaling[28,76], suggesting that at the cell surface PrP^{C} may exit under the compact state. As in the GD the α3 surface constitutes the prion binding site, its shielding by the interdomain lock may also interfere with prion amplification by competing with seed binding[76]. Moreover, the interdomain lock prevents fibrillation of PrP by stabilizing the α-fold, which could be utilized in therapeutic intervention using the lock state as a target.

The charge structure code also operates in the fibrillation path, dictating properties that compromise propagation and toxicity. Despite the differences with PrP^{Sc}, only R-type PrP fibrils exhibit in vivo propagation, which are only found in mutants with a modified charge structure[66]. The PrP charges appear to drive the chain into the fibril structures with attenuated pathogenicity and provide sites for cofactor action. Therefore, cofactors that bind to CC1 may regulate the initial steps,

whereas cofactors that shield CC2, singly or combined with CC1, may drive the progression to the advanced assembly steps. These mechanistic hints agree with the mode of action of polyanions in previous conversion studies[35,59]. Moreover, the limits of assembly evolution due to FT charges are inversely correlated with the POM17 epitope exposure. Because this region contains the DWED sequence, forming part of the α1 in the α-fold and stabilized by salt bridges, it is tempting to postulate that the assembly involves its interaction with CC1. On the other hand, charged residues at either end of the α3, which are part of the β-core but not engaged in β-sheets, mainly govern the fibril length. Changing these charges reduces the length, either impeding growth or favoring fragmentation, which increases the seed concentration and consequently the propagation efficiency[77]. Thus, α3 mutations may strengthen their pathogenicity by optimizing their propagation through the seed concentration.

In conclusion, PrP charge design encodes several of structural and metabolic traits set up for ensuring function and diminishing pathogenic routes. These traits are: 1) shaping an interdomain lock, which prevents the FT from its toxic signaling and the GD from its prion receptor activity, 2) promoting the α-cleavage yielding anti-prion C1 chains and reducing the dose of chains with pro-prion activity, and 3) stabilizing the α-fold against conversion and if so allowing the less pathogenic assembly.

Methods

Production of PrP chains. rHaPrP (23–231) chains were produced from their pET11a constructs as described[48,78], with minor modifications. Briefly, inclusion bodies were solubilized in 20 mM Tris pH 7.5 containing 6 M GdnCl, 05 M NaCl and 2.6 mM imidazole, and after column loading 6 M GdnCl was replaced by 8 M urea. rHaPrP(90–231) was produced from a pET15b construct using thrombin diges- tion to cleave the His-tag. The various mutants were produced via site-directed mutagenesis using the primers listed in **Table S1**. Before use proteins were equilibrated in the desired buffer (10 mM NaAc pH 4.5 or 10 mM Mes at pH 6.5, unless stated) by extensive dialysis and cleared by centrifugation before concentration determinations[48].

Dynamic Light Scattering. Dynamic light scattering (DLS) measurements were performed using a DynaPro spectroscatter (Wyatt Technology) with a 1.5-mm path length and a 12 µl quartz cuvette. The average of 20–25 acquisitions of buffers and protein solutions (15 µM protein concentrations) were filtered using a 0.1 µm Whatman Anodisc-3 filters. The hydrodynamic radii (RH) and mass proportions (%) of the species were derived from the autocorrelation data assuming a model of n-monodisperse globular proteins and using the software provided by the manufacturer[13,48]. Measurements were performed in triplicate using two different protein batches. The theoretical hydrodynamic radius (RHT) for PrP wt chain was calculated using 0.73 cm3 g−1 and 0.35 g H2O (g protein)−1 for the particle specific volume and the hydration, as described[47].

CD Spectroscopy. CD spectra were recorded in a Jasco-810 CD spectrometer with 15 µM protein solutions in either 10 mM Mes at pH 6.5 or 10 mM ammonium acetate pH 5.0 using a 0.1-cm cuvette[48]. Thermal denaturation experiments were performed following the ellipticity changes at 222 nm upon heating from 15 °C to 90 °C at a 1 degree/min heating rate and analyzed as a two-state transition as described48. Briefly, the changes in Θ222 with temperatures were normalized to

the fraction of unfolded protein (fU) using fU(T) = (Θ222(T) − Θ222N(T))/(Θ222U(T)− Θ222N(T)), where N and U refer to the native and unfolded states, respectively. The value of fU was plotted as a function of temperature for the calculation of Tm and ΔHm. The experimental Tm values of mutants were converted into the apparent relative changes in free energy with respect to the wt protein (ΔΔGo) using the equation ΔΔG mut/wt mut/ wt = ΔHwt x (1 – Tmwt / Tmmut), where Tmwt and Tmmut are the Tm values for the wt and mutant protein,respectively, and ΔHwt is the denaturation van´t Hoff enthalpy of the wt protein.

Fibril formation. The proteins in 5 mM MES pH 6.5 were cleared by centrifuging at 13200 rpm for 20 min at 4 °C and placed at 40 μM protein concentrations in 50 mM MES at pH 6.5 containing either 2 M GdnCl and 3 M urea with 50 mM NaCl. For kinetic analyses, 0.2-ml samples containing 15 μM ThT were placed in wells with a 3 mm glass ball. ThT binding was monitored at 37 °C, as described[13,73]. All measurements were performed in triplicate, and the experiments were repeated at least with two different protein batches. For imaging, fibrils were formed in 50 mM MES pH 6.0 containing 2 M GdnCl at 37 °C with continuous rotation at 24 rpm. After 100 h, the products were dialyzed against 10 mM ammonium acetate at pH 5.

Atomic force microscopy. First, 2-μM fibril solutions were deposited onto freshly cleaved mica surfaces. After 10 min of adsorption, the samples were washed with H_2O and dried with a stream of N2. AFM studies were performed using a MultiMode Veeco microscope with a 125-μm lateral range and a 5-μm vertical range equipped with a J-scanner and a NanoScope IIIa controller, using rectangular can- tilevers with tetrahedral tips for the dynamic mode in air (Olympus, OMCL-AC240TS)13. The analysis was performed using WSxM (Nanotec).

Fluorescence Microscopy. PrP fibrils were deposited onto Permanox 8-well Lab-Teks chamber slides and immunostained with rabbit anti-PrP Ab 3531 (1:1000, recognizes 90–102) and mouse POM17 anti-PrP Ab (1:1000, recognizes 140–145), followed by goat anti-rabbit and goat anti-mouse antibodies labeled with Alexa-488 and Alexa-546, respectively (Invitrogen/Molecular Probes, 1:1000). Fluorescence images were captured using an Axioplan Universal Microscope (Zeiss) equipped with a DFC 350 FX digital camera (Leica) and a 100x objective. Processing and analyses were performed using WCIF ImageJ software[79]. Manders overlap coefficients were determined as the amount of Ab3531 signal overlapped with the POM17 stain with at least 20 independent fibrils.

Cell culture, transfections and processing analysis. Mutants were generated using pcDNA4.1-HaPrP(1–254) as a template (**Table 1S**)[80]. Transient transfections were performed using Chinese hamster ovary (CHO) cells and Fugene 6 as a transfection reagent (Roche), as described[80]. After 40 h, the cells were harvested via in situ lysis in a cold RIPA buffer (10 mM Tris-HCl pH 7.5, 100 mM NaCl 10 mM EDTA, 0.5% Triton X-100, 0.5% deoxycholate). The lysates were cleared via 5 min of centrifu- gation at 500 g, supplemented with 0.5 mM Pefabloc, and precipitated with 5 volumes of methanol at −20 °C. Samples were then centrifuged at 10000 × g for 30 min, and the pellets were redissolved in TNE buffer (50 mM Tris-HCl pH 7.5, 150 mM NaCl, 5 mM EDTA). Enzymatic digestions with PNGaseF (New England Biolabs) were performed for 1 h at 37 °C[80]. After digestion, the reactions were stopped by the addition of Laemmli buffer and PrP analyzed via immunoblotting using the POM17 antibody.

Western blot analysis. The samples were resolved using SDS-PAGE (13.5% acrylamide gels) and electrophoretically transferred onto PVDF. The membranes were blocked for 1 h in 5% (w/v) non-fat dried skimmed milk powder in Tris-buffered saline containing 0.05% Tween 20. After incubation with mouse anti-PrP POM17 and HRP (horseradish peroxidase)-conjugated goat-anti mouse antibody (Sigma-Aldrich, 1:5000), the signals were developed using an ECL-Western-blotting reagent (Bio-Rad) and detected using ChemiDoc XRS equipment.

Statistical analysis of experiments. Statistical analysis of experiments was performed either using paired Student's t-test, for comparing two samples, or one-way ANOVA with Dunnett's post-hoc test, for comparison of all columns to a control column. Results are displayed as the average of replicates ± s.d.

Acknowledgements: We thank Prof. A. Estepa, V. Muñoz, and S. Zorrilla for contributing reagents and equipment and for critically reading the manuscript. This work was partially supported by the Ministerio de Economía y Competitividad (BFU2009-07971 and SAF2014-52661 to MG, BIO2011-28092 and CSD2009-00088 to MC), Fundación CIEN (MG), Raman Health (MG) and the National Institutes of Health (grants NS045585 and NS074998 to IVB). JM was supported by an FPI-research contract and an FPI-short staying grant. MC was supported by a Juan de la Cierva Postdoctoral contract.

Author Contributions: M.G. and J.M. conceived the experiments; J.M., R.S., M.C. and N.M. conducted the experiments; J.M., M.G., I.B. and A.A. analyzed the results. M.G. and J.M. draft the manuscript. All authors reviewed the manuscript

Additional Information: Supplementary information accompanies this paper at http://www.nature.com/srep
Competing financial interests: The authors declare no competing financial interests.

References

1. **Nakamura, H.** Roles of electrostatic interaction in proteins. *Quarterly reviews of biophysics* 29, 1–90 (1996).
2. **Bosshard, H. R., Marti, D. N. & Jelesarov, I.** Protein stabilization by salt bridges: concepts, experimental approaches and clarification of some misunderstandings. *Journal of molecular recognition*: JMR 17, 1–16, doi: 10.1002/jmr.657 (2004).
3. **Gitlin, I., Carbeck, J. D. & Whitesides, G. M.** Why are proteins charged? Networks of charge-charge interactions in proteins measured by charge ladders and capillary electrophoresis. *Angew Chem Int Ed Engl* 45, 3022–3060, doi: 10.1002/anie.200502530 (2006).
4. **Uversky, V. N., Gillespie, J. R. & Fink, A. L.** Why are "natively unfolded" proteins unstructured under physiologic conditions? *Proteins* 41, 415–427 (2000).
5. **Chiti, F. et al**. Studies of the aggregation of mutant proteins in vitro provide insights into the genetics of amyloid diseases. *Proceedings of the National Academy of Sciences of the United States of America* 99 Suppl 4, 16419–16426, doi: 10.1073/pnas.212527999 (2002).
6. **Chiti, F., Stefani, M., Taddei, N., Ramponi, G. & Dobson, C. M.** Rationalization of the effects of mutations on peptide and protein aggregation rates. *Nature* 424, 805–808, doi: 10.1038/nature01891 (2003).
7. **Schmittschmitt, J. P. & Scholtz, J. M.** The role of protein stability, solubility, and net charge in amyloid fibril formation. *Protein science*: a publication of the Protein Society 12, 2374–2378, doi: 10.1110/ps.03152903 (2003).
8. **Chang, E., Kim, S., Schafer, K. N. & Kuret, J.** Pseudophosphorylation of tau protein directly modulates its aggregation kinetics. *Biochimica et biophysica acta* 1814, 388–395, doi: 10.1016/j.bbapap.2010.10.005 (2011).
9. **Dima, R. I. & Thirumalai, D.** Proteins associated with diseases show enhanced sequence correlation between charged residues. *Bioinformatics* 20, 2345–2354, doi: 10.1093/bioinformatics/bth245 (2004).
10. **Guest, W. C., Cashman, N. R. & Plotkin, S. S.** Electrostatics in the stability and misfolding of the prion protein: salt bridges, self energy, and solvation. *Biochemistry and cell biology* = Biochimie et biologie cellulaire 88, 371–381, doi: 10.1139/o09-180 (2010).
11. **Funk, K. E. et al.** Lysine methylation is an endogenous post-translational modification of tau protein in human brain and a modulator of aggregation propensity. *The Biochemical journal* 462, 77–88, doi: 10.1042/BJ20140372 (2014).

12. **Sant'Anna, R. et al.** The importance of a gatekeeper residue on the aggregation of transthyretin: implications for transthyretin- related amyloidoses. *The Journal of biological chemistry* 289, 28324–28337, doi: 10.1074/jbc.M114.563981 (2014).
13. **Martínez, J. et al.** Fish β-parvalbumin acquires allergenic properties by amyloid assembly. *Swiss medical weekly* (2015).
14. **Mao, Y. et al.** Charge and charge-pair mutations alter the rate of assembly and structural properties of apolipoprotein C-II amyloid fibrils. *Biochemistry* 54, 1421–1428, doi: 10.1021/bi5014535 (2015).
15. **Aguzzi, A. & Calella, A. M.** Prions: protein aggregation and infectious diseases. *Physiological reviews* 89, 1105–1152, doi: 10.1152/ physrev.00006.2009 (2009).
16. **Soto, C.** Transmissible proteins: expanding the prion heresy. *Cell* 149, 968–977, doi: 10.1016/j.cell.2012.05.007 (2012).
17. **Morillas, M., Swietnicki, W., Gambetti, P. & Surewicz, W. K.** Membrane environment alters the conformational structure of the recombinant human prion protein. *The Journal of biological chemistry* 274, 36859–36865 (1999).
18. **Li, R. et al.** Identification of an epitope in the C terminus of normal prion protein whose expression is modulated by binding events in the N terminus. *Journal of molecular biology* 301, 567–573, doi: 10.1006/jmbi.2000.3986 (2000).
19. **Wuthrich, K. & Riek, R.** Three-dimensional structures of prion proteins. *Advances in protein chemistry* 57, 55–82 (2001).
20. **Cordeiro, Y. et al.** The amino-terminal PrP domain is crucial to modulate prion misfolding and aggregation. *Biophysical journal* 89, 2667–2676, doi: 10.1529/biophysj.105.067603 (2005).
21. **Ostapchenko, V. G., Makarava, N., Savtchenko, R. & Baskakov, I. V.** The polybasic N-terminal region of the prion protein controls the physical properties of both the cellular and fibrillar forms of PrP. *Journal of molecular biology* 383, 1210–1224, doi: 10.1016/j. jmb.2008.08.073 (2008).
22. **Oliveira-Martins, J. B. et al.** Unexpected tolerance of alpha-cleavage of the prion protein to sequence variations. *PloS one* 5, e9107, doi: 10.1371/journal.pone.0009107 (2010).
23. **Boland, M. P. et al.** Anionic phospholipid interactions of the prion protein N terminus are minimally perturbing and not driven solely by the octapeptide repeat domain. *The Journal of biological chemistry* 285, 32282–32292, doi: 10.1074/jbc.M110.123398 (2010).
24. **Miller, M. B., Geoghegan, J. C. & Supattapone, S.** Dissociation of infectivity from seeding ability in prions with alternate docking mechanism. *PLoS pathogens* 7, e1002128, doi: 10.1371/journal.ppat.1002128 (2011).
25. **Turnbaugh, J. A. et al.** The N-terminal, polybasic region of PrP(C) dictates the efficiency of prion propagation by binding to PrP(Sc). *The Journal of neuroscience: the official journal of the Society for Neuroscience* 32, 8817–8830, doi: 10.1523/ JNEUROSCI.1103-12.2012 (2012).
26. **Turnbaugh, J. A., Westergard, L., Unterberger, U., Biasini, E. & Harris, D. A.** The N-terminal, polybasic region is critical for prion protein neuroprotective activity. *PloS one* 6, e25675, doi: 10.1371/journal.pone.0025675 (2011).
27. **Spevacek, A. R. et al.** Zinc drives a tertiary fold in the prion protein with familial disease mutation sites at the interface. *Structure* 21, 236–246, doi: 10.1016/j.str.2012.12.002 (2013).
28. **Sonati, T. et al.** The toxicity of antiprion antibodies is mediated by the flexible tail of the prion protein. *Nature* 501, 102–106, doi: 10.1038/nature12402 (2013).
29. **Zurawel, A. A. et al.** Prion nucleation site unmasked by transient interaction with phospholipid cofactor. *Biochemistry* 53, 68–76, doi: 10.1021/bi4014825 (2014).
30. **Benetti, F. et al.** Structural determinants in prion protein folding and stability. *Journal of molecular biology* 426, 3796–3810, doi: 10.1016/j.jmb.2014.09.017 (2014).
31. **Liu, A. et al.** NMR experiments for resonance assignments of 13C, 15N doubly-labeled flexible polypeptides: application to the human prion protein hPrP(23-230). *Journal of biomolecular NMR* 16, 127–138 (2000).
32. **Morante, S. et al.** Inter- and intra-octarepeat Cu(II) site geometries in the prion protein: implications in Cu(II) binding cooperativity and Cu(II)-mediated assemblies. *The Journal of biological chemistry* 279, 11753–11759, doi: 10.1074/jbc.M312860200 (2004).
33. **Kim, S. J., Rahbar, R. & Hegde, R. S.** Combinatorial control of prion protein biogenesis by the signal sequence and transmembrane domain. *The Journal of biological chemistry* 276, 26132–26140, doi: 10.1074/jbc.M101638200 (2001).
34. **Johanssen, V. A. et al.** C-terminal peptides modelling constitutive PrPC processing demonstrate ameliorated toxicity predisposition consequent to alpha-cleavage. *The Biochemical journal* 459, 103–115, doi: 10.1042/BJ20131378 (2014).
35. **Groveman, B. R. et al.** Charge neutralization of the central lysine cluster in prion protein (PrP) promotes PrP(Sc)-like folding of recombinant PrP amyloids. *The Journal of biological chemistry* 290, 1119–1128, doi: 10.1074/jbc.M114.619627 (2015).
36. **Chiesa, R., Piccardo, P., Ghetti, B. & Harris, D. A.** Neurological illness in transgenic mice expressing a prion protein with an insertional mutation. *Neuron* 21, 1339–1351 (1998).
37. **Leliveld, S. R., Stitz, L. & Korth, C.** Expansion of the octarepeat domain alters the misfolding pathway but not the folding pathway of the prion protein. *Biochemistry* 47, 6267–6278, doi: 10.1021/bi800253c (2008).

38. **Speare, J. O., Rush, T. S.,** 3rd, Bloom, M. E. & Caughey, B. The role of helix 1 aspartates and salt bridges in the stability and conversion of prion protein. *The Journal of biological chemistry* 278, 12522–12529, doi: 10.1074/jbc.M211599200 (2003).
39. **Zahn, R. et al.** NMR solution structure of the human prion protein. *Proceedings of the National Academy of Sciences of the United States of America* 97, 145–150 (2000).
40. **Calzolai, L. & Zahn, R.** Influence of pH on NMR structure and stability of the human prion protein globular domain. *The Journal of biological chemistry* 278, 35592–35596, doi: 10.1074/jbc.M303005200 (2003).
41. **Zuegg, J. & Gready, J. E.** Molecular dynamics simulations of human prion protein: importance of correct treatment of electrostatic interactions. *Biochemistry* 38, 13862–13876 (1999).
42. **Norstrom, E. M. & Mastrianni, J. A.** The charge structure of helix 1 in the prion protein regulates conversion to pathogenic PrPSc. *Journal of virology* 80, 8521–8529, doi: 10.1128/JVI.00366-06 (2006).
43. **Dumetz, A. C., Chockla, A. M., Kaler, E. W. & Lenhoff, A. M.** Effects of pH on protein-protein interactions and implications for protein phase behavior. *Biochimica et biophysica acta* 1784, 600–610, doi: 10.1016/j.bbapap.2007.12.016 (2008).
44. **Gabizon, R. et al.** Insoluble wild-type and protease-resistant mutant prion protein in brains of patients with inherited prion disease. *Nature medicine* 2, 59–64 (1996).
45. **Hsiao, K. et al.** Mutant prion proteins in Gerstmann-Straussler-Scheinker disease with neurofibrillary tangles. *Nature genetics* 1, 68–71, doi: 10.1038/ng0492-68 (1992).
46. **Lee, C. I., Yang, Q., Perrier, V. & Baskakov, I. V.** The dominant-negative effect of the Q218K variant of the prion protein does not require protein X. *Protein science*: a publication of the Protein Society 16, 2166–2173, doi: 10.1110/ps.072954607 (2007).
47. **Georgieva, D. et al.** Oligomerization of the proteolytic products is an intrinsic property of prion proteins. *Biochemical and biophysical research communications* 323, 1278–1286, doi: 10.1016/j.bbrc.2004.08.230 (2004).
48. **Lisa, S. et al.** The structural intolerance of the PrP alpha-fold for polar substitution of the helix-3 methionines. *Cellular and molecular life sciences*: CMLS 67, 2825–2838, doi: 10.1007/s00018-010-0363-1 (2010).
49. **Thakur, A. K., Srivastava, A. K., Srinivas, V., Chary, K. V. & Rao, C. M.** Copper alters aggregation behavior of prion protein and induces novel interactions between its N- and C-terminal regions. *The Journal of biological chemistry* 286, 38533–38545, doi: 10.1074/jbc.M111.265645 (2011).
50. **Liemann, S. & Glockshuber, R.** Influence of amino acid substitutions related to inherited human prion diseases on the thermodynamic stability of the cellular prion protein. *Biochemistry* 38, 3258–3267, doi: 10.1021/bi982714g (1999).
51. **Apetri, A. C., Surewicz, K. & Surewicz, W. K.** The effect of disease-associated mutations on the folding pathway of human prion protein. *The Journal of biological chemistry* 279, 18008–18014, doi: 10.1074/jbc.M313581200 (2004).
52. **Bera, A. & Nandi, P. K.** Nucleic acid induced unfolding of recombinant prion protein globular fragment is pH dependent. *Protein science*: a publication of the Protein Society 23, 1780–1788, doi: 10.1002/pro.2573 (2014).
53. **Canello, T. et al.** Oxidation of Helix-3 methionines precedes the formation of PK resistant PrP. *PLoS pathogens* 6, e1000977, doi: 10.1371/journal.ppat.1000977 (2010).
54. **Xiao, S. et al.** Rational modification of protein stability by targeting surface sites leads to complicated results. *Proceedings of the National Academy of Sciences of the United States of America* 110, 11337–11342, doi: 10.1073/pnas.1222245110 (2013).
55. **Kraus, A., Groveman, B. R. & Caughey, B.** Prions and the potential transmissibility of protein misfolding diseases. *Annual review of microbiology* 67, 543–564, doi: 10.1146/annurev-micro-092412-155735 (2013).
56. **Prusiner, S. B.** Biology and genetics of prions causing neurodegeneration. *Annual review of genetics* 47, 601–623, doi: 10.1146/annurev-genet-110711-155524 (2013).
57. **Cobb, N. J., Sonnichsen, F. D., McHaourab, H. & Surewicz, W. K.** Molecular architecture of human prion protein amyloid: a parallel, in-register beta-structure. *Proceedings of the National Academy of Sciences of the United States of America* 104, 18946–18951, doi: 10.1073/pnas.0706522104 (2007).
58. **Qi, X., Moore, R. A. & McGuirl, M. A.** Dissociation of recombinant prion protein fibrils into short protofilaments: implications for the endocytic pathway and involvement of the N-terminal domain. *Biochemistry* 51, 4600–4608, doi: 10.1021/bi300201e (2012).
59. **Supattapone, S.** Synthesis of high titer infectious prions with cofactor molecules. *The Journal of biological chemistry* 289, 19850–19854, doi: 10.1074/jbc.R113.511329 (2014).
60. **Chen, S. G. et al.** Truncated forms of the human prion protein in normal brain and in prion diseases. The *Journal of biological chemistry* 270, 19173–19180 (1995).
61. **Walmsley, A. R., Watt, N. T., Taylor, D. R., Perera, W. S. & Hooper, N. M**. alpha-cleavage of the prion protein occurs in a late compartment of the secretory pathway and is independent of lipid rafts. *Molecular and cellular neurosciences* 40, 242–248, doi: 10.1016/j.mcn.2008.10.012 (2009).

62. **McDonald, A. J., Dibble, J. P., Evans, E. G. & Millhauser, G. L.** A new paradigm for enzymatic control of alpha-cleavage and beta-cleavage of the prion protein. *The Journal of biological chemistry* 289, 803–813, doi: 10.1074/jbc.M113.502351 (2014).
63. **Gonzalez-Iglesias, R. et al.** Prion protein interaction with glycosaminoglycan occurs with the formation of oligomeric complexes stabilized by Cu(II) bridges. *Journal of molecular biology* 319, 527–540, doi: 10.1016/S0022-2836(02)00341-8 (2002).
64. **Leucht, C. et al.** The 37 kDa/67 kDa laminin receptor is required for PrP(Sc) propagation in scrapie-infected neuronal cells. *EMBO reports* 4, 290–295, doi: 10.1038/sj.embor.embor768 (2003).
65. **Sanghera, N. et al.** Deciphering the molecular details for the binding of the prion protein to main ganglioside GM1 of neuronal membranes. *Chemistry & biology* 18, 1422–1431, doi: 10.1016/j.chembiol.2011.08.016 (2011).
66. **Ostapchenko, V. G. et al.** Two amyloid States of the prion protein display significantly different folding patterns. *Journal of molecular biology* 400, 908–921, doi: 10.1016/j.jmb.2010.05.051 (2010).
67. **Klimova, N., Makarava, N. & Baskakov, I. V.** The diversity and relationship of prion protein self-replicating states. *Virus research*. doi: 10.1016/j.virusres.2014.10.002 (2014).
68. **Miller, M. B. et al.** Cofactor molecules induce structural transformation during infectious prion formation. *Structure* 21, 2061–2068, doi: 10.1016/j.str.2013.08.025 (2013).
69. **Noble, G. P., Walsh, D. J., Miller, M. B., Jackson, W. S. & Supattapone, S.** Requirements for mutant and wild-type prion protein misfolding in vitro. *Biochemistry* 54, 1180–1187, doi: 10.1021/bi501495j (2015).
70. **McKinley, M. P. & Prusiner, S. B.** Ultrastructural studies of prions. *Current topics in microbiology and immunology* 172, 75–91 (1991).
71. **Juanes, M. E., Elvira, G., Garcia-Grande, A., Calero, M. & Gasset, M.** Biosynthesis of prion protein nucleocytoplasmic isoforms by alternative initiation of translation. *The Journal of biological chemistry* 284, 2787–2794, doi: 10.1074/jbc.M804051200 (2009).
72. **Colombo, G., Meli, M., Morra, G., Gabizon, R. & Gasset, M.** Methionine sulfoxides on prion protein Helix-3 switch on the alpha-fold destabilization required for conversion. *PloS one* 4, e4296, doi: 10.1371/journal.pone.0004296 (2009).
73. **Martinez, J. et al.** Selenomethionine incorporation into amyloid sequences regulates fibrillogenesis and toxicity. *PloS one* 6, e27999, doi: 10.1371/journal.pone.0027999 (2011).
74. **Millhauser, G. L.** Copper and the prion protein: methods, structures, function, and disease. *Annual review of physical chemistry* 58, 299–320, doi: 10.1146/annurev.physchem.58.032806.104657 (2007).
75. **Lau, A. et al.** Octarepeat region flexibility impacts prion function, endoproteolysis and disease manifestation. *EMBO molecular medicine* 7, 339–356, doi: 10.15252/emmm.201404588 (2015).
76. **Horiuchi, M. & Caughey, B.** Specific binding of normal prion protein to the scrapie form via a localized domain initiates its conversion to the protease-resistant state. *The EMBO journal* 18, 3193–3203, doi: 10.1093/emboj/18.12.3193 (1999).
77. **Tycko, R., Savtchenko, R., Ostapchenko, V. G., Makarava, N. & Baskakov, I. V.** The alpha-helical C-terminal domain of full-length recombinant PrP converts to an in-register parallel beta-sheet structure in PrP fibrils: evidence from solid state nuclear magnetic resonance. *Biochemistry* 49, 9488–9497, doi: 10.1021/bi1013134 (2010).
78. **Rezaei, H. et al.** High yield purification and physico-chemical properties of full-length recombinant allelic variants of sheep prion protein linked to scrapie susceptibility. *European journal of biochemistry/FEBS* 267, 2833–2839 (2000).
79. **Ostapchenko, V., Gasset, M. & Baskakov, I. V.** Atomic force fluorescence microscopy in the characterization of amyloid fibril assembly and oligomeric intermediates. *Methods Mol Biol* 849, 157–167, doi: 10.1007/978-1-61779-551-0_11 (2012).
80. **Lisa, S. et al.** Failure of prion protein oxidative folding guides the formation of toxic transmembrane forms. *The Journal of biological chemistry* 287, 36693–36701, doi: 10.1074/jbc.M112.398776 (2012).

Supplementary Information

Table S1. List of primers used in this study

Mutation	Template	Primer (forward)
K2	pETHaPrP(23-231)	5'-CATATGAAGGAGCGGCCAGAGCCTGGAG-3'
K2-E200K	pETHaPrP(23-231) K2	5'-GGAGAACTTCACGAAGACCGACATCAAG-3'
K2	pcDNA-HaPrP(1-254)	5´-GCCTCTGCAAGGAGCGGCCAGAGCCTGGAG-3
K4	pETHaPrP(23-231)	5´-GTGGAACGAGCCCAGTGAGCCAGAAACCAACATGGAGCACATGG-3´
K4	pcDNA-HaPrP(1-254)	5´-CAGTGGAACGAGCCTTCGGACCCAGAAACCAACATGGAGCACATGG-3´
K6	pETHaPrP(23-231) K4	5'-CATATGAAGGAGCGGCCAGAGCCTGGAG-3'
K6	pcDNA-HaPrP(1-254) K4	5´-GCCTCTGCAAGGAGCGGCCAGAGCCTGGAG-3
E200K	pETHaPrP(23-231) pcDNA-HaPrP(1-254)	5'-GGAGAACTTCACGAAGACCGACATCAAG-3'
Q217R	pETHaPrP(23-231) pcDNA-HaPrP(1-254)	5'-GTGTACCACCCGGTATCAGAAGGAG-3'
Q219K	pETHaPrP(23-231) pcDNA-HaPrP(1-254)	5´-CAGATGTGTACCACCCAGTATAAGAAGGAG-3'
E221K	pETHaPrP(23-231) pcDNA-HaPrP(1-254)	5'- CAGTATCAGAAGAAGTCCCAGGCCTACTAC-3'

Objetivo III. La adquisición de propiedades alergénicas en la β-Parvalbumina de pescado requiere la formación del estado amiloide.

ANTECEDENTES: Muchos estudios modelo de formación de amiloides hacen uso de medios ácidos, que se asemejan a las condiciones a las que se exponen los alérgenos alimentarios de tipo-I durante el proceso de digestión gastrointestinal y en las que adquieren unas propiedades de resistencia similares a las de dichos polímeros [98,313-315,341]. De los alérgenos alimentarios tipo I, las β-parvalbúminas son responsables del 90% de las alergias al pescado y de la elevada reactividad cruzada entre especies [322,326,342]. Estructuralmente, las β-parvalbúminas están constituidas por una única secuencia con tres motivos hélice-loop-hélice (AB,CD y EF), de los que sólo CD y EF constituyen sitios funcionales de unión a Ca^{2+} [326,342], cuya saturación parece ser esencial para el reconocimiento por IgE [329,342].

OBJETIVO: Determinar el papel de la formación de amiloides en el proceso de estabilización de Gad m 1 durante la digestión gastrointestinal y en la generación de especies con capacidad de interacción de igE.

METODOS: La determinación de la existencia y localización de segmentos adhesivos en las secuencias de β-parvalbúmina de peces con valor comercial se realizó empleando el algoritmo ZipperDB. La formación de amiloides y su reactividad frente a IgE de sueros de pacientes se determinaron empleando medidas de unión de ThT, SDS-PAGE, CD, DLS, AFM, proteólisis y dot-blot con condiciones de simulación gástrica (SGF), intestinal (SIF) o gastro-intestinal (SGIF), en presencia y ausencia de Ca^{2+}.

RESULTADOS: El estudio teórico de las secuencias de β-parvalbúminas de peces con valor comercial demostró la presencia de segmentos adhesivos en las regiones A, C, y E/F que flanquean los sitios de unión de Ca^{2+}, y que en el caso de E/F solapa con los epítopos de IgE. Tomando como modelo rGad m 1 por su alta reactividad cruzada con IgE, los experimentos de unión de ThT, SDS-PAGE, CD y AFM, demostraron la existencia de un proceso de formación de amiloides asociado a la estabilización de la forma Apo bien a pH ácido (SGF) o en presencia del quelante EDTA (SIF). Estos amiloides son resistentes a la proteólisis gastrointestinal, y en función de la disponibilidad de Ca^{2+} y de la concentración de proteína, se disocian liberando monómeros y oligómeros. De las tres especies (monómeros, oligómeros y fibras) solo los polímeros fibrosos interaccionan con IgE de suero de pacientes alérgicos al pescado.

CONCLUSIONES: rGad m 1, modelo de alérgeno alimentario de tipo I, permite la resistencia a la digestión gastro-intestinal, su facilidad para atravesar el epitelio intestinal y la aparición de epítopos estructurales de la forma fibrilar reconocido por IgE.

Contribución: generación de rGad m 1 (producción, aislamiento y purificación), realización y análisis de las cinéticas de unión de ThT, caracterización de los productos mediante AFM, DLS, proteólisis, dicroísmo y unión de IgE de sueros de pacientes mediante dot-blot.

Swiss Medical Weekly

Fish β-parvalbumin acquires allergenic properties by amyloid assembly

Javier Martínez[a], Rosa Sánchez[a], Milagros Castellanos[b], Ana M. Fernández-Escamilla[c], Sonia Vázquez-Cortés[d], Montserrat Fernández- Rivas[d], María Gasset[a]

a Instituto Química-Física "Rocasolano", Consejo Superior de Investigaciones Científicas, Madrid, Spain.
b Centro Nacional de Biotecnología, Consejo Superior de Investigaciones Científicas, Madrid, Spain.
c Estación Experimental del Zaidín, Consejo Superior de Investigaciones Científicas, Granada, Spain.
d Allergy Department, Hospital Clínico San Carlos, IdISSC, Madrid, Spain

Original article | Published 29 May 2015, doi:10.4414/smw.2015.14128, **Cite this as:** Swiss Med Wkly. 2015;145:w14128

Summary

PRINCIPLES: Amyloids are highly cross-β-sheet rich aggregated states that confer protease resistance, membrane activity and multivalence properties to proteins, all essential features for the undesired preservation of food proteins transiting the gastrointestinal tract and causing type I allergy.

METHODS: Amyloid propensity of β-parvalbumin, the major fish allergen, was theoretically analysed and assayed under gastrointestinal-relevant conditions using the binding of thioflavin T, the formation of sodium dodecyl sulphate-(SDS) resistant aggregates, circular dichroism spectroscopy and atomic force microscopy fibril imaging. Impact of amyloid aggregates on allergenicity was assessed with dot blot.

RESULTS: Sequences of β-parvalbumin from species with commercial value contain several adhesive hexapeptides capable of driving amyloid formation. Using Atlantic cod β-parvalbumin (rGad m 1) displaying high IgE cross-reactivity, we found that formation of amyloid fibres under simulated gastrointestinal conditions accounts for the resistance to acid and neutral proteases, for the presence of membrane active species under gastrointestinal relevant conditions and for the IgE-recognition in the sera of allergic patients. Incorporation of the anti-amyloid compound epigallocatechin gallate prevents rGad m 1 fibrillation, facilitates its protease digestion and impairs its recognition by IgE.

CONCLUSIONS: the formation of amyloid by rGad m 1 explains its degradation resistance, its facilitated passage across the intestinal epithelial barrier and its epitope architecture as allergen.

Key words: type I food allergy; fish allergens; fish β-parvalbumin; amyloids

Introduction

More than 5% of the population suffer from type I food al- lergy, an immunoglobulin E-(IgE) mediated hypersensitivity disease provoked by food proteins [1–3]. Type I food allergy involves two main phases; a sensitisation step and an effector phase [3–5]. The sensitisation occurs in the gastrointestinal tract (GIT) after the contact with the ingested allergen and consists in a series of events leading to an overproduction of allergen-specific IgE able to bind to the high-affinity IgE receptor FcεRI on the surface of basophils and mast cells. In the effector phase, the causative al- lergen crosses the intestinal epithelium and cross-links the IgE-FcεRI complexes, provoking effector cell activation and the release of allergy mediators. Although individual reactivity depends on genetic and environmental factors, stability of food allergens through the GIT is an essential requirement for their pathogenicity [3, 6–9]. The stability confers resistance to heat treatments, to drastic pH changes (pH 2–7.5), to acid and neutral proteases and to detergents, and permits the preservation of immunogenic motifs for interaction with the epithelial immune system or passage through the epithelial barrier in order to induce sensitisation and systemic symptoms [8, 9]. These properties are shared by more than 120 molecular architectures with different folds, suggesting as yet unknown common structural threats [10, 11].

Pathogenic proteins such as prions display such stability by virtue of their amyloid fibrillar state [12, 13]. Amyloid fibrils are insoluble protein aggregates with a highly compact spine based on a cross-β-sheet structure [14–18]. This structure comprises an indefinitely repeating intermolecular β-sheet motif, in which each pair of intermolecular β sheets interdigitate their side chains as a steric zipper. Amyloids are very stable and more resistant to hydrolysis than the folded globular protein, and upon the proper signal they can release monomers and create a population of different oligomeric and polymeric intermediates [18, 19]. Amyloid fibrils are considered poorly immunogenic, but their aggregated fragments as prefibrillar oligomers and fibrillar oligomers have yielded very valuable conformational antibodies [20, 21]. Therefore, assembly into amyloid-like structures by food allergens could explain some of their pathogenic properties.

Results

To address the question of whether degradation properties and preservation of monomers involves amyloid-like aggregates we chose β-parvalbumins, the main elicitors of IgE-mediated reactions in fish-allergic individuals [26]. The β-parvalbumins are Ca^{2+} binding proteins of about 12 kDa and contribute >2.5 mg per gram to raw fish muscle [26–28]. They fold into a structure consisting of three EF-hand motifs (AB, CD and EF) (**fig. 1A**), of which only CD and EF can bind divalent cations (Ca^{2+} and/or Mg^{2+}) [26,27]. The major immunologically reactive sites have been found on the junction between the motifs (regions 33–44, 65–74) and on the EF region (segments 88–96 and 95–109) [26, 29–31]. Ca-bound forms are extremely stable and even cooking cannot alter their allergenicity [26]. However, loss of calcium causes an altered conformation, with decreased stability and impaired IgE recognition [26,32].

To adopt the amyloid conformation, proteins must contain segments which are able to form a steric zipper [17, 18]. These segments must be exposed to solvent and achieve a local concentration high enough to overcome the entropy of fibre formation [14–16]. We first asked whether β-par- valbumin sequences from fish with commercial value contain adhesive hexapeptides forming steric zippers using the Zipper Db algorithm [17]. All sequences tested displayed at least two regions with adhesive properties, mainly overlapping A, E and F helical regions (**fig. 1**). Importantly, the adhesive sequence AETKAF located at helix E and linking IgE epitopes is highly conserved and only some herring and mackerel sequences do not have it (**fig. 1**).

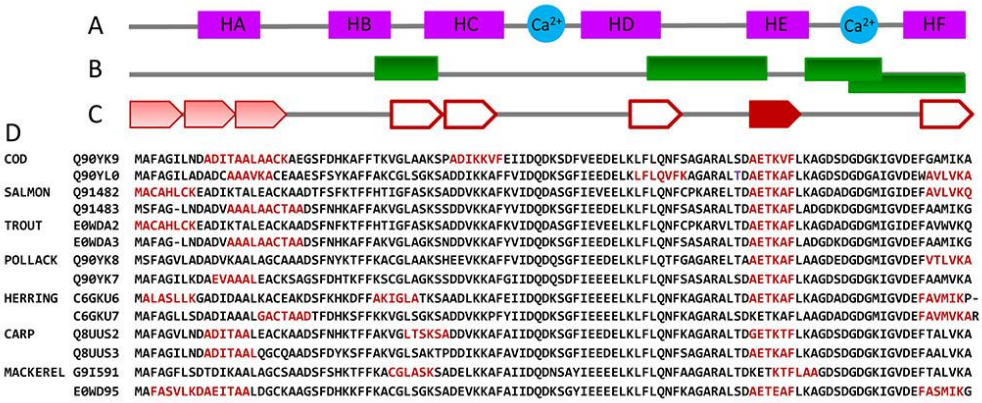

Figure 1. **Propensity of fish β-parvalbumin sequences to form amyloids.** (A) Fish β-parvalbumin fold described for cod (PDB ID:2MBX), carp (PDB ID: 4CPV), hake (PDB ID: 1BU3), pike (PDB ID: 1PVB) and whiting (PDB ID: 1A75) chains is largely conserved and consist of six α-helices pairing as AB, CD and EF forming three EF-hand motifs, two of which (CD and EF) coordinate Ca^{2+}. (B) Immunological reactive sites described for fish β-parvalbumins, shown as green rectangles, embrace the spacers between motifs and on the C-terminal motif [29-31]. (C) Some hexapeptides with adhesive properties found in β-parvalbumin sequences from commercially valuable fish and known allergic potential using Zipper Db flank the immunological reactive sites. Hexapeptides (single or extended) are depicted in red, by (C) arrows (the saturation of the color is proportional to the similarity of the segments) and by (D) their sequences.

Once the theoretical capacity had been identified, to test amyloid formation we selected Atlantic cod β-parvalbumin (Gad m 1) as a model given its high IgE cross reactivity, and assayed the binding of the amyloid-specific dye thioflavin T (ThT), the formation of SDS-resistant aggregates by means of SDS-PAGE, the presence of β-sheet structures measured with circular dichroism (CD) spectroscopy, and the presence of fibrils in atomic force microscopy (AFM) images. These analyses were performed while simulating the gastric (SGF: 50 mM HCl-Gly pH 2, 35 mM NaCl) and the intestinal (SIF: 50 mM Tris-HCl pH 7.4, 35 mM NaCl) fluids, both in the presence of 5 mM EDTA or 5 mM $CaCl^{2+}$ to account for cation-free and bound forms. Recombinant Gad m 1 showed fast fibrillation under intestinal conditions in the presence of EDTA as assessed with ThT binding (**fig. 2A**), solubility assays (**fig. 2B**), SDS- PAGE (**fig. 2C**), CD (**fig. 2D**) and AFM (**fig. 2E**). At acid pH where Ca^{2+} binding is impeded by protonation of the side chains involved in its binding site, rGad m 1 aggregated both in the presence of EDTA or Ca^{2+} (**fig. 2A–E**). Aggregation is initiated from the α-helix-poor conformation of the apoform that evolves into a β-sheet-rich conformation (**fig. 2D**). Under these conditions fibrils were notably present, but aggregation was predominated by lentil shaped oligomers (oblate ellipsoids) about 2 nm high and 40 nm wide. Since transit through the gastrointestinal tract involves exposure first to pH 2 and then to pH>6.5, we simulated the process by

performing a 10-min preincuba- tion at pH 2 followed by dilution to pH 7.4. Under these conditions, rGad m 1 formed fibrils in the presence of both EDTA and Ca^{2+} (**fig. 2A–E**). Importantly, exposure to pH<2.5 plays a key role in permitting Ca^{2+}-bound rGad m 1 tofibrillate, since incubation at pH>4.5 impeded the process (**fig. 2A**, **fig. 2E**). On the other hand, the slower rate and efficiency observed in the presence of Ca^{2+} compared with EDTA under simulated gastrointestinal conditions suggest competition between aggregation and cation binding.

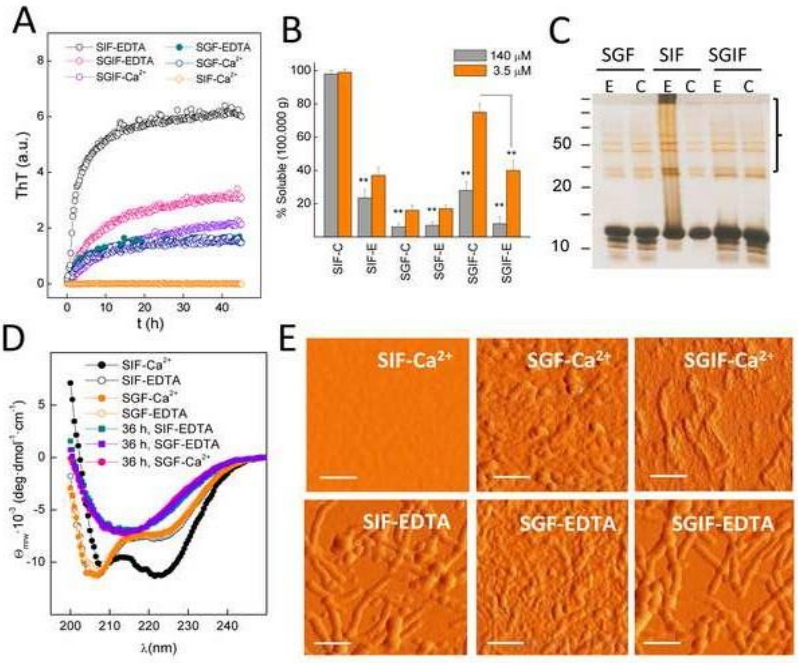

Figure 2. Amyloid-like aggregation of cod β-parvalbumin (A) Kinetics of Thioflavin T (ThT) binding indicate rGad m 1 fibril formation under simulated gastric fluid (SGF), simulated intestinal fluid (SIF) supplemented with 5 mM EDTA and simulated gastrointestinal fluid (SGIF) containing either 5 mM EDTA or 5 mM $CaCl_2$. Reactions were performed at 37 °C using 140 µM rGad m1, and the measured fluorescence counts normalized. (B) Percentage of soluble rGad m 1 recovered in the supernatants of a 100.000 x g centrifugation of 36 h incubations in SIF, SGF and SIGF, supplemented with 5 mM EDTA (E) or 5 mM $CaCl_2$ (C) show formation of insoluble aggregates under those conditions with increased ThT binding. Incubations were performed at 3.5 and 140 µM rGad m 1. Solubility percentages were determined measuring the protein concentration in both the soluble and the pellet fraction using triplicates. Bar charts are presented as mean ± standard deviation (n = 3); $^{**}P < 0.05$. (C) Analysis of rGad m 1 aggregates by use of sodium dodecyl sulfate polyacrilamide gel electrphoresis (SDS-PAGE) and silver staining shows bands at high molecular weight corresponding to SDS-resistance aggregates. (D) Circular dichroism (CD) spectra of 60 µM rGad m 1 in SGF and SIF supplemented with either 5 mM EDTA or 5 mM $CaCl_2$ indicate β-sheet structures after 36 h incubation of the apoforms. (E) Atomic forcé microscopy (AFM) images of rGad m1 incubated for 36 h under SGF, SIF and SGIF supplemented with 5 mM EDTA or 5 mM $CaCl_2$ indicating the formation of aggregates and of their fibrillar shape. Scale bars 100 nm.

To assess whether amyloid formation confers protease resistance, we analysed the rGad m 1 proteolytic pattern under GIT-relevant conditions (**fig. 3A**). In SGF (pH 2) containing either EDTA or Ca^{2+} at 5 mM, rGad m 1, freshly dissolved or preincubated for 36 h in such media, resists the action of pepsin and generates full length and truncated chains. Increasing the pH to 7.4 and adding proteinase K instead of the mixture of trypsin and chymotrypsin to minimise the strong Ca^{2+} dependence of protease activity, showed no further digestion. On the contrary, when rGad m 1 was

treated with 20 µM of the anti-amyloid compound epigallocatechin gallate (ECGC) [33] to impair fibril assembly (**fig. 3B**), acid and neutral digestion proceed with significantly higher efficiency (**fig. 3A**).

To demonstrate that amyloid fibrils function as depots and release species, we performed a fibre release assay under GIT-relevant conditions [34]. For this purpose, rGad m 1 fibrils were harvested by centrifugation and diluted in SIF, both in the presence and absence of Ca^{2+}, and the process was analysed by means of ThT binding (**fig. 3C**), CD (**fig. 3D**) and DLS (**fig. 3E**). Incubation of fibrils in SIF containing EDTA concurs with about 50% reduction of ThT fluorescence and minor changes in the CD spectrum, indicating the dissociation of fibrils into entities with similar secondary structure. DLS analysis of the supernatant of a 100,000 x g centrifugation revealed, as function of pro- tein concentration, species with RH of 2.2 ± 0.2 nm, 4.5 ± 0.5 nm and 21 ± 0.5 nm which correspond to Ca^{2+}-free monomers and oligomers. In contrast, fibrils incubated in SIF with Ca^{2+} underwent a larger reduction in ThT binding and changes in the CD indicating an increase in α-helix structure. In this case, the supernatant contained only Ca^{2+}-bound (RH = 1.85 ± 0.1 nm) and Ca^{2+}-free (RH = 2.2 ± 0.2 nm) monomers. Taken together, these results indicated that rGad m 1 fibrils release oligomers and monomers, whose relative populations depend on Ca^{2+} availability and the protein concentration.

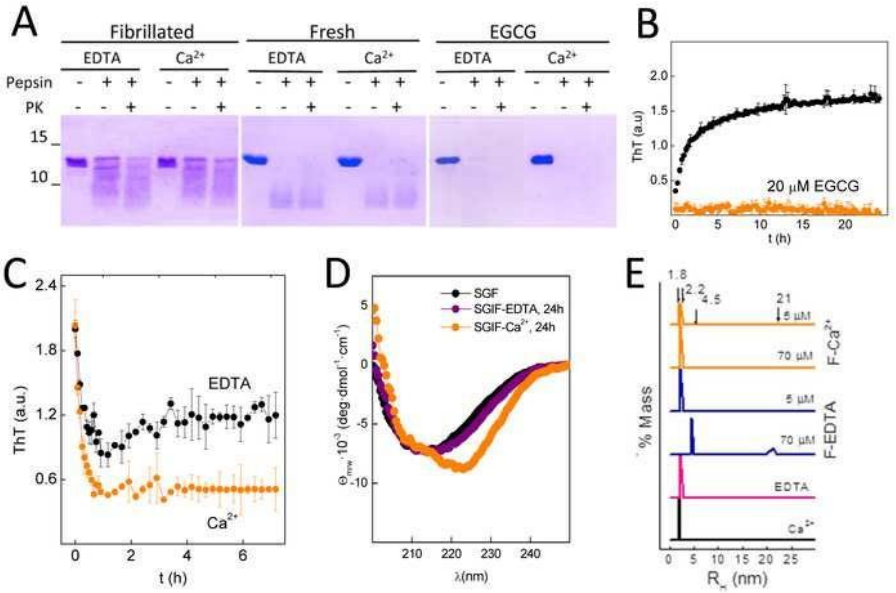

Figure 3. Amyloid fibrils protect rGad m1 from protease digestion and function as depots releasing distinct species. (A) sodium dodecyl sulfate polyacrylamide gel electrophoresis (SDS-PAGE) analysis of gastric (pepsin at pH 2.0) and gastrointestinal (pepsin at pH 2.0 followed by proteinase K at pH 7.4) digestions of freshly prepared solutions or after 36 h of fibrillation in SGF, in the absence and presence of 20 µM of epigallatocatechin (ECGC), show amyloid-assembly protects monomers from proteolysis. Gels were stained with Coomassie blue. (B) Incubation of rGad m 1 with ECGC (20 µM) prevents the thioflavine T (ThT) fluorescence increase due to fibrillation. Incubation was performed for 15 min in simulated gastric fluid (SGF) and then brought to simulated intestinal fluid (SIF) conditions. Data correspond to two independent experiments performed in triplicate. (C) Time-course decrease of ThT fluorescence of rGad m 1 fibrils resuspended in SIF containing either 5 mM EDTA or 5 mM $CaCl_2$ indicates amyloid disassembly. (D) Evolution of the CD spectrum of rGad m1 fibrils after resuspension in SIF containing either 5 mM EDTA or 5 mM $CaCl_2$ reveal effects of amyloid disassembly on secondary structure. Spectra were recorded 3h after resuspension. (E) DLS analysis of soluble rGad m 1 obtained in the supernatant of a 100,000 x g centrifugation of amyloid fibrils resuspended in SGF and SIF containing either 5 mM EDTA or 5 mM $CaCl_2$ show the release of monomers and oligomers. Species with R_H of 1.8 ± 0.1 nm 2.2 ± 0.2 nm correspond to Ca^{2+}-bound and free monomers, and those with 4.5 ± 0.5 nm and 21 ± 0.5 nm to oligomers.

Importantly, both amyloid fibrils and oligomers are membrane-active structures with the ability to increase permeability, which could play a role in facilitation of passage of the allergen through the intestinal epithelium, which is required for the sensitisation and the effector phases [35, 36].

To assess the allergenicity of the different rGad m 1 species (monomers, oligomers and fibrils) we tested their IgE recognition by means of dot blot analysis using sera of two patients allergic to fish and sensitised to fish parvalbumin (**fig. 4A**). Unexpectedly, all forms involving presence of amyloid aggregates were recognised by the sera of fish-allergic patients with an affinity pattern similar to that of the anti-amyloid fibrils OC antibody but different from that of anti-oligomers A11 antibody. Indeed, IgE reactivity was associated with the insoluble aggregates isolated in the pellet fraction of a 100,000 x g centrifugation (**fig. 4B**) and was prevented by incubation with the anti-amyloid compound EGCG and by their denaturation with GdnCl (**fig. 4A**). Moreover, IgE reactivity is specific for rGad m 1 amyloids since Aβ1–40 and PrP fibrils displaying anti-amyloid fib ril OC antibody reactivity were not recognised by patient sera (**fig. 4C**). These data indicated that serum recognition involved amyloid assembly and resulted from a fibril-induced protein specific epitope (**fig. 4A**).

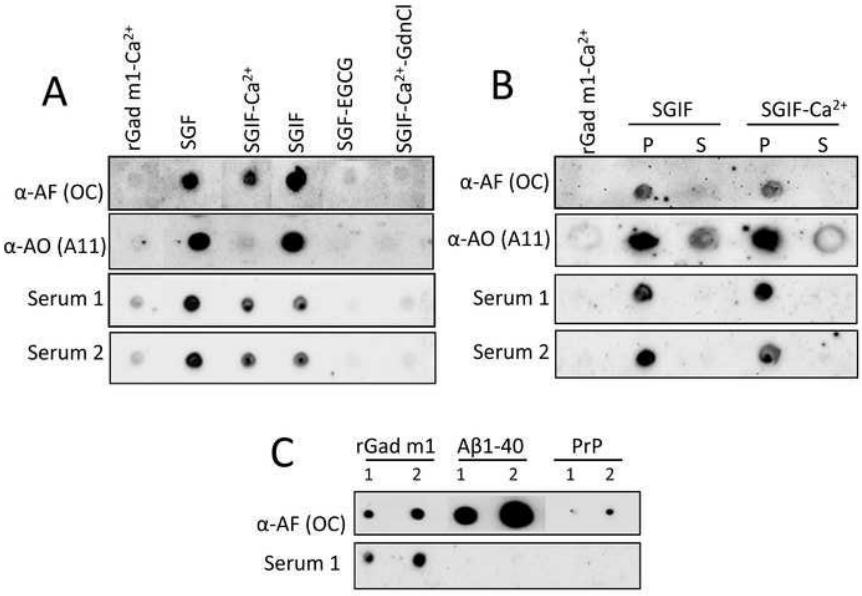

Figure 4. IgE from fish allergic patients sera recognises the rGad m 1 amyloid fibrils. (A) Dot-blot analysis of the immunoreactivity of rGad m 1 species probed with anti-amyloid fibrils (OC), anti-amyloid oligomer (A11) antibodies and with the sera from two fish-allergic patients indicate IgE binding to native amyloid fibrils. Dots correspond to 20 ng of fresh rGad m 1 solution in simulated intestinal fluid (SIF) containing 5 mM Ca^{2+}, rGad m 1 fibrillated for 36 h in simulated gastric fluid (SGF) and then diluted 1/50 in SGF, SIF with 5 mM EDTA (SGIF), SIF with 5 mM CaCl (SGIF-Ca^{2+}) and SIF with 5 mM $CaCl_2$ and 6 M GdnCl. SGF- epigallocatechin gallate (EGCG) corresponds to rGad m1 incubated in the presence of 20 μM EGCG for 36 h and then diluted 1/50 in SGF. (B) Separation of soluble (S) and pellet (P) fractions reveal that allergic patients IgE recognise insoluble amyloid fibrils. Fibrils formed at 140 μM protein concentration in SGF were diluted 1/50 in SIF either with 5 mM EDTA (SGIF) or 5 mM $CaCl_2$ (SGIF-Ca) and centrifuged at 100,000xg for 1 h at 4 °C. (C) Anti-amyloid fibrils antibody (OC) reacts with amyloid assemblies of rGad m 1, Aβ1–40 and HaPrP 23–231, but IgE from allergic patients sera recognised specifically rGad m 1 fibrils. Labels 1 and 2 correspond to the load of 10 and 20 ng of protein, respectively.

Discussion

Despite the large variety of proteins present in foods, only a few of them are capable of sensitising and eliciting an IgE response [1–3]. These food allergens are mainly present in milk, egg, peanut, wheat, fish and shellfish, and consist of a limited number of protein families with various functions (hydrolases, binding and transport of ligands, storage and cytoskeleton scaffolds) [11, 37, 38]. Food allergens undergo large environmental changes during digestion, triggering profound structural alterations that can be crucial for their pathogenicity. Formation of amyloid aggregates under GIT conditions has been reported for several model proteins, some of which, such as ovalbumin, β-lactoglobulin and lysozyme, behave as food allergens [34, 39, 40–42]. It must be stressed that the amyloid structural signature was established in protein extracts rich in ovalbumin and legumin [39]. Here, we show that rGad m 1, the major type I fish allergen, also forms amyloids in the GIT, and that these assemblies are crucial for allergenicity. This amyloidogenesis explains the role of the GIT, the concentration and ligand dependence, the degradation resistance, the facilitated passage across the intestinal epithelial barrier and the architecture of the IgE epitope.

Aggregation of fish parvalbumin into fibrils occurs through its apo-form, which is consistent with the proamyloid properties of the ligand-free state of proteins such as apomyoglobin and apolipoproteins [43, 44]. It also suggests that the milk allergen apo-Bos d 5 may undergo a similar aggregation event [45]. For fish parvalbumin, the proamyloid form is stabilised by either acid pH or chelates, indicating that gastric pH and food composition (citrates, polyanions, etc) may regulate the efficiency of the aggregation process. On the other hand, the dependence of amyloid formation, both seeding and growing, on the monomer concentration also agrees with the reported variations in pepsin resistance and in the allergenicity of different fish species [28]. Transit through the intestine increases the pH, conditions that favour fibrillation of rGad m 1. At this stage, Ca^{2+} availability (ligand in general), which depends on its concentration and on the presence of other entities binding it, modulates the efficiency of the dissociation process and the species thus produced.

By virtue of their membrane activity, fibrils and oligomers can cooperate in the disruption of the intestinal barrier permeability, and facilitate the passage of fibrillar oligomers to initiate the sensitisation route. Indeed, these amyloid assemblies share with mucosal adjuvants such as cholera toxin (CT) a deleterious lipid binding activity [6, 35, 36, 46]. On the other hand, as shown for the amyloid-β in retinal pigment epithelium cells, amyloid aggregates could also play a key role in stimulating intestinal epithelial cells to produce IL-33 and trigger type 2 responses, overcoming tolerance and provoking sensitisation [6, 47]. Other amyloid aggregates as *Salmonella enterica* serovar Typhimurium curli fibrils activate the Toll-like receptor 2 / phos- phatidylinositol 3-kinase pathway, enhancing the intestinal epithelial barrier function, which is also tightly regulated by gut microbiota [48–50].

The finding of the amyloid assembly as the Gad m 1 architecture recognised by the IgE sera of patients allergic to fish adds new functions for the amyloid fold and novel routes for fish allergy intervention. Although the amyloid fold was initially recognised in the context of toxic functions, its functional repertoire has been expanded to include storage, coating, catalysis and acquired inheritance roles [12, 14–18]. Fish parvalbumin amyloid adds to the list the function of scaffolding

the IgE epitopes of this type I food allergen. The search for the IgE epitopes in fish parvalbumins has yielded several segments around Ca^{2+}-stabilised EF-hands, by use of antigens both denatured proteins and peptides [29–31]. These regions fail to accomplish the mul- tivalence required to cross-link IgE-FcεRI complexes on effector cells in sensitised patients and hence triggering the release of allergy mediators. On the contrary, the structural repetitiveness of the amyloid polymer provides the basis for such multivalence. Generalisation of this finding to other type I food allergens requires the consideration of the in soluble and polymeric protein forms and the use of native conditions during IgE recognition testing. Furthermore, the feasibility of epigallocatechin gallate for preventing rGad m 1 fibrillation suggests a role of anti-amyloid compounds present in food or supplied by the gastrointestinal microbiota as the natural antidotes to food allergens.

Materials and methods

Chemicals and proteins. All reagents were of the highest grade commercially available. Thioflavin T was obtained from Sigma. A Chelex resin (Bio-Rad) was used to remove contaminant trace metals from all solutions. Recombinant Gad m 1 (rGad m 1) was produced from a pET15b construct containing the synthetic open reading frame sequence of Atlantic cod parvalbumin A51874 (Genscript). Protein was isolated from the soluble fraction of sonicated bacterial cells and purified by Ni^{2+}-NTA (nickel-nitrilotriacetic acid) chromatography. Removal of His-tag was performed by a 3h digestion with thrombin, following ultrafiltration through a 30 kDa cutoff filter. Filtrates containing rGad m 1 were extensively dialysed against mQ H20 and then lyophilised. Protein was quantified using Bio-Rad protein assay. Before use, rGad m 1 was equilibrated by dialysis in 5 mM Hepes pH 7.4 and centri- fuge at 12,000 × g for 15 min at 4 °C to remove any insoluble material. Fibrils from Aβ1–40 and HaPrP23–231 were formed as described [22, 23].

Human sera. Fish allergic patients had convincing case histories of fish allergy, positive skin prick tests to codfish (≥5 mm mean wheal diameter), and serum specific IgE to cod (30.3 and 9.6 kU/l) and to rGad c 1 (14.2 and 18.5 ku/l, respectively) and a positive double-blind placebo-controlled food challenge with codfish (ImmunoCAP, ThermoFisher Scientific, Uppsala, Sweden). Sera were stored at –20 °C until use. Written informed consent was obtained from patients and the study was approved by the Ethics Committee of the Hospital Clínico San Carlos (Madrid).

Amyloidogenic propensity analysis. The amyloidogenic propensity of fish β-parvalbumins was analysed using the ZipperDb algorithm [17]. The sequences considered were: Atlantic cod (*Gadus morhua*) – Q90YK9, Q90YL0, A51874; Atlantic salmon (*Salmo salar*) – Q91482, Q91483, B5DH15, B5DH16, E0WD98, E0WD99; Rainbow trout (*Salmo gairdneri, Onco- rhynchusmykiss*) – E0WDA2, E0WDA3; Alaska pollock (*Theragra chalcogramma, Gadus chalcogramma*) – Q90YK8, Q90YK7; Atlantic herring (*Clupea harengus*) – C6GKU6, C6GKU7; carp (Cyprinus carpio) – Q8UUS2, Q8UUS3, E0W92, E0W93; mackerel (*Scomber japonicus, Trachurus japonicas, Scomber vernalis*) – G9I591, E0WD95, Q3C2C3, Q3C2C4, D3GME4, C0LEK8; hake (*Merluccius bilinearis, Merluccius merluccius, Merluccius australis, Merluccius senegalensis*) – P56503, P02620, P86745, P86778.

Aggregation assays. Recombinant Gad m 1 solutions at concentrations of 0.5–5 mg/ml were prepared in simulated gastric fluid (SGF: 50 mM glycine pH 2.0, 35 mM NaCl) or simulated intestinal fluid (SIF:

50 mM Tris pH 7.5, 35 mM NaCl), in both cases supplemented with either 5 mM EDTA or 5 mM $CaCl_2$. Simulated gastrointestinal fluid (SGIF) was achieved by a 30-min incubation in SGF followed by the addition of 1/5 (V/V) of 1.5 M Tris pH 8.0. When required, fibres were harvested by a 100,000 x g centrifugation for 1 h using an Optima™ MAX Beckman ultracentrifuge, and the pellet and supernatant fractions used for analysis. The binding of ThT for the detection of amyloid was performed as described [22]. Detergent resistant aggregates were assayed by means of SDS-polyacrylamide gel electrophoreses (SDS–PAGE) in 17% polyacrylamide gels; the proteins were loaded without heating and visualised with either Coomassie blue or silver staining.

Circular dichroism spectroscopy. Circular dichroism (CD) spectroscopy experiments were performed with a Jasco J-820 spectropolarimeter equipped with a Peltier-controlled thermostated cell holder. Far-UV CD spectra were recorded for 30 µM rGad m 1 in SGF and SIF supplemented with either 1 mM EDTA or 1 mM $CaCl_2$. Spectral analysis was performed as described [24].

Dynamic light scattering. Dynamic light scattering (DLS) data were acquired at 25 °C by use of Wyatt Dyna-Pro DLS system with a 1-mm path length 12 µl quartz cuvette. Samples were filtered with a 0.22 µm Whatman Anodisc-13 filter. Data were collected with a 5-second acquisition time, 20 acquisitions per measurement at laser power 100% (buffer) and 85% (protein samples) and were analysed with the Dynamics software.

Atomic force microscopy. For visualisation with atomic force microscopy (AFM), 5-µl sample aliquots of 0.5 mg/ml protein concentration were absorbed to freshly cleaved mica. Images were obtained using a MultiMode Veeco microscope with 125-µm lateral range and 5-µm vertical range J-scanner and Nan- oScope IIIa controller. Rectangular cantilevers with tetra- hedral tips for dynamic (tapping) mode in air were pur- chased from Olympus (OMCL-AC240TS). Software to ob- tain and treat the images was supplied with the instrument- ation (NanoScope). For specific AFM analysis, we used the free software WSxM 4.0 develop 13 (Nanotec).

Simulated gastrointestinal digestión. Recombinant Gad m 1 was both freshly dissolved or in- cubated for 36 h in SGF (1–10 mg/ml protein concentration) with or without 20 µM epigallocatechin gallate (EGCG, Sigma). The mixture was maintained at 37 °C with gentle shaking, and the reaction was started with the addition of pepsin (Sigma) at a ratio 1:70 w/w enzyme: substrate. After 30 min, the digestion was stopped by increasing the pH to 7.5 with 1.5 M Tris-HCl. For simulating the intestinal digestion, the reaction products were supplemented with proteinase K (1:70 w/w, protease:substrate) and digestion was allowed for 30 min at 37 °C. The digestion was stopped by adding phenylmethylsulfonyl fluoride (PMSF) at a final concentration of 2 mM. Control experiments without proteases or with bovine serum albumin (BSA) instead of rGad m 1 were also performed. The reac- tion products were analysed by means of SDS-PAGE using 17% polyacrylamide gels.

Dot-blot analysis. The reactivity of protein species against conformation-dependent antibodies was evaluated in a dot-blot analysis using the anti-amyloid fibrils OC antibody (AB2286 Merck Millipore, 1/2000 dilution), the A11 anti-amyloid oligomer antibody (AB9234 Merck Millipore, 1/2000 dilution), and sera from patients allergic to cod fish (1/10 dilution). Briefly, aliquots of rGad m1 (1–50 ng) under the different treatments were spotted in triplicates on a nitrocellulose membrane and treated with and without 6 M GdnCl. Immunodetection was performed by 1 h of incubation with primary antibodies, followed by extensive washes and 30 min incubation with horseradish peroxidase-

labelled anti-body, either mouse monoclonal B3102E8 anti-human IgE (Abcam, diluted 1:2000) or goat anti-rabbit IgG (1:5000 diluted; Sigma). The signal was developed with the ECL- western-blotting reagent (Biorad), and detected with ChemiDoc XRS equipment [25].

Acknowledgements: We thank Drs Manuel Espinosa-Urgel, Rafael Giraldo, Douglas V. Laurents, Victor Muñoz, Rosalía Rodríguez and Silvia Zorrilla for share of reagents and critical reading of the manuscript. JM was supported by a FPI-research contract, MC by a Juan de la Cierva Postdoctoral contract, and AMFE is a Ramón y Cajal fellow.

Disclosures: This work was partially supported by Ministerio de Economía y Competitividad (BFU2009–07971 and SAF2014–52661 to MG, BIO2011–28092 and CSD2009–00088 to MC), Fundación CIEN (MG) and Raman Health (MG).

Correspondence: María Gasset, IQFR, Consejo Superior de Investigaciones Científicas, Serrano 119, E-28006 Madrid, maria.gasset@csic.es

References

1. **Nwaru BI, Hickstein L, Panesar SS, Roberts G, Muraro A, Sheikh A.** Prevalence of common food allergies in Europe: a systematic review and meta-analysis. *Allergy*. 2014;69:992–1007.

2. **Muraro A, Werfel T, Hoffmann-Sommergruber K, Roberts G, Beyer K, Bindslev-Jensen C, et al.** EAACI food allergy and anaphylaxis guidelines: diagnosis and management of food allergy. *Allergy*. 2014;69:1008–25.

3. **Sicherer SH, Sampson HA. Food allergy**: Epidemiology, pathogenesis, diagnosis, and treatment. *J Allergy Clin Immunol*. 2014;133:291–307; quiz 8.

4. **Akdis CA.** Therapies for allergic inflammation: refining strategies to induce tolerance. *Nature Med.* 2012;18:736–49.

5. **Palomares O.** The role of regulatory T cells in IgE-mediated food allergy. *J Investig Allergol Clin Immunol.* 2013;23:371–82; quiz 2 p pre- ceding 82.

6. **Oyoshi MK, Oettgen HC, Chatila TA, Geha RS, Bryce PJ.** Food allergy: Insights into etiology, prevention, and treatment provided by murine models. *J Allergy Clin Immunol*. 2014;133:309–17.

7. **Taylor SL, Lehrer SB.** Principles and characteristics of food allergens. *Crit Rev Food Sci Nutr*. 1996;36 Suppl:S91–118.

8. **Traidl-Hoffmann C, Jakob T, Behrendt H.** Determinants of allergenicity. *J Allergy Clin Immunol*. 2009;123:558–66.

9. **Astwood JD, Leach JN, Fuchs RL.** Stability of food allergens to digestion in vitro. *Nat Biotechnol*. 1996;14:1269–73.

10. **Chapman MD, Pomes A, Breiteneder H, Ferreira F.** Nomenclature and structural biology of allergens. *J Allergy Clin Immunol.* 2007;119:414–20.

11. **Aalberse RC.** Structural biology of allergens. *J Allergy Clin Immunol*. 2000;106:228–38.

12. **Prusiner SB, McKinley MP, Bowman KA, Bolton DC, Bendheim PE, Groth DF, et al.** Scrapie prions aggregate to form amyloid-like birefringent rods. *Cell.* 1983;35:349–58.

13. **Concha-Marambio L, Diaz-Espinoza R, Soto C.** The extent of protease resistance of misfolded prion protein is highly dependent on the salt concentration. *J Biol Chem*. 2014;289:3073–9.

14. **Tycko R, Wickner RB**. Molecular structures of amyloid and prion fibrils: consensus versus controversy. *Acc Chem Res*. 2013;46:1487–96.

15. **Greenwald J, Riek R.** Biology of amyloid: structure, function, and regulation. *Structure*. 2010;18:1244–60.

16. **Eisenberg D, Jucker M.** The amyloid state of proteins in human diseases. *Cell*. 2012;148:1188–203.

17. **Goldschmidt L, Teng PK, Riek R, Eisenberg D.** Identifying the amylome, proteins capable of forming amyloid-like fibrils. *Proceed Natl Acad Sci U S A*. 2010;107:3487–92.

18. **Maji SK, Perrin MH, Sawaya MR, Jessberger S, Vadodaria K, Rissman RA, et al.** Functional amyloids as natural storage of peptide hormones in pituitary secretory granules. *Science.* 2009;325:328–32.

19. **Sanchez L, Madurga S, Pukala T, Vilaseca M, López-Iglesias C, Robinson CV, et al.** Abeta40 and Abeta42 amyloid fibrils exhibit distinct molecular recycling properties. *J Am Chem Soc*. 2011;133:6505–8.

20. **O'Nuallain B, Wetzel R.** Conformational Abs recognizing a generic amyloid fibril epitope. *Proc Natl Acad Sci U S A.* 2002;99:1485–90.

21. **Kayed R, Head E, Sarsoza F, Saing T, Cotman CW, Necula M, et al.** Fibril specific, conformation dependent antibodies recognize a generic epitope common to amyloid fibrils and fibrillar oligomers that is absent in prefibrillar oligomers. *Mol Neurodegener.* 2007;2:18.
22. **Martinez J, Lisa S, Sanchez R, Kowalczyk W, Zurita E, Teixidó M, et al**. Selenomethionine incorporation into amyloid sequences regulates fibrillogenesis and toxicity. *PloS One* 2011;6:e27999.
23. **Makarava N, Baskakov IV.** Purification and fibrillation of full-length recombinant PrP. *Methods Mol Biol*. 2012;849:33–52.
24. **Lisa S, Meli M, Cabello G, Gabizon R, Colombo G, Gasset M.** The structural intolerance of the PrP alpha-fold for polar substitution of the helix-3 methionines. *Cell Mol Life Sci*. 2010;67:2825–38.
25. **Lisa S, Domingo B, Martinez J, Gilch S, Llopis JF, Schätzl HM, et al.** Failure of prion protein oxidative folding guides the formation of toxic transmembrane forms. *J Biol Chem*. 2012;287:36693–701.
26. **Kuehn A, Swoboda I, Arumugam K, Hilger C, Hentges F.** Fish allergens at a glance: variable allergenicity of parvalbumins, the major fish allergens. *Front Immunol*. 2014;5:179.
27. **Moraes AH, Ackerbauer D, Kostadinova M, Bublin M, de Oliveira GA, Ferreira F, et al.** Solution and high-pressure NMR studies of the structure, dynamics, and stability of the cross-reactive allergenic cod parval- bumin Gad m 1. *Proteins*. 2014;82:3032–42.
28. **Griesmeier U, Vazquez-Cortes S, Bublin M, Radauer C, Ma Y, Briza P, et al.** Expression levels of parvalbumins determine allergenicity of fish species. *Allergy.* 2010;65:191–8.
29. **Elsayed S, Apold J.** Immunochemical analysis of cod fish allergen M: locations of the immunoglobulin binding sites as demonstrated by the native and synthetic peptides. *Allergy*. 1983;38:449–59.
30. **Untersmayr E, Szalai K, Riemer AB, Hemmer W, Swoboda I, Hantusch B, et al.** Mimotopes identify conformational epitopes on parvalbumin, the major fish allergen. *Mol Immunol*.2006;43:1454–61.
31. **Perez-Gordo M, Pastor-Vargas C, Lin J, Cases B, Ibáñez MD, Vivanco F, et al**. Epitope mapping of the major allergen from Atlantic cod in Spanish population reveals different IgE-binding patterns. *Mol Nutr Food Res.* 2013;57:1283–90.
32. **Swoboda I, Balic N, Klug C, Focke M, Weber M, Spitzauer S, et al.** A general strategy for the generation of hypoallergenic molecules for the immunotherapy of fish allergy. *J Allergy Clin Immunol*. 2013;132:979–81 e1.
33. **Ehrnhoefer DE, Duennwald M, Markovic P, Wacker JL, Engemann S, Roark M, et al.** Green tea (-)-epigallocatechin-gallate modulates early events in huntingtin misfolding and reduces toxicity in Huntington's disease models. Hum Mol Genet. 2006;15:2743–51.
34. **Tufail S, Owais M, Kazmi S, Balyan R, Kaur Khalsa J, Faisal SM, et al**. Amyloid form of Ovalbumin evokes native antigen specific immune response in the host: prospective immunoprophylactic potential. *J Biol Chem.* 2014.
35. **Last NB, Miranker AD.** Common mechanism unites membrane poration by amyloid and antimicrobial peptides. *Proc Natl Acad Sci U S A.* 2013;110:6382–7.
36. **Reynolds NP, Soragni A, Rabe M, Verdes D, Liverani E, Handschin S, et al.** Mechanism of membrane interaction and disruption by alpha-synuclein. *J Am Chem Soc.* 2011;133:19366–75.
37. **Hoffmann-Sommergruber K, Mills EN.** Food allergen protein families and their structural characteristics and application in component-resolved diagnosis: new data from the EuroPrevall project. *Anal Bioanal Chem.* 2009;395:25–35.
38. **Breiteneder H, Mills EN.** Molecular properties of food allergens. J Allergy Clin Immunol. 2005;115:14–23.
39. Astbury WT, Dickinson S, Bailey K. The X-ray interpretation of denaturation and the structure of the seed globulins. *Biochem J.* 1935;29:2351–601.
40. **Lara C, Gourdin-Bertin S, Adamcik J, Bolisetty S, Mezzenga R.** Self-assembly of ovalbumin into amyloid and non-amyloid fibrils. *Biomacromolecules.* 2012;13:4213–21.
41. **Jones OG, Adamcik J, Handschin S, Bolisetty S, Mezzenga R.** Fibrillation of beta-lactoglobulin at low pH in the presence of a complexing anionic polysaccharide. *Langmuir*. 2010;26:17449–58.
42. **Mulaj M, Foley J, Muschol M.** Amyloid oligomers and protofibrils, but not filaments, self-replicate from native lysozyme. *J Am Chem Soc*. 2014;136:8947–56.
43. **Fandrich M, Fletcher MA, Dobson CM**. Amyloid fibrils from muscle myoglobin. *Nature.* 2001;410:165–6.
44. **Hatters DM, Howlett GJ.** The structural basis for amyloid formation by plasma apolipoproteins: a review. *Eur Biophys J*. 2002;31:2–8.
45. **Roth-Walter F, Pacios LF, Gomez-Casado C, Hofstetter G, Roth GA, Singer J, et al.** The major cow milk allergen Bos d 5 manipulates T-helper cells depending on its load with siderophore-bound iron. *PloS One* 2014;9:e104803.
46. **Lencer WI, Tsai B.** The intracellular voyage of cholera toxin: going retro. *Trends Biochem Sci.* 2003;28:639–45.
47. **Liu XC, Liu XF, Jian CX, Li CJ, He SZ**. IL-33 is induced by amyloid-beta stimulation and regulates inflammatory cytokine production in retinal pigment epithelium cells. *Inflammation*. 2012;35:776–84.
48. **Noval Rivas M, Burton OT, Wise P, Zhang YQ, Hobson SA, Garcia Lloret M, et al.** A microbiota signature associated with experimental food allergy promotes allergic sensitization and anaphylaxis. *J Allergy Clin Immunol*. 2013;131:201–12.

49. **Oppong GO, Rapsinski GJ, Newman TN, Nishimori JH, Biesecker SG, Tukel C.** Epithelial cells augment barrier function via activation of the Toll-like receptor 2/phosphatidylinositol 3–kinase pathway upon recognition of Salmonella enterica serovar Typhimurium curli fibrils in the gut. *Infect Immun.* 2013;81:478–86.
50. **Cao S, Feehley TJ, Nagler CR.** The role of commensal bacteria in the regulation of sensitization to food allergens. *FEBS letters* 2014;588:4258–66.

IV. Discusión

Desde su descubrimiento hasta la actualidad, el concepto de amiloides ha evolucionado en paralelo a la introducción y desarrollo de nuevas técnicas instrumentales en el campo de la biofísica, la microscopía, y la biología computacional que nos han permitido incrementar la resolución estructural y permitido ampliar el concepto pasando de ser considerado en sus orígenes una basura tisular producto de errores en el plegamiento y siempre relacionado con la aparición de patologías, a alcanzar la consideración de estado estructural con atributos funcionales que varían desde citotoxicidad, función estructural, de almacenamieto, memoria o incluso a ser un elemento en la transmisión de información de forma similar a los ácidos nucleicos. La generalización del estado amiloide como consecuencia de la descripción de cada vez un número mayor de cadenas polipeptídicas no relacionadas evolutivamente de procariotas, hongos y metazoos, ha rastreado su origen a las etapas iniciales de la evolución sugiriendo su naturaleza de plegamiento ancestral [9-13,52,168,169,343].

El estado amiloide no está al alcance de todas las proteínas, sino que la predisposición teórica está codificada en la secuencia en forma de hexapéptidos capaces de empaquetarse en láminas β-cruzadas [69]. Estos segmentos se denominan segmentos adhesivos los cuales pueden tener una extensión superior a seis aminoácidos y el conjunto de proteínas que los contiene se denomina amiloma. En ausencia de cambios debido a mutaciones genéticas, la naturaleza de una secuencia y su predisposición intrínseca a formar amiloides puede modularse postraduccionalmente mediante su modificación covalente. De este modo, fosforilaciones y acetilaciones alteran la carga de residuos mientras que las glicosilaciones introducen impedimentos estéricos. Además de estas posibilidades, en la etapa sintética de traducción, los residuos de Met y SeM pueden intercambiarse dado que compiten por un mismo codón e introducirse indistintamente en la cadena polipeptídica [331,332,344]. Este intercambio se conoce como mutación metabólica y para aquellos organismos para los que ambos aminoácidos son esenciales, su regulación está dictada por la dieta [331,332,344]. Met y SeMet difieren únicamente en la naturaleza de un átomo pero sus propiedades de tamaño mayor en el selenio que en el azufre con radios atómicos de 1.17 vs 1.04Å respectivamente (Se>S), la hidrofobicidad, el selenio es más hidrofóbico que el azufre (Se>S) y la reactividad química son distintas y determinantes en reacciones de asociación como los empaquetamientos que determinan la formación de una lámina β-cruzada, [69,272,303,306,307,333,334,345-347]. Pequeñas diferencias estéricas pueden perturbar la formación de las cremalleras estéricas formadas por las interacciones entre cadenas laterals de los residuos implicados en la polimerización de las láminas β que dan lugar a la estructura amiloide.

La introducción de esta mutación metabólica mediante síntesis química empleando métodos optimizados de fase sólida en las cadenas proamiloidogénicas de Aβ40 y HuPrP(106-140) ha permitido determinar el efecto de esta sustitución tiene sobre dichos péptidos. En el caso de Aβ40, en el que M35 forma parte del segmento adhesivo GAIIGLM, su sustitución por SeM impide la formación de fibras amiloides y conduce a agregados con escasa, si alguna, neurotoxicidad. Esta inhbición ocurre tanto en reacciones de homo- (GAIIGLSeM) como hetero

(GAIIGLSeM y GAIIGLM)-asociación, sugiriendo que una dieta enriquecida en SeMet podría atenuar la formación de los amiloides de Aβ40 y de sus implicaciones en el deterioro cognitivo. En secuencias más complejas como HuPrP(106-140), en la que M129 forma parte del segmento adhesivo GGYMLG, M112 es el flanco N-terminal de la núcleo de agregación AGAAAAG, y M109 y M134 son residuos ajenos a la asociación, las distintitas sustituciones individuales por SeM dan lugar a una gama de efectos entre los que se encuentra la inhibición (M129), la aceleración (M109 y M112), la disminución de la eficacia (M134) y la forma de las fibras amiloides (M109 y M112) con impactos más o menos severos en la actividad citotóxica de los agregados. Así con las evidencias obtenidas la incorporación de SeM en secuencias proamiloides actúa en varios niveles en función de su localización y sugiere por tanto que el incremento de SeM de la dieta generaría un escenario complejo con suma de efectos y difícil de predecir con el conocimiento actual.

Si bien la presencia en una cadena de segmentos adhesivos determina su predisposición para alcanzar el estado amiloide, el proceso de formación requiere que dichas regiones se activen por exposición y que se encuentren a una concentración suficiente para superar a barrera entrópica del proceso de orden. De este modo, un segundo elemento modulador dependiente de la secuencia es el que surge de la distribución de carga y sus consecuencias en las interacciones intra- e intermoleculares que determinan las estabilidades de los estados nativos, amiloides e intermedios en el proceso de conversión entre ambos [12,14,16,69,84]. En el caso de PrP cuya cadena consta de dos dominios diferenciados, uno desordenado y portador de carga electropositiva en dos regiones situadas al inicio y al final de dicho dominio, y uno globular donde se concentra dispersada la carga negativa y las propiedades amiloides, la distribución de carga actúa a modo de código complejo que opera en todos los estados. Así, en el estado nativo (α-PrP o tipo PrP^{C}) la distribución de carga en la región α3 del dominio globular define una superficie electronegativa que permite la interacción con la región básica distal del dominio flexible y desencadena la compactación del estado en una forma cerrada. Por su naturaleza difusa, la interacción es lábil pero dispone de elementos estabilizadores como son los que resultan de la formación de quelatos de Zn(II) [245] mediada por la región del octarepeat. Estabilizada o no, la compactación del estado nativo actúa de barrera dificultando la conversión en estado amiloide. Además de esta barrera, in vivo existe una segunda que está codificada en las cargas del dominio flexible y que dictan un procesamiento tal que se generan las cadenas del dominio globular conocidas como C1 debido a la escisión-α de la cadena de PrP y los cuales funcionan como inhibidores del estado amiloide tóxico [348].

Por otra parte, la distribución de la carga de la cadena juega también un papel fundamental en la estructura del estado amiloide dictando el tipo de estructura secundaria (tipo S o tipo R) las cuales están relacionadas con la no o baja toxicidad de las tipo S o la aparición de infectividad *in vivo* en las tipo R como demostraron los estudios de Baskakov y colaboradores [253,349]. Además la disposición de las cargas afecta a aspectos de forma que incluyen la longitud de la fibra (límite de crecimiento o fragmentación óptima) mayor en los mutantes que afectan a la región α3 punto de interacción del N-terminal originándose fibras más eficientes en la

propagación lo cual podría implicar mayor patogenicidad, así como el límite de asociación entre filamentos (pre-filamento, filamento, etc), y la reactividad superficial a un determinado anticuerpo como en este caso el POM17. Todas estas características, cuya variabilidad subyace bajo el concepto de cepa (*strain, confórmero de forma*, etc), apuntan a que aunque la naturaleza del esqueleto de lámina β-cruzada sea una información contenida en la secuencia de la cadena y su empaquetamiento dictado por factores estéricos, los ensamblajes de orden superior están sujetos a factores adicionales reguladores complejos como los debidos a apantallamientos de carga a larga distancia. Estos efectos difíciles de observan y cuantificar in vivo podrían ser la bases de los procesos de adaptación de cepas y que generan fenotipos cambiantes en los procesos de transmisión de priones [248].

Un tercer elemento regulador son los cambios de entorno drástico con pérdida o ganancia de ligandos estructurales, como son los que acontecen durante la digestión gastrointestinal de las proteínas contenidas en los alimentos. Así, las condiciones de entorno gástricas (pH 2) y tratamientos térmicos estabilizan el estado amiloide de las ovoalbúminas, β-lactoglobulinas y las lisozimas [27,350-352], todas ellas con función alergénica. En el caso de los alérgenos alimentarios de tipo-I han de poseer unas características determinadas de estabilidad frente a condiciones desnaturalizantes como tratamientos térmicos, cambios bruscos de pH, acción de proteasas y detergentes etc, que les permitan mantener las regiones inmunorreactivas [314,341,353,354]. Uno de los mayores alérgenos alimentarios tipo I y con elevada reactividad cruzada como es Gad m 1 forma amiloides a partir de su forma Apo estabilizada tanto en condiciones de entorno gástrico (pH 2) como en presencia de quelantes de su ligando Ca^{2+}. Estos amiloides son precisamente las entidades responsables de la resistencia a proteasas ácidas y neutras, en comparación con los estados monoméricos. Si bien la resistencia a la proteólisis es una propiedad del estado amiloide, en el caso de los polímero de Gad m 1 y de muchas otras proteínas alimentarias tiene una significado adicional ya permite que sus cadenas enteras o truncadas escapen al proceso de digestión y alcancen el epitelio intestinal bajo distintos estados de asociación [355].

Basado en estudios relacionados con Aβ, además del estado monomérico y fibrilar existen almenos dos tipos de oligómeros [106]. Así, los oligómeros de tipo II poseen el motivo de láminas paralelas β y en registro que son reconocidos por el anticuerpo OC y están relacionados con la formación y fragmentación de fibras siendo considerados como profibrilares [101,106,356]. Por el contrario, los oligómeros de tipo 1 presentan inmunorreactividad frente a A11 y divergen de la ruta de plegamiento que conduce al amiloide y generalmente son elevadamente tóxicos [106]. Ambos tipos de oligómeros se detectan en las preparaciones de Gad m 1 sometidas a condiciones que simulan el tránsito gastrointestinal y ambos desempeñan funciones complementarias. Por un lado, los oligómeros de tipo I son entidades difusoras con propiedades de permeabilización de membranas y podrían ser las estructuras que facilitan del paso a través del epitelio intestinal. Por otro lado, los oligómeros de tipo II son las entidades reconocidas por

las IgEs de sueros de pacientes alérgicos a pescado y por tanto desencadenantes de las reacciones patógenas.

La unión del efecto proamiloide de los cambios drásticos de entorno con los alérgenos alimentarios de tipo I hace pensar que éstos podrían tener propiedades de prionoide. Sin embargo, esto no parece ser así ya que la calificación de prionoide implica una migración transcelular y una amplificación en la célula de destino. En el caso de los alérgenos, los análisis de secuencia no han permitido detectar una identidad en los segmentos adhesivos entre el alergéno y el proteoma humano, descartando la amplificación homóloga y relegándola a una posible reacción heteróloga en un principio menos eficiente.

De forma global, los resultados de todo este trabajo realizado han contribuido al conocimiento del estado amiloide ofreciendo nuevos elementos reguladores claves en su formación y con un potencial uso como diana de intervención, si bien es cierto, la complejidad del entorno celular hace imaginar como las diferentes secuencias polipeptídicas se verán expuestas a la acción de múltiples moduladores a la vez, lo que supone un complejo sistema de estudio y un reto apasionante con el fin de conseguir actuar de forma correcta en posibles terapias principalmente en aquellas dirigidas frente a amiloides con función tóxica.

V. Conclusiones

El trabajo aquí descrito contribuye al conocimiento del campo de amiloides en:

- La sustitución Met por SeM en secuencias proamiloidogénicas es un elemento intrínseco que modula:
    - las propiedades de ensamblaje, dictando la capacidad o no de formación del estado amiloide.
    - las características cinéticas del proceso y la estructura del producto.
    - La sustitución de Met por SeM muestra una capacidad reguladora que se ubica en los posibles efectos de la dieta en el envejecimiento, así como en el origen de las cepas o *strains* de priones.

- La estructura de la carga (expuesta o superficial) en PrP actúa como un código interno que regula la interacción entre dominios.
    - En el estado nativo (forma α) las cargas superficiales definen la estabilización de un estado compacto (CC1 y α3) y la extensión del procesamiento que conduce a una cadena no convertible (CC1 y CC2).
    - En el estado amiloide, las cargas de las regiones CC1, CC2 y α3 determinan el tipo de estructura secundaria, la jerarquía del ensamblaje y la longitud de las fibras.

- La formación de amiloides en la β-parvalbúmina del pescado rGad m 1, modelo recombinante de alérgeno alimentario de tipo I:
    - Ocurre a través de la forma apo.
    - Es responsable de la resistencia a la digestión gastrointestinal por la acción de proteasas ácidas y neutras.
    - Es responsable de la formación de especies capaces de atravesar el epitelio intestinal.
    - Permite la conservación de la estructura del epítopo reconocido por la IgE de sueros de pacientes alérgicos.

VI. Bibliografía

journal. date;537(1-3):215-21.

1 Glenner, G. G. & Wong, C. W. Alzheimer's disease: initial report of the purification and characterization of a novel cerebrovascular amyloid protein. *Biochemical and biophysical research communications* **120**, 885-890 (1984).

2 Prusiner, S. B. Novel proteinaceous infectious particles cause scrapie. *Science* **216**, 136-144 (1982).

3 Bolton, D. C., McKinley, M. P. & Prusiner, S. B. Identification of a protein that purifies with the scrapie prion. *Science* **218**, 1309-1311 (1982).

4 Selkoe, D. J. Disease-related protein changes in purified neurons from Alzheimer's and Huntington's diseases. *Transactions of the American Neurological Association* **104**, 70-74 (1979).

5 Selkoe, D. J., Salazar, F. J., Abraham, C. & Kosik, K. S. Huntington's disease: changes in striatal proteins reflect astrocytic gliosis. *Brain research* **245**, 117-125 (1982).

6 Wickner, R. B. [URE3] as an altered URE2 protein: evidence for a prion analog in Saccharomyces cerevisiae. *Science* **264**, 566-569 (1994).

7 Maji, S. K. *et al.* Functional amyloids as natural storage of peptide hormones in pituitary secretory granules. *Science* **325**, 328-332, doi:10.1126/science.1173155 (2009).

8 Chapman, M. R. *et al.* Role of Escherichia coli curli operons in directing amyloid fiber formation. *Science* **295**, 851-855, doi:10.1126/science.1067484 (2002).

9 Shorter, J. & Lindquist, S. Prions as adaptive conduits of memory and inheritance. *Nature reviews. Genetics* **6**, 435-450, doi:10.1038/nrg1616 (2005).

10 Halfmann, R. & Lindquist, S. Epigenetics in the extreme: prions and the inheritance of environmentally acquired traits. *Science* **330**, 629-632, doi:10.1126/science.1191081 (2010).

11 Lindquist, S. Protein folding sculpting evolutionary change. *Cold Spring Harbor symposia on quantitative biology* **74**, 103-108, doi:10.1101/sqb.2009.74.043 (2009).

12 Greenwald, J. & Riek, R. Biology of amyloid: structure, function, and regulation. *Structure* **18**, 1244-1260, doi:10.1016/j.str.2010.08.009 (2010).

13 Greenwald, J. & Riek, R. On the possible amyloid origin of protein folds. *Journal of molecular biology* **421**, 417-426, doi:10.1016/j.jmb.2012.04.015 (2012).

14 Eisenberg, D. & Jucker, M. The amyloid state of proteins in human diseases. *Cell* **148**, 1188-1203, doi:10.1016/j.cell.2012.02.022 (2012).

15 Bennett, M. J., Sawaya, M. R. & Eisenberg, D. Deposition diseases and 3D domain swapping. *Structure* **14**, 811-824, doi:10.1016/j.str.2006.03.011 (2006).

16 Knowles, T. P., Vendruscolo, M. & Dobson, C. M. The amyloid state and its association with protein misfolding diseases. *Nature reviews. Molecular cell biology* **15**, 384-396, doi:10.1038/nrm3810 (2014).

17 Divry, P. & Florkin, M. Sur les proprietes optiques de l'amyloide. *C. R. Soc. Biol* **97**, 1808-1810 (1927).

18 Missmahl, H. P. & Hartwig, M. [Optical polarization studies of amyloid substance]. *Virchows Archiv : an international journal of pathology* **324**, 489-508 (1953).

19 Glenner, G. G. & Bladen, H. A. Purification and reconstitution of the periodic fibril and unit structure of human amyloid. *Science* **154**, 271-272 (1966).

20 DeLellis, R. A., Glenner, G. G. & Ram, J. S. Histochemical observations on amyloid with reference to polarization microscopy. *The journal of histochemistry and cytochemistry : official journal of the Histochemistry Society* **16**, 663-665 (1968).

21 Cohen, A. S. & Calkins, E. Electron microscopic observations on a fibrous component in amyloid of diverse origins. *Nature* **183**, 1202-1203 (1959).

22 Cohen, A. S., Shirahama, T. & Skinner, M. in *Electron Microscopy of Proteins* Vol. 3 (ed J.R. Harris) 165-205 (Academic Press, 1982).

23 Shirahama, T. & Cohen, A. S. High-resolution electron microscopic analysis of the amyloid fibril. *The Journal of cell biology* **33**, 679-708 (1967).

24 Cohen, A. S. & Calkins, E. The Isolation of Amyloid Fibrils and a Study of the Effect of Collagenase and Hyaluronidase. *The Journal of cell biology* **21**, 481-486 (1964).

25 Pras, M., Schubert, M., Zucker-Franklin, D., Rimon, A. & Franklin, E. C. The characterization of soluble amyloid prepared in water. *The Journal of clinical investigation* **47**, 924-933, doi:10.1172/JCI105784 (1968).

26 Sipe, J. D. & Cohen, A. S. Review: history of the amyloid fibril. *Journal of structural biology* **130**, 88-98, doi:10.1006/jsbi.2000.4221 (2000).

27 Astbury, W. T., Dickinson, S. & Bailey, K. The X-ray interpretation of denaturation and the structure of the seed globulins. *Biochem. J.* **29**, 2351-2360 (1935).

28 Sarroukh, R., Goormaghtigh, E., Ruysschaert, J. M. & Raussens, V. ATR-FTIR: a "rejuvenated" tool to investigate amyloid proteins. *Biochimica et biophysica acta* **1828**, 2328-2338, doi:10.1016/j.bbamem.2013.04.012 (2013).

29 Stohr, J. Prion protein aggregation and fibrillogenesis in vitro. *Sub-cellular biochemistry* **65**, 91-108, doi:10.1007/978-94-007-5416-4_5 (2012).

30 Liu, C., Sawaya, M. R. & Eisenberg, D. beta(2)-microglobulin forms three-dimensional domain-swapped amyloid fibrils with disulfide linkages. *Nature structural & molecular biology* **18**, 49-55, doi:10.1038/nsmb.1948 (2011).

31 Carulla, N., Zhou, M., Giralt, E., Robinson, C. V. & Dobson, C. M. Structure and intermolecular dynamics of aggregates populated during amyloid fibril formation studied by hydrogen/deuterium exchange. *Accounts of chemical research* **43**, 1072-1079, doi:10.1021/ar9002784 (2010).

32 Tycko, R. Solid-state NMR as a probe of amyloid fibril structure. *Current opinion in chemical biology* **4**, 500-506 (2000).

33 White, H. E. *et al.* Globular tetramers of beta(2)-microglobulin assemble into elaborate amyloid fibrils. *Journal of molecular biology* **389**, 48-57, doi:10.1016/j.jmb.2009.03.066 (2009).

34 Bonar, L., Cohen, A. S. & Skinner, M. M. Characterization of the amyloid fibril as a cross-beta protein. *Proceedings of the Society for Experimental Biology and Medicine. Society for Experimental Biology and Medicine* **131**, 1373-1375 (1969).

35 Glenner, G. G., Eanes, E. D., Bladen, H. A., Linke, R. P. & Termine, J. D. Beta-pleated sheet fibrils. A comparison of native amyloid with synthetic protein fibrils. *The journal of histochemistry and cytochemistry : official journal of the Histochemistry Society* **22**, 1141-1158 (1974).

36 Fraser, P. E., Nguyen, J. T., Surewicz, W. K. & Kirschner, D. A. pH-dependent structural transitions of Alzheimer amyloid peptides. *Biophysical journal* **60**, 1190-1201, doi:10.1016/S0006-3495(91)82154-3 (1991).

37 Gasset, M. *et al.* Predicted alpha-helical regions of the prion protein when synthesized as peptides form amyloid. *Proceedings of the National Academy of Sciences of the United States of America* **89**, 10940-10944 (1992).

38 Sunde, M. & Blake, C. C. From the globular to the fibrous state: protein structure and structural conversion in amyloid formation. *Quarterly reviews of biophysics* **31**, 1-39 (1998).

39 Eanes, E. D. & Glenner, G. G. X-ray diffraction studies on amyloid filaments. *The journal of histochemistry and cytochemistry : official journal of the Histochemistry Society* **16**, 673-677 (1968).

40 Pauling, L. & Corey, R. B. The pleated sheet, a new layer configuration of polypeptide chains. *Proceedings of the National Academy of Sciences of the United States of America* **37**, 251-256 (1951).

41 Prusiner, S. B. *et al.* Scrapie prions aggregate to form amyloid-like birefringent rods. *Cell* **35**, 349-358 (1983).

42 Gasset, M., Baldwin, M. A., Fletterick, R. J. & Prusiner, S. B. Perturbation of the secondary structure of the scrapie prion protein under conditions that alter infectivity. *Proceedings of the National Academy of Sciences of the United States of America* **90**, 1-5 (1993).

43 Eichner, T. & Radford, S. E. A diversity of assembly mechanisms of a generic amyloid fold. *Molecular cell* **43**, 8-18, doi:10.1016/j.molcel.2011.05.012 (2011).

44 Prusiner, S. B. Prion diseases and the BSE crisis. *Science* **278**, 245-251 (1997).

45 Barnhart, M. M. & Chapman, M. R. Curli biogenesis and function. *Annual review of microbiology* **60**, 131-147, doi:10.1146/annurev.micro.60.080805.142106 (2006).

46 Liu, J. J., Sondheimer, N. & Lindquist, S. L. Changes in the middle region of Sup35 profoundly alter the nature of epigenetic inheritance for the yeast prion [PSI+]. *Proceedings of the National Academy of Sciences of the United States of America* **99 Suppl 4**, 16446-16453, doi:10.1073/pnas.252652099 (2002).

47 Dannies, P. S. Protein hormone storage in secretory granules: mechanisms for concentration and sorting. *Endocrine reviews* **20**, 3-21, doi:10.1210/edrv.20.1.0354 (1999).

48 Fowler, D. M., Koulov, A. V., Balch, W. E. & Kelly, J. W. Functional amyloid--from bacteria to humans. *Trends in biochemical sciences* **32**, 217-224, doi:10.1016/j.tibs.2007.03.003 (2007).

49 McGlinchey, R. P. *et al.* The repeat domain of the melanosome fibril protein Pmel17 forms the amyloid core promoting melanin synthesis. *Proceedings of the National Academy of Sciences of the United States of America* **106**, 13731-13736, doi:10.1073/pnas.0906509106 (2009).

50 Badtke, M. P., Hammer, N. D. & Chapman, M. R. Functional amyloids signal their arrival. *Science signaling* **2**, pe43, doi:10.1126/scisignal.280pe43 (2009).

51 Sipe, J. D. *et al.* Amyloid fibril protein nomenclature: 2010 recommendations from the nomenclature committee of the International Society of Amyloidosis. *Amyloid : the international journal of experimental and clinical investigation : the official journal of the International Society of Amyloidosis* **17**, 101-104, doi:10.3109/13506129.2010.526812 (2010).

52 Chiti, F. & Dobson, C. M. Protein misfolding, functional amyloid, and human disease. *Annual review of biochemistry* **75**, 333-366, doi:10.1146/annurev.biochem.75.101304.123901 (2006).

53 Nelson, R. & Eisenberg, D. Recent atomic models of amyloid fibril structure. *Current opinion in structural biology* **16**, 260-265, doi:10.1016/j.sbi.2006.03.007 (2006).

54 Nelson, R. *et al.* Structure of the cross-beta spine of amyloid-like fibrils. *Nature* **435**, 773-778, doi:10.1038/nature03680 (2005).

55 Perutz, M. F., Staden, R., Moens, L. & De Baere, I. Polar zippers. *Current biology : CB* **3**, 249-253 (1993).

56 Sawaya, M. R. *et al.* Atomic structures of amyloid cross-beta spines reveal varied steric zippers. *Nature* **447**, 453-457, doi:10.1038/nature05695 (2007).

57 Fitzpatrick, A. W. *et al.* Atomic structure and hierarchical assembly of a cross-beta amyloid fibril. *Proceedings of the National Academy of Sciences of the United States of America* **110**, 5468-5473, doi:10.1073/pnas.1219476110 (2013).

58 Knowles, T. P. *et al.* Role of intermolecular forces in defining material properties of protein nanofibrils. *Science* **318**, 1900-1903, doi:10.1126/science.1150057 (2007).

59 Toyama, B. H. & Weissman, J. S. Amyloid structure: conformational diversity and consequences. *Annual review of biochemistry* **80**, 557-585, doi:10.1146/annurev-biochem-090908-120656 (2011).

60 Baldwin, A. J. *et al.* Metastability of native proteins and the phenomenon of amyloid formation. *Journal of the American Chemical Society* **133**, 14160-14163, doi:10.1021/ja2017703 (2011).

61 Hartl, F. U., Bracher, A. & Hayer-Hartl, M. Molecular chaperones in protein folding and proteostasis. *Nature* **475**, 324-332, doi:10.1038/nature10317 (2011).

62 Blanco, L. P., Evans, M. L., Smith, D. R., Badtke, M. P. & Chapman, M. R. Diversity, biogenesis and function of microbial amyloids. *Trends in microbiology* **20**, 66-73, doi:10.1016/j.tim.2011.11.005 (2012).

63 Conchillo-Sole, O. *et al.* AGGRESCAN: a server for the prediction and evaluation of "hot spots" of aggregation in polypeptides. *BMC bioinformatics* **8**, 65, doi:10.1186/1471-2105-8-65 (2007).

64 Fernandez-Escamilla, A. M., Rousseau, F., Schymkowitz, J. & Serrano, L. Prediction of sequence-dependent and mutational effects on the aggregation of peptides and proteins. *Nature biotechnology* **22**, 1302-1306, doi:10.1038/nbt1012 (2004).

65 Dobson, C. M. Protein misfolding, evolution and disease. *Trends in biochemical sciences* **24**, 329-332 (1999).

66 Maurer-Stroh, S. *et al.* Exploring the sequence determinants of amyloid structure using position-specific scoring matrices. *Nature methods* **7**, 237-242, doi:10.1038/nmeth.1432 (2010).

67 de Groot, N. S., Aviles, F. X., Vendrell, J. & Ventura, S. Mutagenesis of the central hydrophobic cluster in Abeta42 Alzheimer's peptide. Side-chain properties correlate with aggregation propensities. *The FEBS journal* **273**, 658-668, doi:10.1111/j.1742-4658.2005.05102.x (2006).

68 Tartaglia, G. G. & Vendruscolo, M. The Zyggregator method for predicting protein aggregation propensities. *Chemical Society reviews* **37**, 1395-1401, doi:10.1039/b706784b (2008).

69 Goldschmidt, L., Teng, P. K., Riek, R. & Eisenberg, D. Identifying the amylome, proteins capable of forming amyloid-like fibrils. *Proceedings of the National Academy of Sciences of the United States of America* **107**, 3487-3492, doi:10.1073/pnas.0915166107 (2010).

70 Tycko, R. Physical and structural basis for polymorphism in amyloid fibrils. *Protein science : a publication of the Protein Society* **23**, 1528-1539, doi:10.1002/pro.2544 (2014).

71 Wang, M. *et al.* The relationship between ADAM17 promoter polymorphisms and sporadic Alzheimer's disease in a Northern Chinese Han population. *Journal of clinical neuroscience : official journal of the Neurosurgical Society of Australasia* **17**, 1276-1279, doi:10.1016/j.jocn.2010.01.008 (2010).

72 Petkova, A. T. *et al.* Self-propagating, molecular-level polymorphism in Alzheimer's beta-amyloid fibrils. *Science* **307**, 262-265, doi:10.1126/science.1105850 (2005).

73 Chen, B., Thurber, K. R., Shewmaker, F., Wickner, R. B. & Tycko, R. Measurement of amyloid fibril mass-per-length by tilted-beam transmission electron microscopy. *Proceedings of the National Academy of Sciences of the United States of America* **106**, 14339-14344, doi:10.1073/pnas.0907821106 (2009).

74 Tycko, R. & Wickner, R. B. Molecular structures of amyloid and prion fibrils: consensus versus controversy. *Accounts of chemical research* **46**, 1487-1496, doi:10.1021/ar300282r (2013).

75 Paravastu, A. K., Petkova, A. T. & Tycko, R. Polymorphic fibril formation by residues 10-40 of the Alzheimer's beta-amyloid peptide. *Biophysical journal* **90**, 4618-4629, doi:10.1529/biophysj.105.076927 (2006).

76 Paravastu, A. K., Leapman, R. D., Yau, W. M. & Tycko, R. Molecular structural basis for polymorphism in Alzheimer's beta-amyloid fibrils. *Proceedings of the National Academy of Sciences of the United States of America* **105**, 18349-18354, doi:10.1073/pnas.0806270105 (2008).

77 Kodali, R., Williams, A. D., Chemuru, S. & Wetzel, R. Abeta(1-40) forms five distinct amyloid structures whose beta-sheet contents and fibril stabilities are correlated. *Journal of molecular biology* **401**, 503-517, doi:10.1016/j.jmb.2010.06.023 (2010).

78 Lu, J. X. *et al.* Molecular structure of beta-amyloid fibrils in Alzheimer's disease brain tissue. *Cell* **154**, 1257-1268, doi:10.1016/j.cell.2013.08.035 (2013).

79 Qiang, W., Yau, W. M. & Tycko, R. Structural evolution of Iowa mutant beta-amyloid fibrils from polymorphic to homogeneous states under repeated seeded growth. *Journal of the American Chemical Society* **133**, 4018-4029, doi:10.1021/ja109679q (2011).

80 Qiang, W., Kelley, K. & Tycko, R. Polymorph-specific kinetics and thermodynamics of beta-amyloid fibril growth. *Journal of the American Chemical Society* **135**, 6860-6871, doi:10.1021/ja311963f (2013).

81 McDonald, M. *et al.* Fiber diffraction data indicate a hollow core for the Alzheimer's abeta 3-fold symmetric fibril. *Journal of molecular biology* **423**, 454-461, doi:10.1016/j.jmb.2012.08.004 (2012).

82 Tanaka, M., Collins, S. R., Toyama, B. H. & Weissman, J. S. The physical basis of how prion conformations determine strain phenotypes. *Nature* **442**, 585-589, doi:10.1038/nature04922 (2006).

83 Baskakov, I. V. Switching in amyloid structure within individual fibrils: implication for strain adaptation, species barrier and strain classification. *FEBS letters* **583**, 2618-2622, doi:10.1016/j.febslet.2009.05.044 (2009).

84 Eichner, T., Kalverda, A. P., Thompson, G. S., Homans, S. W. & Radford, S. E. Conformational conversion during amyloid formation at atomic resolution. *Molecular cell* **41**, 161-172, doi:10.1016/j.molcel.2010.11.028 (2011).

85 Wiltzius, J. J. *et al.* Molecular mechanisms for protein-encoded inheritance. *Nature structural & molecular biology* **16**, 973-978, doi:10.1038/nsmb.1643 (2009).

86 Jarrett, J. T. & Lansbury, P. T., Jr. Seeding "one-dimensional crystallization" of amyloid: a pathogenic mechanism in Alzheimer's disease and scrapie? *Cell* **73**, 1055-1058 (1993).

87 Ye, W. *et al.* Insight into the stability of cross-beta amyloid fibril from VEALYL short peptide with molecular dynamics simulation. *PloS one* **7**, e36382, doi:10.1371/journal.pone.0036382 (2012).

88 Jang, H. *et al.* Mechanisms for the Insertion of Toxic, Fibril-like beta-Amyloid Oligomers into the Membrane. *Journal of chemical theory and computation* **9**, 822-833, doi:10.1021/ct300916f (2013).

89 Lee, J., Culyba, E. K., Powers, E. T. & Kelly, J. W. Amyloid-beta forms fibrils by nucleated conformational conversion of oligomers. *Nature chemical biology* **7**, 602-609, doi:10.1038/nchembio.624 (2011).

90 Cox, B., Ness, F. & Tuite, M. Analysis of the generation and segregation of propagons: entities that propagate the [PSI+] prion in yeast. *Genetics* **165**, 23-33 (2003).

91 Cohen, S. I. *et al.* Proliferation of amyloid-beta42 aggregates occurs through a secondary nucleation mechanism. *Proceedings of the National Academy of Sciences of the United States of America* **110**, 9758-9763, doi:10.1073/pnas.1218402110 (2013).

92 Collins, S. R., Douglass, A., Vale, R. D. & Weissman, J. S. Mechanism of prion propagation: amyloid growth occurs by monomer addition. *PLoS biology* **2**, e321, doi:10.1371/journal.pbio.0020321 (2004).

93 Knowles, T. P. *et al.* An analytical solution to the kinetics of breakable filament assembly. *Science* **326**, 1533-1537, doi:10.1126/science.1178250 (2009).

94 Sanchez, L. *et al.* Abeta40 and Abeta42 amyloid fibrils exhibit distinct molecular recycling properties. *Journal of the American Chemical Society* **133**, 6505-6508, doi:10.1021/ja1117123 (2011).

95 Prusiner, S. B., Groth, D., Serban, A., Stahl, N. & Gabizon, R. Attempts to restore scrapie prion infectivity after exposure to protein denaturants. *Proceedings of the National Academy of Sciences of the United States of America* **90**, 2793-2797 (1993).

96 Brown, P., Liberski, P. P., Wolff, A. & Gajdusek, D. C. Conservation of infectivity in purified fibrillary extracts of scrapie-infected hamster brain after sequential enzymatic digestion or polyacrylamide gel electrophoresis. *Proceedings of the National Academy of Sciences of the United States of America* **87**, 7240-7244 (1990).

97 Giraldo, R. Amyloid assemblies: protein legos at a crossroads in bottom-up synthetic biology. *Chembiochem : a European journal of chemical biology* **11**, 2347-2357, doi:10.1002/cbic.201000412 (2010).

98 Chiti, F. & Dobson, C. M. Amyloid formation by globular proteins under native conditions. *Nature chemical biology* **5**, 15-22, doi:10.1038/nchembio.131 (2009).

99 Elam, J. S. *et al.* Amyloid-like filaments and water-filled nanotubes formed by SOD1 mutant proteins linked to familial ALS. *Nature structural biology* **10**, 461-467, doi:10.1038/nsb935 (2003).

100 Wang, L., Maji, S. K., Sawaya, M. R., Eisenberg, D. & Riek, R. Bacterial inclusion bodies contain amyloid-like structure. *PLoS biology* **6**, e195, doi:10.1371/journal.pbio.0060195 (2008).

101 Glabe, C. G. Structural classification of toxic amyloid oligomers. *The Journal of biological chemistry* **283**, 29639-29643, doi:10.1074/jbc.R800016200 (2008).

102 Lasagna-Reeves, C. A., Glabe, C. G. & Kayed, R. Amyloid-beta annular protofibrils evade fibrillar fate in Alzheimer disease brain. *The Journal of biological chemistry* **286**, 22122-22130, doi:10.1074/jbc.M111.236257 (2011).

103 Lesne, S. E. *et al.* Brain amyloid-beta oligomers in ageing and Alzheimer's disease. *Brain : a journal of neurology* **136**, 1383-1398, doi:10.1093/brain/awt062 (2013).

104 Noguchi, A. *et al.* Isolation and characterization of patient-derived, toxic, high mass amyloid beta-protein (Abeta) assembly from Alzheimer disease brains. *The Journal of biological chemistry* **284**, 32895-32905, doi:10.1074/jbc.M109.000208 (2009).

105 Shankar, G. M. *et al.* Amyloid-beta protein dimers isolated directly from Alzheimer's brains impair synaptic plasticity and memory. *Nature medicine* **14**, 837-842, doi:10.1038/nm1782 (2008).

106 Liu, P. *et al.* Quaternary Structure Defines a Large Class of Amyloid-beta Oligomers Neutralized by Sequestration. *Cell reports* **11**, 1760-1771, doi:10.1016/j.celrep.2015.05.021 (2015).

107 Breydo, L. & Uversky, V. N. Structural, morphological, and functional diversity of amyloid oligomers. *FEBS letters* **589**, 2640-2648, doi:10.1016/j.febslet.2015.07.013 (2015).

108 Moshe, A., Landau, M. & Eisenberg, D. Preparation of Crystalline Samples of Amyloid Fibrils and Oligomers. *Methods in molecular biology* **1345**, 201-210, doi:10.1007/978-1-4939-2978-8_13 (2016).

109 Kayed, R. *et al.* Fibril specific, conformation dependent antibodies recognize a generic epitope common to amyloid fibrils and fibrillar oligomers that is absent in prefibrillar oligomers. *Molecular neurodegeneration* **2**, 18, doi:10.1186/1750-1326-2-18 (2007).

110 Wu, J. W. *et al.* Fibrillar oligomers nucleate the oligomerization of monomeric amyloid beta but do not seed fibril formation. *The Journal of biological chemistry* **285**, 6071-6079, doi:10.1074/jbc.M109.069542 (2010).

111 Huang, D. *et al.* Antiparallel beta-Sheet Structure within the C-Terminal Region of 42-Residue Alzheimer's Amyloid-beta Peptides When They Form 150-kDa Oligomers. *Journal of molecular biology* **427**, 2319-2328, doi:10.1016/j.jmb.2015.04.004 (2015).

112 Laganowsky, A. *et al.* Atomic view of a toxic amyloid small oligomer. *Science* **335**, 1228-1231, doi:10.1126/science.1213151 (2012).

113 Liu, C. *et al.* Out-of-register beta-sheets suggest a pathway to toxic amyloid aggregates. *Proceedings of the National Academy of Sciences of the United States of America* **109**, 20913-20918, doi:10.1073/pnas.1218792109 (2012).

114 Bemporad, F. & Chiti, F. Protein misfolded oligomers: experimental approaches, mechanism of formation, and structure-toxicity relationships. *Chemistry & biology* **19**, 315-327, doi:10.1016/j.chembiol.2012.02.003 (2012).

115 Mannini, B. *et al.* Toxicity of protein oligomers is rationalized by a function combining size and surface hydrophobicity. *ACS chemical biology* **9**, 2309-2317, doi:10.1021/cb500505m (2014).

116 Campioni, S. *et al.* A causative link between the structure of aberrant protein oligomers and their toxicity. *Nature chemical biology* **6**, 140-147, doi:10.1038/nchembio.283 (2010).

117 Wogulis, M. *et al.* Nucleation-dependent polymerization is an essential component of amyloid-mediated neuronal cell death. *The Journal of neuroscience : the official journal of the Society for Neuroscience* **25**, 1071-1080, doi:10.1523/JNEUROSCI.2381-04.2005 (2005).

118 Feng, S., Song, X. H. & Zeng, C. M. Inhibition of amyloid fibrillation of lysozyme by phenolic compounds involves quinoprotein formation. *FEBS letters* **586**, 3951-3955, doi:10.1016/j.febslet.2012.09.037 (2012).

119 Poirier, M. A. *et al.* Huntingtin spheroids and protofibrils as precursors in polyglutamine fibrilization. *The Journal of biological chemistry* **277**, 41032-41037, doi:10.1074/jbc.M205809200 (2002).

120 Langer, F. *et al.* Soluble Abeta seeds are potent inducers of cerebral beta-amyloid deposition. *The Journal of neuroscience : the official journal of the Society for Neuroscience* **31**, 14488-14495, doi:10.1523/JNEUROSCI.3088-11.2011 (2011).

121 Walker, L. C., Diamond, M. I., Duff, K. E. & Hyman, B. T. Mechanisms of protein seeding in neurodegenerative diseases. *JAMA neurology* **70**, 304-310, doi:10.1001/jamaneurol.2013.1453 (2013).

122 Wu, W. H. *et al.* Fibrillar seeds alleviate amyloid-beta cytotoxicity by omitting formation of higher-molecular-weight oligomers. *Biochemical and biophysical research communications* **439**, 321-326, doi:10.1016/j.bbrc.2013.08.088 (2013).

123 Lasagna-Reeves, C. A. *et al.* Alzheimer brain-derived tau oligomers propagate pathology from endogenous tau. *Sci Rep* **2**, 700, doi:10.1038/srep00700 (2012).

124 Aguzzi, A. & Rajendran, L. The transcellular spread of cytosolic amyloids, prions, and prionoids. *Neuron* **64**, 783-790, doi:10.1016/j.neuron.2009.12.016 (2009).

125 Ashe, K. H. & Aguzzi, A. Prions, prionoids and pathogenic proteins in Alzheimer disease. *Prion* **7**, 55-59, doi:10.4161/pri.23061 (2013).

126 Aguzzi, A. & Lakkaraju, A. K. Cell Biology of Prions and Prionoids: A Status Report. *Trends in cell biology*, doi:10.1016/j.tcb.2015.08.007 (2015).

127 Sawyer, E. B., Claessen, D., Haas, M., Hurgobin, B. & Gras, S. L. The assembly of individual chaplin peptides from Streptomyces coelicolor into functional amyloid fibrils. *PloS one* **6**, e18839, doi:10.1371/journal.pone.0018839 (2011).

128 Harbi, D. & Harrison, P. M. Interaction networks of prion, prionogenic and prion-like proteins in budding yeast, and their role in gene regulation. *PloS one* **9**, e100615, doi:10.1371/journal.pone.0100615 (2014).

129 Harbi, D. & Harrison, P. M. Classifying prion and prion-like phenomena. *Prion* **8** (2014).

130 Giraldo, R., Moreno-Diaz de la Espina, S., Fernandez-Tresguerres, M. E. & Gasset-Rosa, F. RepA-WH1 prionoid: a synthetic amyloid proteinopathy in a minimalist host. *Prion* **5**, 60-64 (2011).

131 Scherzinger, E. *et al.* Huntingtin-encoded polyglutamine expansions form amyloid-like protein aggregates in vitro and in vivo. *Cell* **90**, 549-558 (1997).

132 Braak, H. *et al.* Amyotrophic lateral sclerosis--a model of corticofugal axonal spread. *Nature reviews. Neurology* **9**, 708-714, doi:10.1038/nrneurol.2013.221 (2013).

133 Cushman, M., Johnson, B. S., King, O. D., Gitler, A. D. & Shorter, J. Prion-like disorders: blurring the divide between transmissibility and infectivity. *Journal of cell science* **123**, 1191-1201, doi:10.1242/jcs.051672 (2010).

134 Ren, P. H. *et al.* Cytoplasmic penetration and persistent infection of mammalian cells by polyglutamine aggregates. *Nature cell biology* **11**, 219-225, doi:10.1038/ncb1830 (2009).

135 Harbi, D. *et al.* PrionHome: a database of prions and other sequences relevant to prion phenomena. *PloS one* **7**, e31785, doi:10.1371/journal.pone.0031785 (2012).

136 Hou, F. *et al.* MAVS forms functional prion-like aggregates to activate and propagate antiviral innate immune response. *Cell* **146**, 448-461, doi:10.1016/j.cell.2011.06.041 (2011).

137 Fioriti, L. *et al.* The Persistence of Hippocampal-Based Memory Requires Protein Synthesis Mediated by the Prion-like Protein CPEB3. *Neuron* **86**, 1433-1448, doi:10.1016/j.neuron.2015.05.021 (2015).

138 Si, K., Choi, Y. B., White-Grindley, E., Majumdar, A. & Kandel, E. R. Aplysia CPEB can form prion-like multimers in sensory neurons that contribute to long-term facilitation. *Cell* **140**, 421-435, doi:10.1016/j.cell.2010.01.008 (2010).

139 Prusiner, S. B. Prions. *Proceedings of the National Academy of Sciences of the United States of America* **95**, 13363-13383 (1998).

140 Soto, C. Transmissible proteins: expanding the prion heresy. *Cell* **149**, 968-977, doi:10.1016/j.cell.2012.05.007 (2012).

141 Saa, P., Castilla, J. & Soto, C. Cyclic amplification of protein misfolding and aggregation. *Methods in molecular biology* **299**, 53-65 (2005).

142 Soto, C. *et al.* Pre-symptomatic detection of prions by cyclic amplification of protein misfolding. *FEBS letters* **579**, 638-642, doi:10.1016/j.febslet.2004.12.035 (2005).

143 Baskakov, I. V. & Breydo, L. Converting the prion protein: what makes the protein infectious. *Biochimica et biophysica acta* **1772**, 692-703, doi:10.1016/j.bbadis.2006.07.007 (2007).

144 Castilla, J., Saa, P., Hetz, C. & Soto, C. In vitro generation of infectious scrapie prions. *Cell* **121**, 195-206, doi:10.1016/j.cell.2005.02.011 (2005).

145 Prusiner, S. B. *et al.* Evidence for alpha-synuclein prions causing multiple system atrophy in humans with parkinsonism. *Proceedings of the National Academy of Sciences of the United States of America* **112**, E5308-5317, doi:10.1073/pnas.1514475112 (2015).

146 Lundmark, K., Westermark, G. T., Olsen, A. & Westermark, P. Protein fibrils in nature can enhance amyloid protein A amyloidosis in mice: Cross-seeding as a disease mechanism. *Proceedings of the National Academy of Sciences of the United States of America* **102**, 6098-6102, doi:10.1073/pnas.0501814102 (2005).

147 Solomon, A. *et al.* Amyloidogenic potential of foie gras. *Proceedings of the National Academy of Sciences of the United States of America* **104**, 10998-11001, doi:10.1073/pnas.0700848104 (2007).

148 Jaunmuktane, Z. *et al.* Evidence for human transmission of amyloid-beta pathology and cerebral amyloid angiopathy. *Nature* **525**, 247-250, doi:10.1038/nature15369 (2015).

149 Chattopadhyay, M. *et al.* The Disulfide Bond, but not Zinc or Dimerization, Controls Initiation and Seeded Growth in Amyotrophic Lateral Sclerosis-linked Cu-Zn Superoxide Dismutase (SOD1) Fibrillation. *The Journal of biological chemistry*, doi:10.1074/jbc.M115.666503 (2015).

150 Alberti, S., Halfmann, R., King, O., Kapila, A. & Lindquist, S. A systematic survey identifies prions and illuminates sequence features of prionogenic proteins. *Cell* **137**, 146-158, doi:10.1016/j.cell.2009.02.044 (2009).

151 Brachmann, A., Baxa, U. & Wickner, R. B. Prion generation in vitro: amyloid of Ure2p is infectious. *The EMBO journal* **24**, 3082-3092, doi:10.1038/sj.emboj.7600772 (2005).

152 King, C. Y. & Diaz-Avalos, R. Protein-only transmission of three yeast prion strains. *Nature* **428**, 319-323, doi:10.1038/nature02391 (2004).

153 Patel, B. K. & Liebman, S. W. "Prion-proof" for [PIN+]: infection with in vitro-made amyloid aggregates of Rnq1p-(132-405) induces [PIN+]. *Journal of molecular biology* **365**, 773-782, doi:10.1016/j.jmb.2006.10.069 (2007).

154 Shorter, J. & Lindquist, S. Destruction or potentiation of different prions catalyzed by similar Hsp104 remodeling activities. *Molecular cell* **23**, 425-438, doi:10.1016/j.molcel.2006.05.042 (2006).

155 Coustou, V., Deleu, C., Saupe, S. & Begueret, J. The protein product of the het-s heterokaryon incompatibility gene of the fungus Podospora anserina behaves as a prion analog. *Proceedings of the National Academy of Sciences of the United States of America* **94**, 9773-9778 (1997).

156 Espinosa Angarica, V. *et al.* PrionScan: an online database of predicted prion domains in complete proteomes. *BMC genomics* **15**, 102, doi:10.1186/1471-2164-15-102 (2014).

157 Gebbink, M. F., Claessen, D., Bouma, B., Dijkhuizen, L. & Wosten, H. A. Amyloids--a functional coat for microorganisms. *Nature reviews. Microbiology* **3**, 333-341, doi:10.1038/nrmicro1127 (2005).

158 Shewmaker, F., McGlinchey, R. P. & Wickner, R. B. Structural insights into functional and pathological amyloid. *The Journal of biological chemistry* **286**, 16533-16540, doi:10.1074/jbc.R111.227108 (2011).

159 Falsone, A. & Falsone, S. F. Legal but lethal: functional protein aggregation at the verge of toxicity. *Frontiers in cellular neuroscience* **9**, 45, doi:10.3389/fncel.2015.00045 (2015).

160 Pham, C. L., Kwan, A. H. & Sunde, M. Functional amyloid: widespread in Nature, diverse in purpose. *Essays in biochemistry* **56**, 207-219, doi:10.1042/bse0560207 (2014).

161 Larsen, P. *et al.* Amyloid adhesins are abundant in natural biofilms. *Environmental microbiology* **9**, 3077-3090, doi:10.1111/j.1462-2920.2007.01418.x (2007).

162 McLaurin, J., Yang, D., Yip, C. M. & Fraser, P. E. Review: modulating factors in amyloid-beta fibril formation. *Journal of structural biology* **130**, 259-270, doi:10.1006/jsbi.2000.4289 (2000).

163 White, A. P., Gibson, D. L., Kim, W., Kay, W. W. & Surette, M. G. Thin aggregative fimbriae and cellulose enhance long-term survival and persistence of Salmonella. *Journal of bacteriology* **188**, 3219-3227, doi:10.1128/JB.188.9.3219-3227.2006 (2006).

164 McGlinchey, R. P., Yap, T. L. & Lee, J. C. The yin and yang of amyloid: insights from alpha-synuclein and repeat domain of Pmel17. *Physical chemistry chemical physics : PCCP* **13**, 20066-20075, doi:10.1039/c1cp21376h (2011).

165 McGlinchey, R. P., Jiang, Z. & Lee, J. C. Molecular origin of pH-dependent fibril formation of a functional amyloid. *Chembiochem : a European journal of chemical biology* **15**, 1569-1572, doi:10.1002/cbic.201402074 (2014).

166 Komar, A. A., Melki, R. & Cullin, C. The [URE3] yeast prion: from genetics to biochemistry. *Biochemistry. Biokhimiia* **64**, 1401-1407 (1999).

167 Masison, D. C., Edskes, H. K., Maddelein, M. L., Taylor, K. L. & Wickner, R. B. [URE3] and [PSI] are prions of yeast and evidence for new fungal prions. *Current issues in molecular biology* **2**, 51-59 (2000).

168 Wickner, R. B. *et al.* Prions of yeast as heritable amyloidoses. *Journal of structural biology* **130**, 310-322, doi:10.1006/jsbi.2000.4250 (2000).

169 Halfmann, R. *et al.* Prions are a common mechanism for phenotypic inheritance in wild yeasts. *Nature* **482**, 363-368, doi:10.1038/nature10875 (2012).

170 Keeler, C., Hodsdon, M. E. & Dannies, P. S. Is there structural specificity in the reversible protein aggregates that are stored in secretory granules? *Journal of molecular neuroscience : MN* **22**, 43-49, doi:10.1385/JMN:22:1-2:43 (2004).

171 Carrell, R. W. & Lomas, D. A. Conformational disease. *Lancet* **350**, 134-138, doi:10.1016/S0140-6736(97)02073-4 (1997).

172 Aguzzi, A. & Calella, A. M. Prions: protein aggregation and infectious diseases. *Physiological reviews* **89**, 1105-1152, doi:10.1152/physrev.00006.2009 (2009).

173 Goedert, M. Familial Parkinson's disease. The awakening of alpha-synuclein. *Nature* **388**, 232-233, doi:10.1038/40762 (1997).

174 Goedert, M. Alpha-synuclein and neurodegenerative diseases. *Nature reviews. Neuroscience* **2**, 492-501, doi:10.1038/35081564 (2001).
175 Goedert, M. NEURODEGENERATION. Alzheimer's and Parkinson's diseases: The prion concept in relation to assembled Abeta, tau, and alpha-synuclein. *Science* **349**, 1255555, doi:10.1126/science.1255555 (2015).
176 Dobson, C. M. Protein folding and misfolding. *Nature* **426**, 884-890, doi:10.1038/nature02261 (2003).
177 Soto, C. Unfolding the role of protein misfolding in neurodegenerative diseases. *Nature reviews. Neuroscience* **4**, 49-60, doi:10.1038/nrn1007 (2003).
178 Surguchev, A. & Surguchov, A. Conformational diseases: looking into the eyes. *Brain research bulletin* **81**, 12-24, doi:10.1016/j.brainresbull.2009.09.015 (2010).
179 Kopito, R. R. & Ron, D. Conformational disease. *Nature cell biology* **2**, E207-209, doi:10.1038/35041139 (2000).
180 Soto, C. Protein misfolding and disease; protein refolding and therapy. *FEBS letters* **498**, 204-207 (2001).
181 Balch, W. E., Morimoto, R. I., Dillin, A. & Kelly, J. W. Adapting proteostasis for disease intervention. *Science* **319**, 916-919, doi:10.1126/science.1141448 (2008).
182 Moreno-Gonzalez, I. & Soto, C. Misfolded protein aggregates: mechanisms, structures and potential for disease transmission. *Seminars in cell & developmental biology* **22**, 482-487, doi:10.1016/j.semcdb.2011.04.002 (2011).
183 Last, N. B. & Miranker, A. D. Common mechanism unites membrane poration by amyloid and antimicrobial peptides. *Proceedings of the National Academy of Sciences of the United States of America* **110**, 6382-6387, doi:10.1073/pnas.1219059110 (2013).
184 Reynolds, N. P. *et al.* Mechanism of membrane interaction and disruption by alpha-synuclein. *Journal of the American Chemical Society* **133**, 19366-19375, doi:10.1021/ja2029848 (2011).
185 Selkoe, D. J. Cell biology of protein misfolding: the examples of Alzheimer's and Parkinson's diseases. *Nature cell biology* **6**, 1054-1061, doi:10.1038/ncb1104-1054 (2004).
186 Haass, C. & Selkoe, D. J. Soluble protein oligomers in neurodegeneration: lessons from the Alzheimer's amyloid beta-peptide. *Nature reviews. Molecular cell biology* **8**, 101-112, doi:10.1038/nrm2101 (2007).
187 Hernandez, F. & Avila, J. Tauopathies. *Cellular and molecular life sciences : CMLS* **64**, 2219-2233, doi:10.1007/s00018-007-7220-x (2007).
188 Hernandez, F. & Avila, J. Tau aggregates and tau pathology. *Journal of Alzheimer's disease : JAD* **14**, 449-452 (2008).
189 Hanger, D. P., Seereeram, A. & Noble, W. Mediators of tau phosphorylation in the pathogenesis of Alzheimer's disease. *Expert review of neurotherapeutics* **9**, 1647-1666, doi:10.1586/ern.09.104 (2009).
190 Spires-Jones, T. L., Stoothoff, W. H., de Calignon, A., Jones, P. B. & Hyman, B. T. Tau pathophysiology in neurodegeneration: a tangled issue. *Trends in neurosciences* **32**, 150-159, doi:10.1016/j.tins.2008.11.007 (2009).
191 Busciglio, J., Lorenzo, A., Yeh, J. & Yankner, B. A. beta-amyloid fibrils induce tau phosphorylation and loss of microtubule binding. *Neuron* **14**, 879-888 (1995).
192 Santacruz, K. *et al.* Tau suppression in a neurodegenerative mouse model improves memory function. *Science* **309**, 476-481, doi:10.1126/science.1113694 (2005).
193 Kim, D. & Tsai, L. H. Bridging physiology and pathology in AD. *Cell* **137**, 997-1000, doi:10.1016/j.cell.2009.05.042 (2009).
194 Zheng, H. & Koo, E. H. The amyloid precursor protein: beyond amyloid. *Molecular neurodegeneration* **1**, 5, doi:10.1186/1750-1326-1-5 (2006).

195 Butterfield, D. A., Swomley, A. M. & Sultana, R. Amyloid beta-peptide (1-42)-induced oxidative stress in Alzheimer disease: importance in disease pathogenesis and progression. *Antioxidants & redox signaling* **19**, 823-835, doi:10.1089/ars.2012.5027 (2013).

196 van der Kant, R. & Goldstein, L. S. Cellular functions of the amyloid precursor protein from development to dementia. *Developmental cell* **32**, 502-515, doi:10.1016/j.devcel.2015.01.022 (2015).

197 LaFerla, F. M., Green, K. N. & Oddo, S. Intracellular amyloid-beta in Alzheimer's disease. *Nature reviews. Neuroscience* **8**, 499-509, doi:10.1038/nrn2168 (2007).

198 Hardy, J. A. & Higgins, G. A. Alzheimer's disease: the amyloid cascade hypothesis. *Science* **256**, 184-185 (1992).

199 Kayed, R. *et al.* Common structure of soluble amyloid oligomers implies common mechanism of pathogenesis. *Science* **300**, 486-489, doi:10.1126/science.1079469 (2003).

200 Petkova, A. T. *et al.* Solid state NMR reveals a pH-dependent antiparallel beta-sheet registry in fibrils formed by a beta-amyloid peptide. *Journal of molecular biology* **335**, 247-260 (2004).

201 Bitan, G. *et al.* Amyloid beta -protein (Abeta) assembly: Abeta 40 and Abeta 42 oligomerize through distinct pathways. *Proceedings of the National Academy of Sciences of the United States of America* **100**, 330-335, doi:10.1073/pnas.222681699 (2003).

202 Butterfield, D. A., Drake, J., Pocernich, C. & Castegna, A. Evidence of oxidative damage in Alzheimer's disease brain: central role for amyloid beta-peptide. *Trends in molecular medicine* **7**, 548-554 (2001).

203 Lauderback, C. M. *et al.* The glial glutamate transporter, GLT-1, is oxidatively modified by 4-hydroxy-2-nonenal in the Alzheimer's disease brain: the role of Abeta1-42. *Journal of neurochemistry* **78**, 413-416 (2001).

204 Smith, M. A., Richey Harris, P. L., Sayre, L. M., Beckman, J. S. & Perry, G. Widespread peroxynitrite-mediated damage in Alzheimer's disease. *The Journal of neuroscience : the official journal of the Society for Neuroscience* **17**, 2653-2657 (1997).

205 Zlotnik, I. & Stamp, J. T. Scrapie disease of sheep. *World neurology* **2**, 895-907 (1961).

206 Haik, S. & Brandel, J. P. Biochemical and strain properties of CJD prions: complexity versus simplicity. *Journal of neurochemistry* **119**, 251-261, doi:10.1111/j.1471-4159.2011.07399.x (2011).

207 Masters, C. L., Gajdusek, D. C. & Gibbs, C. J., Jr. Creutzfeldt-Jakob disease virus isolations from the Gerstmann-Straussler syndrome with an analysis of the various forms of amyloid plaque deposition in the virus-induced spongiform encephalopathies. *Brain : a journal of neurology* **104**, 559-588 (1981).

208 DeArmond, S. J. *et al.* Identification of prion amyloid filaments in scrapie-infected brain. *Cell* **41**, 221-235 (1985).

209 Kitamoto, T. *et al.* Amyloid plaques in Creutzfeldt-Jakob disease stain with prion protein antibodies. *Annals of neurology* **20**, 204-208, doi:10.1002/ana.410200205 (1986).

210 Roberts, G. W. *et al.* Prion-protein immunoreactivity in human transmissible dementias. *The New England journal of medicine* **315**, 1231-1233, doi:10.1056/NEJM198611063151919 (1986).

211 Prusiner, S. B., Gabizon, R. & McKinley, M. P. On the biology of prions. *Acta neuropathologica* **72**, 299-314 (1987).

212 Collinge, J. & Palmer, M. S. Human prion diseases. *Bailliere's clinical neurology* **3**, 241-247 (1994).

213 Tateishi, J. & Kitamoto, T. Inherited prion diseases and transmission to rodents. *Brain pathology* **5**, 53-59 (1995).

214 Collinge, J. Variant Creutzfeldt-Jakob disease. *Lancet* **354**, 317-323, doi:10.1016/S0140-6736(99)05128-4 (1999).

215 Gambetti, P. & Parchi, P. Insomnia in prion diseases: sporadic and familial. *The New England journal of medicine* **340**, 1675-1677, doi:10.1056/NEJM199905273402111 (1999).
216 Jackson, G. S. & Collinge, J. The molecular pathology of CJD: old and new variants. *Molecular pathology : MP* **54**, 393-399 (2001).
217 Gambetti, P., Parchi, P. & Chen, S. G. Hereditary Creutzfeldt-Jakob disease and fatal familial insomnia. *Clinics in laboratory medicine* **23**, 43-64 (2003).
218 Montagna, P., Gambetti, P., Cortelli, P. & Lugaresi, E. Familial and sporadic fatal insomnia. *The Lancet. Neurology* **2**, 167-176 (2003).
219 Will, R. G. Acquired prion disease: iatrogenic CJD, variant CJD, kuru. *British medical bulletin* **66**, 255-265 (2003).
220 Basler, K. *et al.* Scrapie and cellular PrP isoforms are encoded by the same chromosomal gene. *Cell* **46**, 417-428 (1986).
221 Yoshimoto, J. *et al.* Comparative sequence analysis and expression of bovine PrP gene in mouse L-929 cells. *Virus genes* **6**, 343-356 (1992).
222 Westaway, D. *et al.* Structure and polymorphism of the mouse prion protein gene. *Proceedings of the National Academy of Sciences of the United States of America* **91**, 6418-6422 (1994).
223 Saeki, K., Matsumoto, Y., Hirota, Y., Matsumoto, Y. & Onodera, T. Three-exon structure of the gene encoding the rat prion protein and its expression in tissues. *Virus genes* **12**, 15-20 (1996).
224 Li, G. & Bolton, D. C. A novel hamster prion protein mRNA contains an extra exon: increased expression in scrapie. *Brain research* **751**, 265-274 (1997).
225 Lee, I. Y. *et al.* Complete genomic sequence and analysis of the prion protein gene region from three mammalian species. *Genome research* **8**, 1022-1037 (1998).
226 Watts, J. C., Balachandran, A. & Westaway, D. The expanding universe of prion diseases. *PLoS pathogens* **2**, e26, doi:10.1371/journal.ppat.0020026 (2006).
227 Ning, Z. Y. *et al.* Quantification of prion gene expression in brain and peripheral organs of golden hamster by real-time RT-PCR. *Animal biotechnology* **16**, 55-65 (2005).
228 Stahl, N. *et al.* Glycosylinositol phospholipid anchors of the scrapie and cellular prion proteins contain sialic acid. *Biochemistry* **31**, 5043-5053 (1992).
229 Taraboulos, A., Raeber, A. J., Borchelt, D. R., Serban, D. & Prusiner, S. B. Synthesis and trafficking of prion proteins in cultured cells. *Molecular biology of the cell* **3**, 851-863 (1992).
230 Englund, P. T. The structure and biosynthesis of glycosyl phosphatidylinositol protein anchors. *Annual review of biochemistry* **62**, 121-138, doi:10.1146/annurev.bi.62.070193.001005 (1993).
231 Vey, M. *et al.* Subcellular colocalization of the cellular and scrapie prion proteins in caveolae-like membranous domains. *Proceedings of the National Academy of Sciences of the United States of America* **93**, 14945-14949 (1996).
232 Malaga-Trillo, E., Salta, E., Figueras, A., Panagiotidis, C. & Sklaviadis, T. Fish models in prion biology: underwater issues. *Biochimica et biophysica acta* **1812**, 402-414, doi:10.1016/j.bbadis.2010.09.013 (2011).
233 Brown, D. R. *et al.* The cellular prion protein binds copper in vivo. *Nature* **390**, 684-687, doi:10.1038/37783 (1997).
234 Stockel, J., Safar, J., Wallace, A. C., Cohen, F. E. & Prusiner, S. B. Prion protein selectively binds copper(II) ions. *Biochemistry* **37**, 7185-7193, doi:10.1021/bi972827k (1998).
235 Brockes, J. P. Topics in prion cell biology. *Current opinion in neurobiology* **9**, 571-577, doi:10.1016/S0959-4388(99)00016-1 (1999).
236 Viles, J. H. *et al.* Copper binding to the prion protein: structural implications of four identical cooperative binding sites. *Proceedings of the National Academy of Sciences of the United States of America* **96**, 2042-2047 (1999).

237 Gonzalez-Iglesias, R. *et al.* Prion protein interaction with glycosaminoglycan occurs with the formation of oligomeric complexes stabilized by Cu(II) bridges. *Journal of molecular biology* **319**, 527-540, doi:10.1016/S0022-2836(02)00341-8 (2002).

238 Hodak, M., Chisnell, R., Lu, W. & Bernholc, J. Functional implications of multistage copper binding to the prion protein. *Proceedings of the National Academy of Sciences of the United States of America* **106**, 11576-11581, doi:10.1073/pnas.0903807106 (2009).

239 Weiss, S. *et al.* RNA aptamers specifically interact with the prion protein PrP. *Journal of virology* **71**, 8790-8797 (1997).

240 Warner, R. G., Hundt, C., Weiss, S. & Turnbull, J. E. Identification of the heparan sulfate binding sites in the cellular prion protein. *The Journal of biological chemistry* **277**, 18421-18430, doi:10.1074/jbc.M110406200 (2002).

241 Deleault, N. R. *et al.* Protease-resistant prion protein amplification reconstituted with partially purified substrates and synthetic polyanions. *The Journal of biological chemistry* **280**, 26873-26879, doi:10.1074/jbc.M503973200 (2005).

242 Ostapchenko, V. G., Makarava, N., Savtchenko, R. & Baskakov, I. V. The polybasic N-terminal region of the prion protein controls the physical properties of both the cellular and fibrillar forms of PrP. *Journal of molecular biology* **383**, 1210-1224, doi:10.1016/j.jmb.2008.08.073 (2008).

243 Wuthrich, K. & Riek, R. Three-dimensional structures of prion proteins. *Advances in protein chemistry* **57**, 55-82 (2001).

244 Chakrabarti, O., Ashok, A. & Hegde, R. S. Prion protein biosynthesis and its emerging role in neurodegeneration. *Trends in biochemical sciences* **34**, 287-295, doi:10.1016/j.tibs.2009.03.001 (2009).

245 Spevacek, A. R. *et al.* Zinc drives a tertiary fold in the prion protein with familial disease mutation sites at the interface. *Structure* **21**, 236-246, doi:10.1016/j.str.2012.12.002 (2013).

246 Colon, W. & Kelly, J. W. Partial denaturation of transthyretin is sufficient for amyloid fibril formation in vitro. *Biochemistry* **31**, 8654-8660 (1992).

247 Makarava, N., Ostapchenko, V. G., Savtchenko, R. & Baskakov, I. V. Conformational switching within individual amyloid fibrils. *The Journal of biological chemistry* **284**, 14386-14395, doi:10.1074/jbc.M900533200 (2009).

248 Baskakov, I. V. The many shades of prion strain adaptation. *Prion* **8** (2014).

249 Cobb, N. J., Apostol, M. I., Chen, S., Smirnovas, V. & Surewicz, W. K. Conformational stability of mammalian prion protein amyloid fibrils is dictated by a packing polymorphism within the core region. *The Journal of biological chemistry* **289**, 2643-2650, doi:10.1074/jbc.M113.520718 (2014).

250 Morgan, C. J., Gelfand, M., Atreya, C. & Miranker, A. D. Kidney dialysis-associated amyloidosis: a molecular role for copper in fiber formation. *Journal of molecular biology* **309**, 339-345, doi:10.1006/jmbi.2001.4661 (2001).

251 Xue, W. F., Hellewell, A. L., Hewitt, E. W. & Radford, S. E. Fibril fragmentation in amyloid assembly and cytotoxicity: when size matters. *Prion* **4**, 20-25 (2010).

252 Makarava, N. & Baskakov, I. V. The same primary structure of the prion protein yields two distinct self-propagating states. *The Journal of biological chemistry* **283**, 15988-15996, doi:10.1074/jbc.M800562200 (2008).

253 Ostapchenko, V. G. *et al.* Two amyloid States of the prion protein display significantly different folding patterns. *Journal of molecular biology* **400**, 908-921, doi:10.1016/j.jmb.2010.05.051 (2010).

254 Makarava, N. *et al.* Stabilization of a prion strain of synthetic origin requires multiple serial passages. *The Journal of biological chemistry* **287**, 30205-30214, doi:10.1074/jbc.M112.392985 (2012).

255 Makarava, N. & Baskakov, I. V. Genesis of tramsmissible protein states via deformed templating. *Prion* **6**, 252-255, doi:10.4161/pri.19930 (2012).

256 Tycko, R., Savtchenko, R., Ostapchenko, V. G., Makarava, N. & Baskakov, I. V. The alpha-helical C-terminal domain of full-length recombinant PrP converts to an in-register parallel beta-sheet structure in PrP fibrils: evidence from solid state nuclear magnetic resonance. *Biochemistry* **49**, 9488-9497, doi:10.1021/bi1013134 (2010).

257 Makarava, N. *et al.* A new mechanism for transmissible prion diseases. *The Journal of neuroscience : the official journal of the Society for Neuroscience* **32**, 7345-7355, doi:10.1523/JNEUROSCI.6351-11.2012 (2012).

258 Makarava, N. & Baskakov, I. V. The evolution of transmissible prions: the role of deformed templating. *PLoS pathogens* **9**, e1003759, doi:10.1371/journal.ppat.1003759 (2013).

259 Foss, T. R., Wiseman, R. L. & Kelly, J. W. The pathway by which the tetrameric protein transthyretin dissociates. *Biochemistry* **44**, 15525-15533, doi:10.1021/bi051608t (2005).

260 Quintas, A., Vaz, D. C., Cardoso, I., Saraiva, M. J. & Brito, R. M. Tetramer dissociation and monomer partial unfolding precedes protofibril formation in amyloidogenic transthyretin variants. *The Journal of biological chemistry* **276**, 27207-27213, doi:10.1074/jbc.M101024200 (2001).

261 Reixach, N., Deechongkit, S., Jiang, X., Kelly, J. W. & Buxbaum, J. N. Tissue damage in the amyloidoses: Transthyretin monomers and nonnative oligomers are the major cytotoxic species in tissue culture. *Proceedings of the National Academy of Sciences of the United States of America* **101**, 2817-2822, doi:10.1073/pnas.0400062101 (2004).

262 Leclerc, E., Sturchler, E. & Vetter, S. W. The S100B/RAGE Axis in Alzheimer's Disease. *Cardiovascular psychiatry and neurology* **2010**, 539581, doi:10.1155/2010/539581 (2010).

263 Jacobson, D. R. *et al.* Variant-sequence transthyretin (isoleucine 122) in late-onset cardiac amyloidosis in black Americans. *The New England journal of medicine* **336**, 466-473, doi:10.1056/NEJM199702133360703 (1997).

264 Saelices, L. *et al.* Uncovering the Mechanism of Aggregation of Human Transthyretin. *The Journal of biological chemistry*, doi:10.1074/jbc.M115.659912 (2015).

265 Bush, A. I. The metallobiology of Alzheimer's disease. *Trends in neurosciences* **26**, 207-214, doi:10.1016/S0166-2236(03)00067-5 (2003).

266 Watson, D. J., Lander, A. D. & Selkoe, D. J. Heparin-binding properties of the amyloidogenic peptides Abeta and amylin. Dependence on aggregation state and inhibition by Congo red. *The Journal of biological chemistry* **272**, 31617-31624 (1997).

267 Giraldo, R. Defined DNA sequences promote the assembly of a bacterial protein into distinct amyloid nanostructures. *Proceedings of the National Academy of Sciences of the United States of America* **104**, 17388-17393, doi:10.1073/pnas.0702006104 (2007).

268 Giraldo, R. & Diaz-Orejas, R. Similarities between the DNA replication initiators of Gram-negative bacteria plasmids (RepA) and eukaryotes (Orc4p)/archaea (Cdc6p). *Proceedings of the National Academy of Sciences of the United States of America* **98**, 4938-4943, doi:10.1073/pnas.081079298 (2001).

269 Levy, E. *et al.* Mutation of the Alzheimer's disease amyloid gene in hereditary cerebral hemorrhage, Dutch type. *Science* **248**, 1124-1126 (1990).

270 Miravalle, L. *et al.* Substitutions at codon 22 of Alzheimer's abeta peptide induce diverse conformational changes and apoptotic effects in human cerebral endothelial cells. *The Journal of biological chemistry* **275**, 27110-27116, doi:10.1074/jbc.M003154200 (2000).

271 Grabowski, T. J., Cho, H. S., Vonsattel, J. P., Rebeck, G. W. & Greenberg, S. M. Novel amyloid precursor protein mutation in an Iowa family with dementia and severe cerebral amyloid angiopathy. *Annals of neurology* **49**, 697-705 (2001).

272 Le, D. T. *et al.* Analysis of methionine/selenomethionine oxidation and methionine sulfoxide reductase function using methionine-rich proteins and antibodies against their oxidized forms. *Biochemistry* **47**, 6685-6694, doi:10.1021/bi800422s (2008).

273 Conway, K. A. *et al.* Acceleration of oligomerization, not fibrillization, is a shared property of both alpha-synuclein mutations linked to early-onset Parkinson's disease: implications for

pathogenesis and therapy. *Proceedings of the National Academy of Sciences of the United States of America* **97**, 571-576 (2000).

274 Fredenburg, R. A. *et al.* The impact of the E46K mutation on the properties of alpha-synuclein in its monomeric and oligomeric states. *Biochemistry* **46**, 7107-7118, doi:10.1021/bi7000246 (2007).

275 Goncalves, S. & Outeiro, T. F. Assessing the subcellular dynamics of alpha-synuclein using photoactivation microscopy. *Molecular neurobiology* **47**, 1081-1092, doi:10.1007/s12035-013-8406-x (2013).

276 Gitlin, I., Carbeck, J. D. & Whitesides, G. M. Why are proteins charged? Networks of charge-charge interactions in proteins measured by charge ladders and capillary electrophoresis. *Angewandte Chemie* **45**, 3022-3060, doi:10.1002/anie.200502530 (2006).

277 Mishra, R. *et al.* Lysozyme amyloidogenesis is accelerated by specific nicking and fragmentation but decelerated by intact protein binding and conversion. *Journal of molecular biology* **366**, 1029-1044, doi:10.1016/j.jmb.2006.11.084 (2007).

278 Morante, S. *et al.* Inter- and intra-octarepeat Cu(II) site geometries in the prion protein: implications in Cu(II) binding cooperativity and Cu(II)-mediated assemblies. *The Journal of biological chemistry* **279**, 11753-11759, doi:10.1074/jbc.M312860200 (2004).

279 Aguzzi, A. Cell biology: Beyond the prion principle. *Nature* **459**, 924-925, doi:10.1038/459924a (2009).

280 Speare, J. O., Rush, T. S., 3rd, Bloom, M. E. & Caughey, B. The role of helix 1 aspartates and salt bridges in the stability and conversion of prion protein. *The Journal of biological chemistry* **278**, 12522-12529, doi:10.1074/jbc.M211599200 (2003).

281 Calzolai, L. & Zahn, R. Influence of pH on NMR structure and stability of the human prion protein globular domain. *The Journal of biological chemistry* **278**, 35592-35596, doi:10.1074/jbc.M303005200 (2003).

282 Zhang, M. Z., Yao, B., McKanna, J. A. & Harris, R. C. Cross talk between the intrarenal dopaminergic and cyclooxygenase-2 systems. *American journal of physiology. Renal physiology* **288**, F840-845, doi:10.1152/ajprenal.00240.2004 (2005).

283 Alexandrescu, A. T. Amyloid accomplices and enforcers. *Protein Sci* **14**, 1-12, doi:10.1110/ps.04887005 (2005).

284 Follmer, C. *et al.* Oligomerization and Membrane-Binding Properties of Covalent Adducts Formed by the Interaction of Alpha-Synuclein with the Toxic Dopamine Metabolite 3,4-Dihydroxyphenylacetaldehyde (DOPAL). *The Journal of biological chemistry*, doi:10.1074/jbc.M115.686584 (2015).

285 Bouma, B. *et al.* Glycation induces formation of amyloid cross-beta structure in albumin. *The Journal of biological chemistry* **278**, 41810-41819, doi:10.1074/jbc.M303925200 (2003).

286 Chan, G. K. *et al.* Myeloperoxidase-mediated Methionine Oxidation Promotes an Amyloidogenic Outcome for Apolipoprotein A-I. *The Journal of biological chemistry* **290**, 10958-10971, doi:10.1074/jbc.M114.630442 (2015).

287 Hrynets, Y., Ndagijimana, M. & Betti, M. Rapid Myoglobin Aggregation through Glucosamine-Induced alpha-Dicarbonyl Formation. *PloS one* **10**, e0139022, doi:10.1371/journal.pone.0139022 (2015).

288 Requena, J. R. *et al.* Oxidation of methionine residues in the prion protein by hydrogen peroxide. *Archives of biochemistry and biophysics* **432**, 188-195, doi:10.1016/j.abb.2004.09.012 (2004).

289 Canello, T. *et al.* Methionine sulfoxides on PrPSc: a prion-specific covalent signature. *Biochemistry* **47**, 8866-8873, doi:10.1021/bi800801f (2008).

290 Radzicka, A., Pedersen, L. & Wolfenden, R. Influences of solvent water on protein folding: free energies of solvation of cis and trans peptides are nearly identical. *Biochemistry* **27**, 4538-4541 (1988).

291 Wolschner, C. *et al.* Design of anti- and pro-aggregation variants to assess the effects of methionine oxidation in human prion protein. *Proceedings of the National Academy of Sciences of the United States of America* **106**, 7756-7761, doi:10.1073/pnas.0902688106 (2009).

292 Moskovitz, J. *et al.* Methionine sulfoxide reductase (MsrA) is a regulator of antioxidant defense and lifespan in mammals. *Proceedings of the National Academy of Sciences of the United States of America* **98**, 12920-12925, doi:10.1073/pnas.231472998 (2001).

293 Moskovitz, J., Berlett, B. S., Poston, J. M. & Stadtman, E. R. The yeast peptide-methionine sulfoxide reductase functions as an antioxidant in vivo. *Proc Natl Acad Sci U S A* **94**, 9585-9589 (1997).

294 Moskovitz, J., Weissbach, H. & Brot, N. Cloning the expression of a mammalian gene involved in the reduction of methionine sulfoxide residues in proteins. *Proceedings of the National Academy of Sciences of the United States of America* **93**, 2095-2099 (1996).

295 Kumar, R. A., Koc, A., Cerny, R. L. & Gladyshev, V. N. Reaction mechanism, evolutionary analysis, and role of zinc in Drosophila methionine-R-sulfoxide reductase. *The Journal of biological chemistry* **277**, 37527-37535, doi:10.1074/jbc.M203496200 (2002).

296 Choi, J. *et al.* Oxidative damage of DJ-1 is linked to sporadic Parkinson and Alzheimer diseases. *J Biol Chem* **281**, 10816-10824, doi:10.1074/jbc.M509079200 (2006).

297 Creamer, T. P. & Rose, G. D. Alpha-helix-forming propensities in peptides and proteins. *Proteins* **19**, 85-97, doi:10.1002/prot.340190202 (1994).

298 Minor, D. L., Jr. & Kim, P. S. Measurement of the beta-sheet-forming propensities of amino acids. *Nature* **367**, 660-663, doi:10.1038/367660a0 (1994).

299 Stahl, N. *et al.* Structural studies of the scrapie prion protein using mass spectrometry and amino acid sequencing. *Biochemistry* **32**, 1991-2002 (1993).

300 Lisa, S. *et al.* The structural intolerance of the PrP alpha-fold for polar substitution of the helix-3 methionines. *Cellular and molecular life sciences : CMLS* **67**, 2825-2838, doi:10.1007/s00018-010-0363-1 (2010).

301 Colombo, G., Meli, M., Morra, G., Gabizon, R. & Gasset, M. Methionine sulfoxides on prion protein Helix-3 switch on the alpha-fold destabilization required for conversion. *PloS one* **4**, e4296, doi:10.1371/journal.pone.0004296 (2009).

302 Lisa, S. *et al.* Failure of prion protein oxidative folding guides the formation of toxic transmembrane forms. *The Journal of biological chemistry* **287**, 36693-36701, doi:10.1074/jbc.M112.398776 (2012).

303 Carroll, L., Davies, M. J. & Pattison, D. I. Reaction of low-molecular-mass organoselenium compounds (and their sulphur analogues) with inflammation-associated oxidants. *Free radical research* **49**, 750-767, doi:10.3109/10715762.2015.1018247 (2015).

304 Grant, C. M. Sup35 methionine oxidation is a trigger for de novo [PSI(+)] prion formation. *Prion* **9**, 257-265, doi:10.1080/19336896.2015.1065372 (2015).

305 Mura, C., Kozhukhovsky, A., Gingery, M., Phillips, M. & Eisenberg, D. The oligomerization and ligand-binding properties of Sm-like archaeal proteins (SmAPs). *Protein science : a publication of the Protein Society* **12**, 832-847, doi:10.1110/ps.0224703 (2003).

306 Budisa, N. *et al.* Atomic mutations in annexin V--thermodynamic studies of isomorphous protein variants. *European journal of biochemistry / FEBS* **253**, 1-9 (1998).

307 Apostol, M. I., Sawaya, M. R., Cascio, D. & Eisenberg, D. Crystallographic studies of prion protein (PrP) segments suggest how structural changes encoded by polymorphism at residue 129 modulate susceptibility to human prion disease. *The Journal of biological chemistry* **285**, 29671-29675, doi:10.1074/jbc.C110.158303 (2010).

308 Bush, A. I. Copper, zinc, and the metallobiology of Alzheimer disease. *Alzheimer disease and associated disorders* **17**, 147-150 (2003).

309 Miura, T., Suzuki, K., Kohata, N. & Takeuchi, H. Metal binding modes of Alzheimer's amyloid beta-peptide in insoluble aggregates and soluble complexes. *Biochemistry* **39**, 7024-7031 (2000).

310 Botelho, H. M. *et al.* S100A6 amyloid fibril formation is calcium-modulated and enhances superoxide dismutase-1 (SOD1) aggregation. *The Journal of biological chemistry* **287**, 42233-42242, doi:10.1074/jbc.M112.396416 (2012).

311 Carvalho, S. B. *et al.* Intrinsically disordered and aggregation prone regions underlie beta-aggregation in S100 proteins. *PloS one* **8**, e76629, doi:10.1371/journal.pone.0076629 (2013).

312 Deleault, N. R., Lucassen, R. W. & Supattapone, S. RNA molecules stimulate prion protein conversion. *Nature* **425**, 717-720, doi:10.1038/nature01979 (2003).

313 Aalberse, R. C. Structural biology of allergens. *The Journal of allergy and clinical immunology* **106**, 228-238, doi:10.1067/mai.2000.108434 (2000).

314 Astwood, J. D., Leach, J. N. & Fuchs, R. L. Stability of food allergens to digestion in vitro. *Nature biotechnology* **14**, 1269-1273, doi:10.1038/nbt1096-1269 (1996).

315 Chapman, M. D., Pomes, A., Breiteneder, H. & Ferreira, F. Nomenclature and structural biology of allergens. *The Journal of allergy and clinical immunology* **119**, 414-420, doi:10.1016/j.jaci.2006.11.001 (2007).

316 Rona, R. J. *et al.* The prevalence of food allergy: a meta-analysis. *The Journal of allergy and clinical immunology* **120**, 638-646, doi:10.1016/j.jaci.2007.05.026 (2007).

317 Venter, C. & Arshad, S. H. Epidemiology of food allergy. *Pediatric clinics of North America* **58**, 327-349, ix, doi:10.1016/j.pcl.2011.02.011 (2011).

318 Bugajska-Schretter, A. *et al.* Parvalbumin, a cross-reactive fish allergen, contains IgE-binding epitopes sensitive to periodate treatment and Ca2+ depletion. *The Journal of allergy and clinical immunology* **101**, 67-74, doi:10.1016/S0091-6749(98)70195-2 (1998).

319 Griesmeier, U. *et al.* Expression levels of parvalbumins determine allergenicity of fish species. *Allergy* **65**, 191-198, doi:10.1111/j.1398-9995.2009.02162.x (2010).

320 Jenkins, J. A., Breiteneder, H. & Mills, E. N. Evolutionary distance from human homologs reflects allergenicity of animal food proteins. *The Journal of allergy and clinical immunology* **120**, 1399-1405, doi:10.1016/j.jaci.2007.08.019 (2007).

321 Lim, D. L. *et al.* Parvalbumin--the major tropical fish allergen. *Pediatric allergy and immunology : official publication of the European Society of Pediatric Allergy and Immunology* **19**, 399-407, doi:10.1111/j.1399-3038.2007.00674.x (2008).

322 Swoboda, I. *et al.* Recombinant carp parvalbumin, the major cross-reactive fish allergen: a tool for diagnosis and therapy of fish allergy. *Journal of immunology* **168**, 4576-4584 (2002).

323 Bernhisel-Broadbent, J., Strause, D. & Sampson, H. A. Fish hypersensitivity. II: Clinical relevance of altered fish allergenicity caused by various preparation methods. *The Journal of allergy and clinical immunology* **90**, 622-629 (1992).

324 Lewit-Bentley, A. & Rety, S. EF-hand calcium-binding proteins. *Current opinion in structural biology* **10**, 637-643 (2000).

325 Ledesma, A. *et al.* Are Ca2+-binding motifs involved in the immunoglobin E-binding of allergens? Olive pollen allergens as model of study. *Clinical and experimental allergy : journal of the British Society for Allergy and Clinical Immunology* **32**, 1476-1483 (2002).

326 Moraes, A. H. *et al.* Solution and high-pressure NMR studies of the structure, dynamics, and stability of the cross-reactive allergenic cod parvalbumin Gad m 1. *Proteins* **82**, 3032-3042, doi:10.1002/prot.24664 (2014).

327 Somkuti, J., Bublin, M., Breiteneder, H. & Smeller, L. Pressure-temperature stability, Ca2+ binding, and pressure-temperature phase diagram of cod parvalbumin: Gad m 1. *Biochemistry* **51**, 5903-5911, doi:10.1021/bi300403h (2012).

328 Swoboda, I. *et al.* A recombinant hypoallergenic parvalbumin mutant for immunotherapy of IgE-mediated fish allergy. *Journal of immunology* **178**, 6290-6296 (2007).

329 Swoboda, I. *et al.* A general strategy for the generation of hypoallergenic molecules for the immunotherapy of fish allergy. *The Journal of allergy and clinical immunology* **132**, 979-981 e971, doi:10.1016/j.jaci.2013.04.027 (2013).

330 Daniels, L. A. Selenium metabolism and bioavailability. *Biological trace element research* **54**, 185-199, doi:10.1007/BF02784430 (1996).

331 Rayman, M. P. Food-chain selenium and human health: emphasis on intake. *The British journal of nutrition* **100**, 254-268, doi:10.1017/S0007114508939830 (2008).

332 Griffiths, N. M., Stewart, R. D. & Robinson, M. F. The metabolism of [75Se]selenomethionine in four women. *The British journal of nutrition* **35**, 373-382 (1976).

333 Gassner, N. C., Baase, W. A., Hausrath, A. C. & Matthews, B. W. Substitution with selenomethionine can enhance the stability of methionine-rich proteins. *Journal of molecular biology* **294**, 17-20, doi:10.1006/jmbi.1999.3220 (1999).

334 Yamniuk, A. P., Ishida, H., Lippert, D. & Vogel, H. J. Thermodynamic effects of noncoded and coded methionine substitutions in calmodulin. *Biophysical journal* **96**, 1495-1507, doi:10.1016/j.bpj.2008.10.060 (2009).

335 Nakamura, H. Roles of electrostatic interaction in proteins. *Quarterly reviews of biophysics* **29**, 1-90 (1996).

336 Bosshard, H. R., Marti, D. N. & Jelesarov, I. Protein stabilization by salt bridges: concepts, experimental approaches and clarification of some misunderstandings. *Journal of molecular recognition : JMR* **17**, 1-16, doi:10.1002/jmr.657 (2004).

337 Liu, A. *et al.* NMR experiments for resonance assignments of 13C, 15N doubly-labeled flexible polypeptides: application to the human prion protein hPrP(23-230). *Journal of biomolecular NMR* **16**, 127-138 (2000).

338 Zhang, Y., Swietnicki, W., Zagorski, M. G., Surewicz, W. K. & Sonnichsen, F. D. Solution structure of the E200K variant of human prion protein. Implications for the mechanism of pathogenesis in familial prion diseases. *The Journal of biological chemistry* **275**, 33650-33654, doi:10.1074/jbc.C000483200 (2000).

339 Norstrom, E. M. & Mastrianni, J. A. The charge structure of helix 1 in the prion protein regulates conversion to pathogenic PrPSc. *Journal of virology* **80**, 8521-8529, doi:10.1128/JVI.00366-06 (2006).

340 Zuegg, J. & Gready, J. E. Molecular dynamics simulations of human prion protein: importance of correct treatment of electrostatic interactions. *Biochemistry* **38**, 13862-13876 (1999).

341 Traidl-Hoffmann, C., Jakob, T. & Behrendt, H. Determinants of allergenicity. *The Journal of allergy and clinical immunology* **123**, 558-566, doi:10.1016/j.jaci.2008.12.003 (2009).

342 Kuehn, A., Swoboda, I., Arumugam, K., Hilger, C. & Hentges, F. Fish allergens at a glance: variable allergenicity of parvalbumins, the major fish allergens. *Frontiers in immunology* **5**, 179, doi:10.3389/fimmu.2014.00179 (2014).

343 Knowles, T. P. & Buehler, M. J. Nanomechanics of functional and pathological amyloid materials. *Nature nanotechnology* **6**, 469-479, doi:10.1038/nnano.2011.102 (2011).

344 Schrauzer, G. N. Selenomethionine: a review of its nutritional significance, metabolism and toxicity. *The Journal of nutrition* **130**, 1653-1656 (2000).

345 Storkey, C., Pattison, D. I., White, J. M., Schiesser, C. H. & Davies, M. J. Preventing protein oxidation with sugars: scavenging of hypohalous acids by 5-selenopyranose and 4-selenofuranose derivatives. *Chemical research in toxicology* **25**, 2589-2599, doi:10.1021/tx3003593 (2012).

346 Wernimont, A. K. *et al.* Crystal structure and dimerization equilibria of PcoC, a methionine-rich copper resistance protein from Escherichia coli. *Journal of biological inorganic chemistry : JBIC : a publication of the Society of Biological Inorganic Chemistry* **8**, 185-194, doi:10.1007/s00775-002-0404-9 (2003).

347 Hakansson, K., Broder, D., Wang, A. H. & Miller, C. G. Crystallization of peptidase T from Salmonella typhimurium. *Acta crystallographica. Section D, Biological crystallography* **56**, 924-926 (2000).

348 Westergard, L., Turnbaugh, J. A. & Harris, D. A. A naturally occurring C-terminal fragment of the prion protein (PrP) delays disease and acts as a dominant-negative inhibitor of PrPSc formation. *The Journal of biological chemistry* **286**, 44234-44242, doi:10.1074/jbc.M111.286195 (2011).

349 Klimova, N., Makarava, N. & Baskakov, I. V. The diversity and relationship of prion protein self-replicating states. *Virus research* **207**, 113-119, doi:10.1016/j.virusres.2014.10.002 (2015).

350 Lara, C., Gourdin-Bertin, S., Adamcik, J., Bolisetty, S. & Mezzenga, R. Self-assembly of ovalbumin into amyloid and non-amyloid fibrils. *Biomacromolecules* **13**, 4213-4221, doi:10.1021/bm301481v (2012).

351 Jones, O. G., Adamcik, J., Handschin, S., Bolisetty, S. & Mezzenga, R. Fibrillation of beta-lactoglobulin at low pH in the presence of a complexing anionic polysaccharide. *Langmuir : the ACS journal of surfaces and colloids* **26**, 17449-17458, doi:10.1021/la1026619 (2010).

352 Mulaj, M., Foley, J. & Muschol, M. Amyloid oligomers and protofibrils, but not filaments, self-replicate from native lysozyme. *Journal of the American Chemical Society* **136**, 8947-8956, doi:10.1021/ja502529m (2014).

353 Oyoshi, M. K., Oettgen, H. C., Chatila, T. A., Geha, R. S. & Bryce, P. J. Food allergy: Insights into etiology, prevention, and treatment provided by murine models. *The Journal of allergy and clinical immunology* **133**, 309-317, doi:10.1016/j.jaci.2013.12.1045 (2014).

354 Taylor, S. L. & Lehrer, S. B. Principles and characteristics of food allergens. *Critical reviews in food science and nutrition* **36 Suppl**, S91-118 (1996).

355 Lasse, M. *et al.* Evaluation of protease resistance and toxicity of amyloid-like food fibrils from whey, soy, kidney bean, and egg white. *Food chemistry* **192**, 491-498, doi:10.1016/j.foodchem.2015.07.044 (2016).

356 Tycko, R. Solid-state NMR studies of amyloid fibril structure. *Annual review of physical chemistry* **62**, 279-299, doi:10.1146/annurev-physchem-032210-103539 (2011).

http://www.niddk.nih.gov/research-funding/at-niddk/labs-branches/LBG/Pages/research-images.aspx (30/10/2015)